

APPENDIX C
Petrographic Analysis Reports

Appendix D: Petrographic Analysis

Introduction

The petrographic analysis for this study was completed by two different registered petrographers. These petrographic examinations were done according to ASTM C 856. Airports I, II, and III were completed by Mr. Don Campbell of Campbell Petrographic Services, Inc., while airports IV – VIII were completed by Mr. James Schmitt of Schmitt Technical Services LLC. The goals of the petrographic analysis were to first determine what the form of deterioration was and what role did the chemical deicers play in the degree of this deterioration. The reports found below are the results of the petrographic analysis of the individual airfield pavements.

Introduction for Airports I – III

Dr. Prasad R. Rangaraju, Ph.D., P.E. of Clemson University, Department of Civil Engineering has contracted Campbell Petrographic Services, Inc. to perform petrographic examinations of core samples from the airfield pavements. The cores are from one of several airfield pavements selected to be included in Innovative Pavement Research Foundation (IPRF) Project No. 01-G-002-05-7, entitled “Performance of Concrete in the Presence of Airfield Pavement Deicers and Identification of Induced Distress Mechanisms.” Petrographic examinations were performed as part of Tasks 5, 7 and 9 of the project regarding forensic investigations of cores taken from the pavements.

Airport I

Identification and Dimensions:

Victor – 2: Length = 203mm; Diameter = 95mm; Intact.

Tango – 3: Length = 215mm; Diameter = 95mm; In two segments, separated transversely along a slanted fracture surface, through aggregates, from a depth of 40 to 85mm.

Tango – 6: Length = 260mm; Diameter = 95mm; Intact.

Echo – 2: Length = 335mm; Diameter = 95mm; Intact.

Echo – 6: Length = 165mm; Diameter = 95mm; Intact.

Core or Fragment Surfaces:

Victor – 2: Core top surface retains faint ridge marks from original finishing operation; numerous fine aggregates exposed. Core side is smoothly drilled. Base of core is fresh transverse fracture surface passing through aggregates.

Tango – 3: Core top surface is weathered but retains very faint marks from the original finish; numerous fine aggregates exposed. Side of core is smoothly drilled. Inclined fracture surface separating the core into segments (as received) at a depth of approximately 85mm exhibits a tan color and apparent paste alteration. Base is a fresh fracture surface, passing through aggregates, but also shows a horizontally drilled 40mm diameter hole, extending approximately ½ the core diameter.

Tango – 6: Core top surface is deeply weathered, removing all traces of previous finish and exposing numerous fine and a few coarse aggregates (topographic relief is approximately 2mm). Side of core is smoothly drilled. Base of core is fresh transverse fracture surface, passing through aggregates.

Echo – 2: Core top retains coarse linear markings from original finish. Side of core is smoothly drilled. Base of core is fresh transverse fracture surface, passing through aggregates.

Echo – 6: Top surface of core is deeply weathered, exposing many fine aggregates, but retaining traces of the original finish. Side of core is smoothly drilled. Base is fresh transverse fracture surface.

Large Voids, Joints, and Macrocracks (easily seen with unaided eye):

- Victor – 2: No significant large voids or joints observed. Vertically oriented macrocrack with a partial filling of clear to cloudy calcite extends approximately $\frac{3}{4}$ of the core diameter, passing out of the core at a depth of 35mm.
- Tango – 3: No significant large voids or joints observed. Top surface exhibits three macrocracks that intersect (almost forming a triple-point junction) on the top; cracks appear to extend downward to a maximum depth of approximately 85mm, ending at the surface dividing the core into the two segments as received.
- Tango – 6: Entrapped air voids with diameters of approximately 4mm are common. No joints or macrocracks observed.
- Echo – 2: A few irregular entrapped air voids were observed with dimensions up to 21x15x10mm. No joints seen. Three macrocracks are visible on the top surface, extending downward as much as 35mm, where they intersect multiple horizontal macrocracks visible throughout the concrete represented in the lapped section. Lapped slices reveal a large number of cracks, many of which are horizontal and vertically spaced at approximately 15-20mm, passing through aggregates. An abundance of macrocracks are developed in the outer 1 to 2mm of the coarse aggregate particles; others occur in the middle portions of the particle. Macrocracks with openings as much 2mm as seen within some of the many coarse aggregates and some fine aggregates (coarse fraction) are numerous.
- Echo – 6: A few round to irregular entrapped air voids observed. No joints. One macrocrack seen on the top surface extends downward to a depth of at least 28mm. Lapped slice reveals a large number of aggregates. Widened cracks in the central part of many coarse aggregates and some fine aggregates (coarse fraction) are numerous.

Reinforcement and Corrosion

- Victor – 2: None Observed.
- Tango – 3: As stated above.
- Tango – 6: As stated above.
- Echo – 2: As stated above.
- Echo – 6: As stated above.

Aggregates

Coarse (C):

- Victor – 2: Crushed light gray to pale yellow limestone, of several varieties (oolitic, microcrystalline, fossiliferous, and others). Some finely microcrystalline, fossiliferous limestone has traces of chalcedony and microcrystalline quartz, apparently as selected replacements of fossil fragments.
- Tango – 3: Crushed medium to light gray to pale green, very sandy limestone and limey sandstone, and a small percentage of chert (the latter containing pseudomorphic fossil shell fragments).

Tango – 6: Crushed limestone apparently identical to that in Echo – 2 and Echo – 6.

Echo – 2: Crushed tan to brown to dark gray limestone of mostly a finely microcrystalline type with fossils and traces of secondary chert; some limestones are sandy.

Echo – 6: As described above for Echo – 2.

Fine:

Victor – 2: Sand containing ordinary quartz, metaquartzite, siltstone, fine-grained sandstone, limestone, feldspar, chert, basalt, and other rocks and minerals.

Tango – 3: Sand containing ordinary quartz, metaquartzite, chert, sandstone and limestone (as described above), feldspar, and other rocks and minerals.

Tango – 6: As described for Tango – 3.

Echo – 2: Sand containing ordinary quartz, metaquartzite, well-rounded siltstone and sandstone (greywacke type), feldspar, chert, well-rounded limestone, and other rocks and minerals. Some coarse sand particles, mainly the greywacke type, show microcracking and associated ASR gel.

Echo – 6: As described above for Echo – 2.

Gradation and Top Size:

Victor – 2: Evenly graded to top size of approximately 16mm (0.62 inch).

Tango – 3: Evenly graded to top size of approximately 17mm (0.66 inch).

Tango – 6: Evenly graded to top size of approximately 20mm (0.78 inch).

Echo – 2: Evenly graded to top size of approximately 14mm (0.55 inch).

Echo – 6: Evenly graded to top size of approximately 14mm (0.55 inch).

Shape and Distribution:

Victor – 2: Angular, equidimensional uniformly distributed CA. Angular to well-rounded equidimensional to elongated, uniformly distributed FA.

Tango – 3: Angular, equidimensional uniformly distributed CA. Angular to well-rounded equidimensional to elongated, uniformly distributed FA.

Tango – 6: CA is angular, equidimensional to prominently elongated, uniformly distributed. FA is well rounded to angular, equidimensional to elongated, uniformly distributed.

Echo – 2: CA is angular, equidimensional to elongated, uniformly distributed. FA is well rounded to angular, equidimensional to elongated, uniformly distributed.

Echo – 6: As described above for Echo – 2.

Paste Aggregate Bond:

Evaluated according to number of cross-fractured hard aggregates.

Victor – 2: Tight, indicated by numerous cross-fractured quartz grains.

Tango – 3: Tight.

Tango – 6: Tight.

Echo – 2: Generally tight in areas not riddled with microcracks, the latter causing the sample to disintegrate with a light hammer blow.

Echo – 6: As above for Echo – 2.

Paste

Air Content:

Estimated on finely lapped saw-cut section and in thin section.

Victor – 2: 3 to 5%, marginal air entrainment system, pending ASTM C 457.

Tango – 3: 3 to 6%, entrained air voids are relatively coarse.

Tango – 6: 5 to 7%, air entrained.

Echo – 2: 5 to 7%, air entrained.

Echo – 6: 5 to 7%, air entrained.

Depth of Carbonation:**

Detected with use of variable pH indicator spray and in thin section.

Victor – 2: Less than 0.5mm.

Tango – 3: Less than 1.0mm, with slight irregularity.

Tango – 6: Less than 1.0mm.

Echo – 2: Not measured.

Echo – 6: Not measured.

Color:

Observed on fresh fracture surface under the stereomicroscope with intense light.

Victor – 2: Light gray to light tan to green, mottled.

Tango – 3: Buff color.

Tango – 6: Medium to light gray, mottled.

Echo – 2: Medium gray.

Echo – 6: Medium gray.

Hardness:

Resistance to scratching with a curved, sharpened, steel dental pick under the stereomicroscope.

Victor – 2: Hard.

Tango – 3: Hard.

Tango – 6: Hard.

Echo – 2: Moderately hard.

Echo – 6: Moderately hard.

Luster:

Reflectivity of fresh fracture surface under the stereomicroscope with intense light.

Victor – 2: Vitreous.

Tango – 3: Vitreous.

Tango – 6: Vitreous.

Echo – 2: Vitreous.

Echo – 6: Vitreous.

Calcium Hydroxide (CH):

Observed in thin section.

Victor – 2: 0.5 to 1.0%, occurring as relatively small poikilitic crystals in the body of the paste, and to a minor extent, on aggregate surfaces.

Tango – 3: 2 to 4%, occurring as relatively small poikilitic crystals in the body of the paste, and to a minor extent, on aggregate surfaces.

Tango – 6: 2 to 4%, occurring as relatively small poikilitic crystals in the body of the paste, and to a minor extent, on aggregate surfaces.

Echo – 2: 1 to 2%, occurring as relatively small irregular poikilitic crystals and blade form crystals, generally well scattered in the paste, rarely developed as coarse crystals on aggregate particles.

Echo – 6: 1 to 2%, occurring as relatively small irregular poikilitic crystals and blade form crystals, generally well scattered in the paste, rarely developed as coarse crystals on aggregate particles.

Unhydrated Portland Cement Clinker Particles (UPCs)*:

Observed in thin section.

Victor – 2: 2 to 4%, gray Portland cement clinker. Clinker constituents are impure C_3S (alite), C_2S (belite), and a matrix of mostly calcium alumino-ferrite, individual phases in particles or combined, well scattered in the paste.

Tango – 3: 2 to 4%, gray Portland cement clinker. Clinker constituents are impure C_3S (alite), C_2S (belite), and a matrix of mostly calcium alumino-ferrite, individual phases in particles or combined, well scattered in the paste.

Tango – 6: 2 to 4%, gray Portland cement clinker. Clinker constituents are impure C_3S (alite), C_2S (belite), and a matrix of mostly calcium alumino-ferrite, individual phases in particles or combined, well scattered in the paste.

Echo – 2: 2 to 4%, gray Portland cement clinker. Clinker constituents are impure C_3S (alite), C_2S (belite), and a matrix of mostly calcium alumino-ferrite, individual phases in particles or combined, well scattered in the paste.

Echo – 6: 2 to 4%, gray Portland cement clinker. Clinker constituents are impure C_3S (alite), C_2S (belite), and a matrix of mostly calcium alumino-ferrite, individual phases in particles or combined, well scattered in the paste.

Fly Ash (fa)*:

Observed in thin section.

- Victor – 2: 10 to 15% of the paste as glassy blast-furnace slag.
Tango – 3: 9 to 12%, Class C on the basis of scarcity of carbon particles.
Tango – 6: 9 to 12%, Class C on the basis of scarcity of carbon particles.
Echo – 2: 10 to 15%, Class C on the basis of scarcity of carbon particles.
Echo – 6: 10 to 15%, Class C on the basis of scarcity of carbon particles.

Secondary Deposits:

Observed in stereomicroscope and thin section.

- Victor – 2: Ettringite observed in trace amounts in voids. No ASR gel observed. Brucite possible in carbonated paste adjacent to ACR dolostone and tan, reaction-rimmed, clayey dolomitic limestone.
- Tango – 3: Ettringite fills a small proportion of the air voids. No ASR gel observed.
- Tango – 6: Virtually no secondary deposits observed, except thin linings of ettringite in voids. No ASR gel seen.
- Echo – 2: Ettringite fills, or partially fills, almost every entrained air void. White and clear finely microcrystalline ASR gel occurs beside many of the limestones (particularly those containing chert) and within microcracks in soft, tan finely microcrystalline chert on the core base and on the drill-cut side where gel fills drill-bit grooves. ASR gel is abundant in the core, occurring mostly in voids and on fracture surfaces within reaction-rimmed limestone; some of the gel accumulations have an opaline luster and color. ASR gel is also associated with particles of chert, siltstone, and fine sandstone of the coarse fraction of the fine aggregate. Gel-filled voids associated with microcracked limestone marked by zones and seams containing clay were notable in one of the thin sections.
- Echo – 6: Virtually identical secondary deposits (ettringite and ASR gel) as described above for Echo – 2. Gel is commonly found in siltstone and sandstone microcracks, the gel occurring mostly in the outer 200 to 300 microns of the reacting particle, and continuing into the adjacent paste. White and clear finely microcrystalline ASR gel occurs beside dark limestone and soft tan finely microcrystalline chert on the core base and on the drill-cut side. Gel was observed in microcracked limestone aggregates but only in the few microns in the outer parts of the particle where the paste is near.

Microcracking:

Observed in fluorescent-epoxy impregnated thin section and finely lapped specimen.

- Victor – 2: Examination of the lapped section, counting numbered coarse-aggregate particles, revealed 27 of 37 particles with microcracks originating within the rock and passing into the adjacent paste. Study of a thin-section, representing a 110-mm depth in V-2 reveals numerous microcracks, some of which are somewhat radially arranged, apparently beginning within tan, reaction-rimmed, clayey dolomitic limestone coarse aggregate, and many other aggregates, with the partially surrounding white-to cream-colored carbonated paste. The number of microcracks is astounding.

Tango – 3: Examination of the fluorescent-epoxy impregnated surface, counting a total of 45 coarse aggregates, revealed only three (3) occurrences of microcracks passing from within the particle and extending into the adjacent paste.

Tango – 6: Of 50 coarse aggregates counted on the fluorescent-epoxy impregnated section, only one (1) particle with a microcrack appearing to originate within the particle and extending into the adjacent paste was observed.

Echo – 2: Microcracks are unusually abundant in the fluorescent-epoxy impregnated slice, some clearly passing from within limestone aggregate particles into the adjacent paste, but many more, along their mostly horizontal paths, cut through several aggregates, mostly the limestone. Many clear examples of thin microcracks, originating from within well-rounded sandstone and siltstone particles and tan to brown limestone and chert of the coarse fraction of the fine aggregate, pass into the adjacent paste and terminate therein, voids containing alkali silica gel appear to be slightly more commonly associated with nearby limestone than the fine-aggregate sandstone and siltstone, however, no statistical counts of this association have been made.

The number of microcracks is far more than can be counted and appear to originate within the chert-bearing limestones of the coarse aggregate, and well-rounded siltstones and fine sandstones, mainly in the coarse fraction of the fine aggregate, showing a well developed ASR microcracking with abundant, adjacent, gel-filled voids. Utilizing fluorescent epoxy and counting coarse aggregates, resulted in 106 microcracks originating within the rock and passing into the paste. thin-section study reveals microcracks partially lined with ASR gel within some of these particles, the cracks leading into the surrounding paste. The offending mineral appears to be chalcedonic and microcrystalline quartz in chert of the coarse aggregate, and siltstone to medium-grained sandstone (classified petrographically as a subgraywacke, containing quartz, fine-grained metamorphic rock fragments, feldspar, chert, mica, and other constituents).

Echo – 6: as described above for Core Echo – 2. Examination of the fluorescent-epoxy impregnated surface, reveals 35 particles (from a total of 63 particles) with microcracks passing into the adjacent paste.

Estimated Water-to- (Cement + Fly Ash) Ratio:

Victor – 2: 0.37 to 0.42.

Tango – 3: As above.

Tango – 6: As above.

Echo – 2: As above.

Echo – 6: As above.

Miscellaneous:

- Victor – 2: Lapped section from top surface to depth of 140 mm. Vertically oriented thin sections from top surface to depth of 20 mm, and from 70 to 90 mm, and from 72 to 135 mm were studied.
- Tango – 3: Lapped section from top surface to a depth of 117 mm. Transversely oriented thin section represents the 118 to 128-mm interval.
- Tango – 6: Lapped section from the top surface to a depth of 150 mm. Thin section made from Transverse surface at approximately 170 mm.
- Echo – 2: Lapped sections extend from the top surface to a depth of 180 mm and from approximately 202 to 325 mm. Thin sections vertically oriented, extending from 182 to 202 mm, the selected blanks cut with the Isomet.
- Echo – 6: Lapped section extends from the top surface to a depth of 180 mm. Thin sections vertically oriented, selected from Isomet-cut blanks extending from 122 to 140 mm.

Figure 1: (Upper) Typical ACR macrocracking and microcracking in Victor – 2 Core at a depth of 90 mm in an epoxy-impregnated surface (without lapped removal of the excess epoxy) under the stereomicroscope in oblique, reflected, diffuse light. Similar cracking was observed throughout the entire length of the core. Millimeter scale divisions. (Lower) Tan dolomitic coarse aggregate limestone under the stereomicroscope in Victor – 2 Core at a depth of approximately 140 mm, partially surrounded by a thin discontinuous band of white carbonated paste (mows), the carbonation believed to result from an alkali carbonate reaction. LP = 16 mm.



Figure 2: (Upper) Thin-section view at 100X of Victor – 2 Core at a depth of 90 mm in transmitted polarized light with simultaneous reflected UV light. Left side of photo illustrates relatively low permeability reaction rim on dolomitic limestone aggregate (arrow) through which a microcrack passes into the adjacent paste. LP = 1.0 mm. (Lower) Thin-section of Victor – 2 Core at a level of 135 mm in cross-polarized transmitted light at 100X. Dolomitic limestone aggregates on left and right sides of photo with intervening carbonated paste (from ACR) and rounded quartz grain (black). The carbonated paste is white to off-white in the lapped section viewed under the stereomicroscope. LP = 1.0 mm.

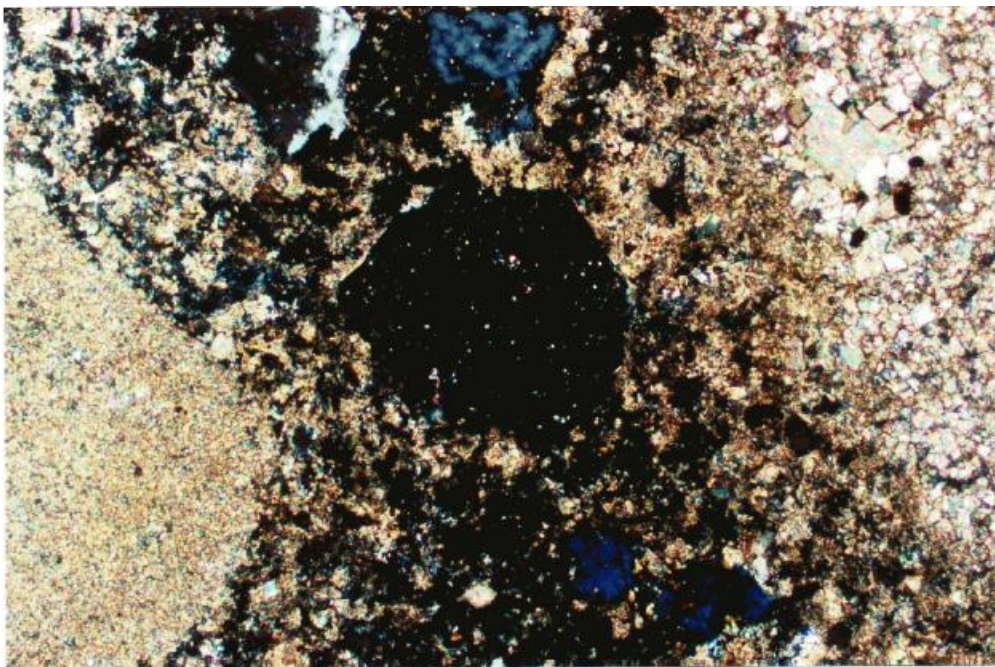
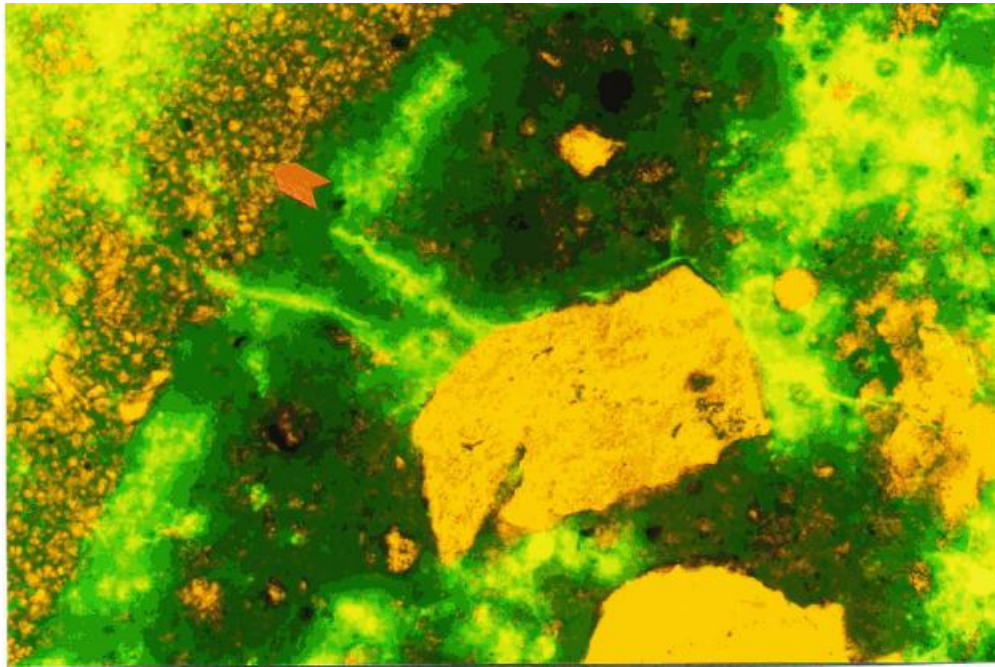


Figure 3: (Upper) Exterior side of Echo – 2 Core, as received, under the stereomicroscope, illustrating white ASR gel that accumulated at a depth of 110 millimeters after core drilling, and suggesting mobilization of gel by the drilling LP = 10 mm, (Lower) Fracture surface at depth of 65 mm in Echo – 2 Core under the stereomicroscope, exposing a reaction-rim crack, coated with white ASR gel in a dark coarse-aggregate limestone (orange arrow) and yellowish tan siltstone of the fine aggregate (green arrow). Dark area in lower right is shadow of core, LP = 20 mm.

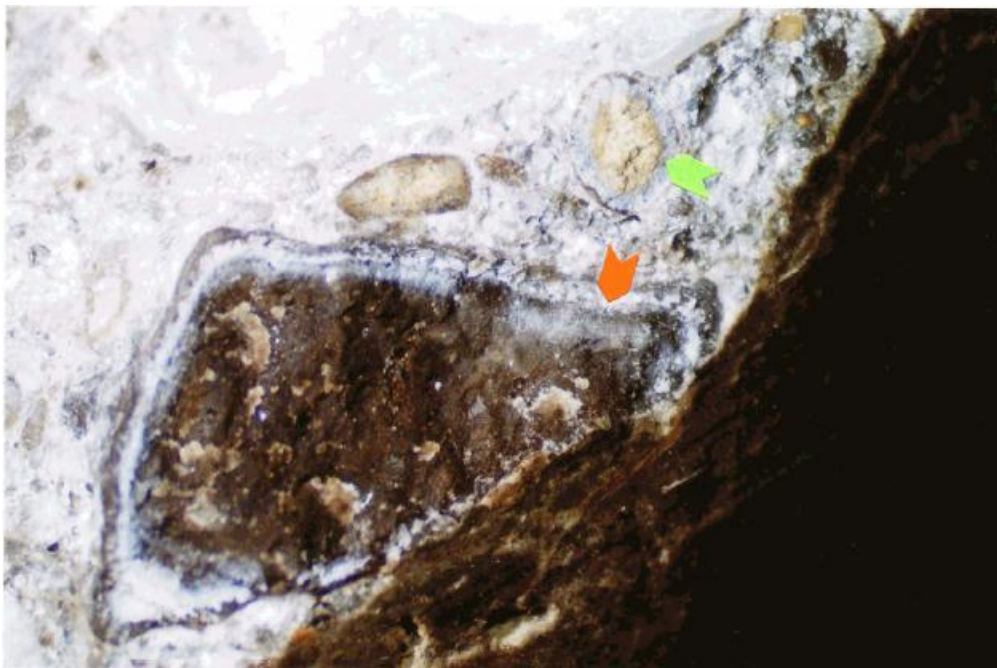


Figure 4: (Upper) Vertically oriented thin section of "box" crack in limestone aggregate in Echo – 2 Core in transmitted plane-polarized light and simultaneous reflected UV light at a magnification of 40X and depth of approximately 195 mm. One of many intricate crack patterns abundant in these limestone aggregates. LP = 2.6 mm, (Lower) Dark limestone in thin section at 200X, showing peripheral microcrack partially lined with ASR gel (orange mows). Crack enters paste and terminates nearby. LP = 0.5mm.

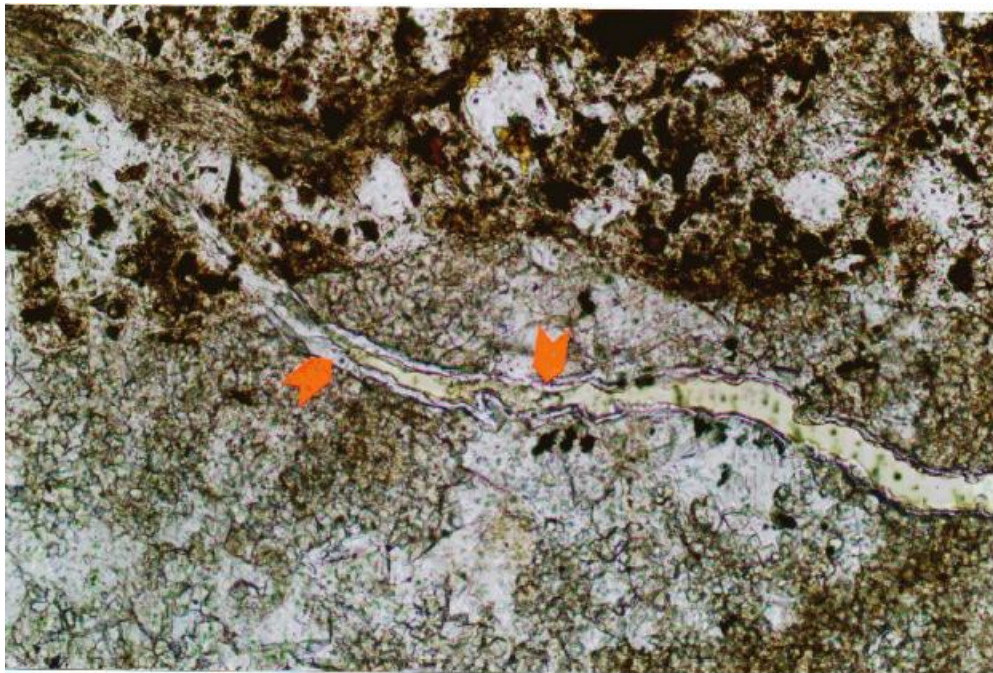
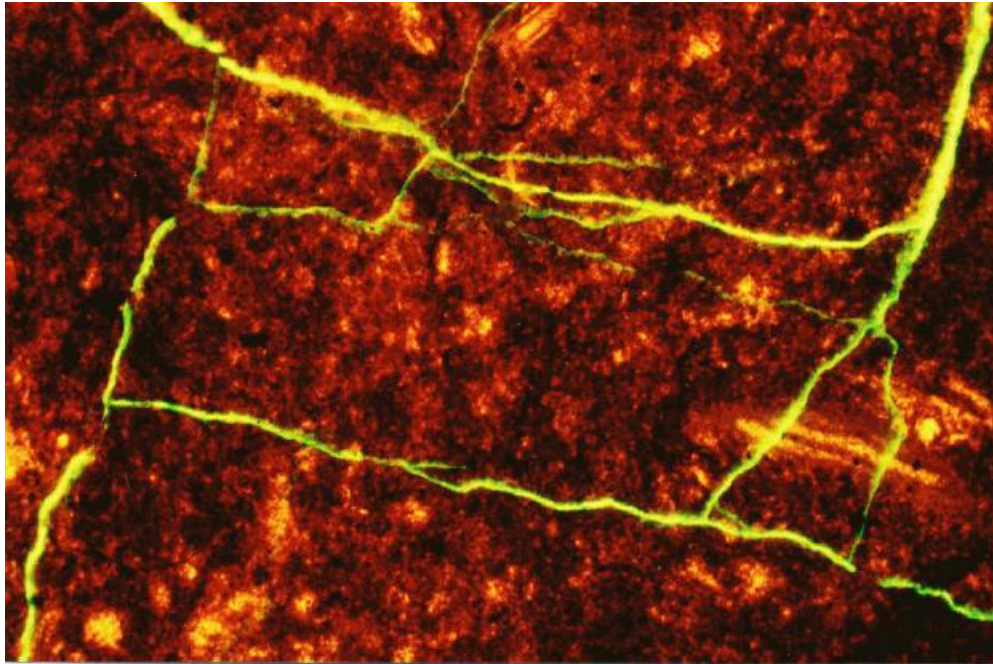


Figure 5: (Upper) Thin section of Echo – 2 Core at 40X, illustrating a fine-aggregate chert particle with microcracking and adjacent ASR gel in voids (arrows). LP = 26 mm (Lower) Typical ASR microcracking in a chert-cemented siltstone in the fine aggregate at 40X. Transmitted polarized light and simultaneous reflected UV light LP = 2.6 mm.

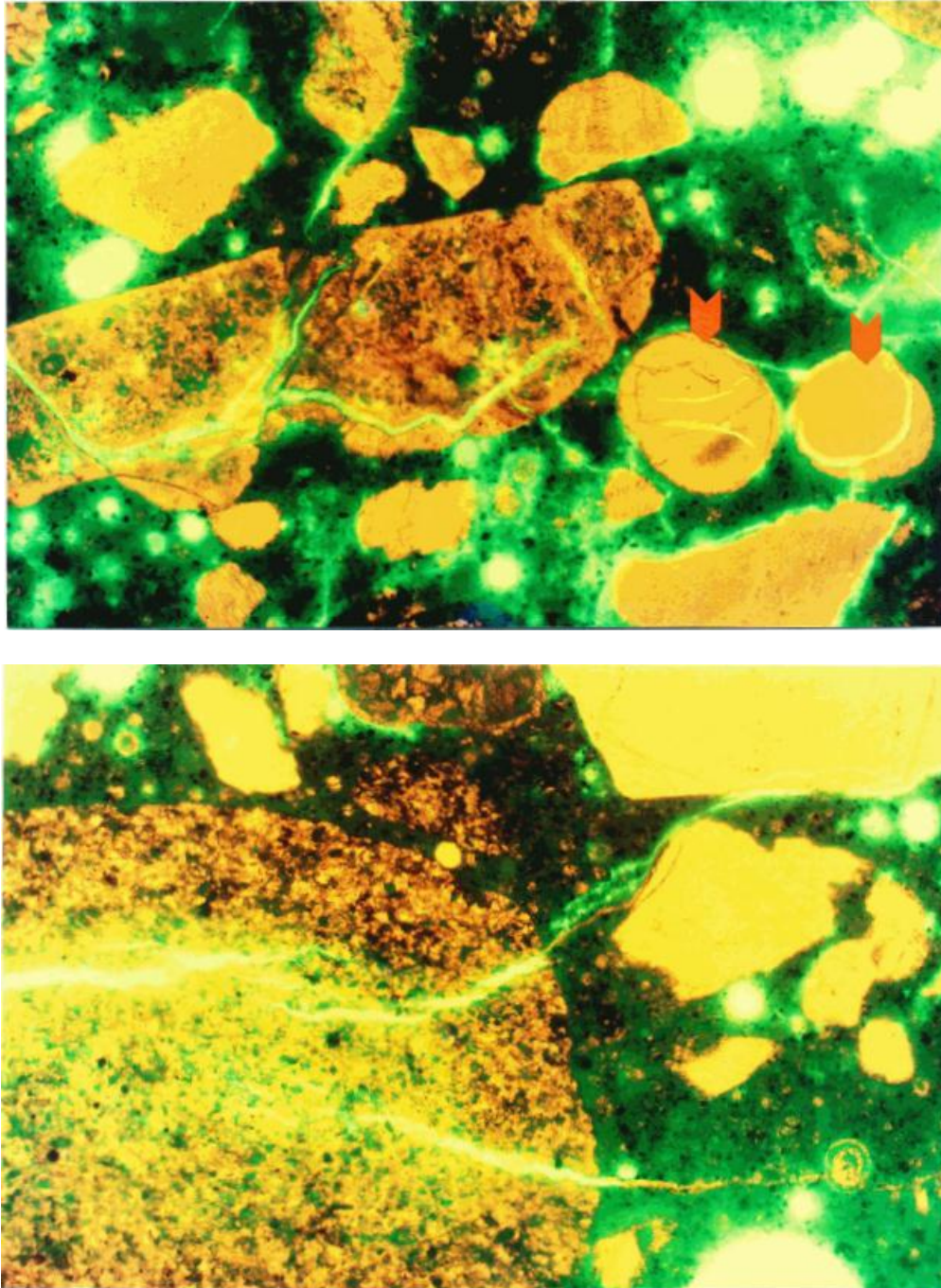


Figure 6: (Upper) Thin section of Echo – 2 Core at 200X in transmitted plane-polarized light. Arrows point to a cluster of radiating crystals of calcium hydroxide (epezite) formed from free lime (not shown in the photo), an unusual occurrence in concrete. No associated damage was found. Round air voids contain fillings and linings of ettringite. LP = 0.5 mm. (Lower) Lapped section of Echo – 6 Core under the stereomicroscope. Limestone at top of photo. Central area shows well-rounded siltstone particles with horizontal microcracks, reaction rims or weathering rims (or combination), and white ASR gel in void (arrow). Depth in core = 140 mm. LP = 13 mm.

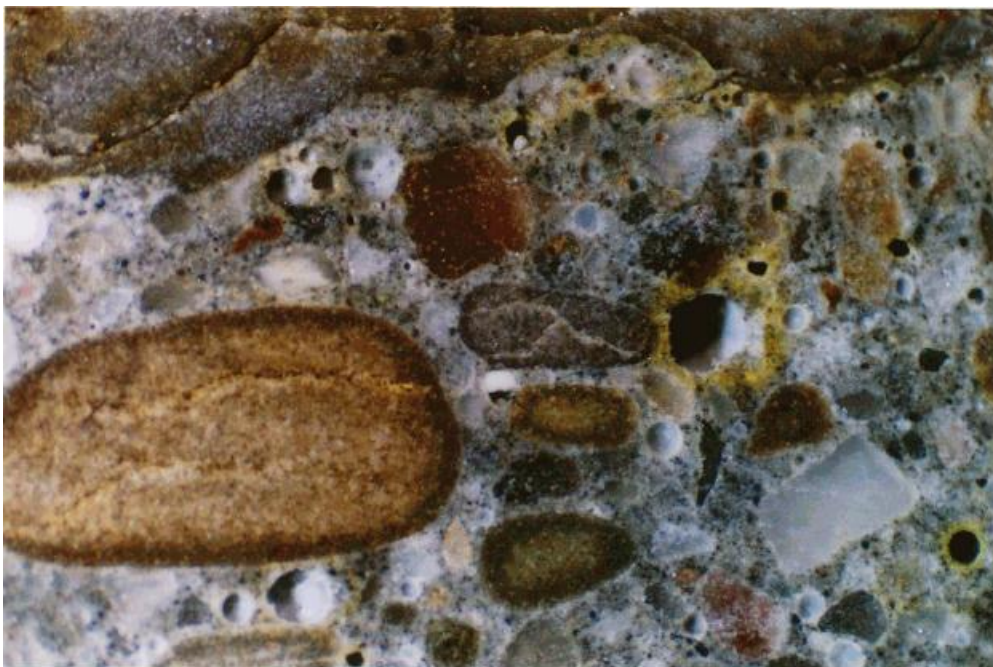
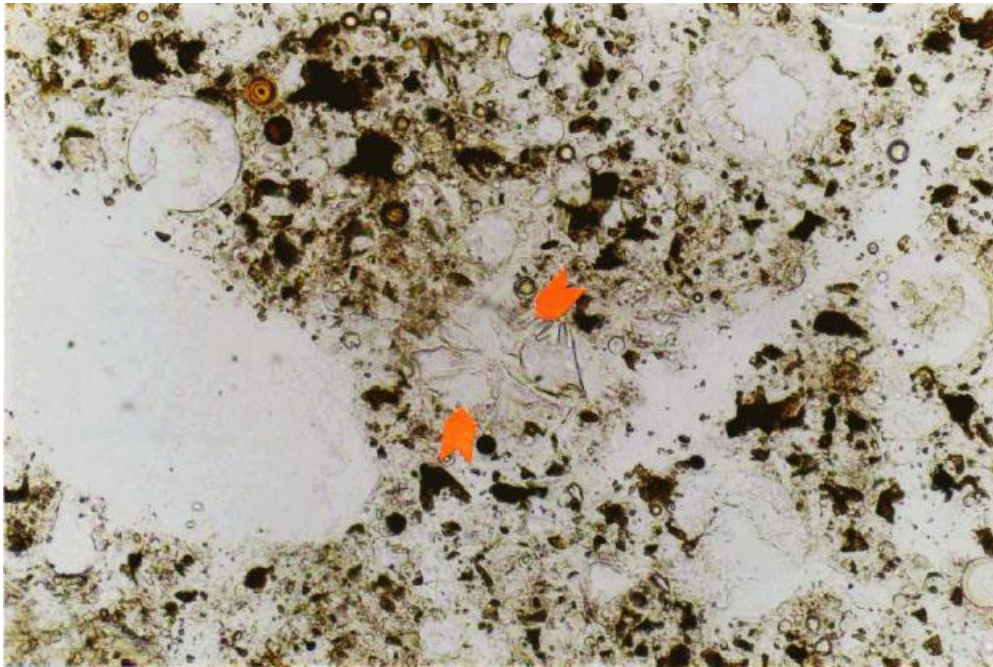


Figure 7: (Upper) Vertically oriented thin section of ASR-microcracked siltstone, abundant in the coarse fraction of the fine aggregate in Echo – 6 Core. Depth is approximately 150 mm. Adjacent voids contain ASR gel. Simultaneous reflected UV light and transmitted plane-polarized light at 40X. LP = 2.6 mm. (Lower) Thin-section view of limestone in Echo – 6 Core at a depth of 140 mm, showing a crack containing a partial lining of ASR gel (arrow) at and across the aggregate-paste interface, one of several similar observations. LP = 0.5 mm.

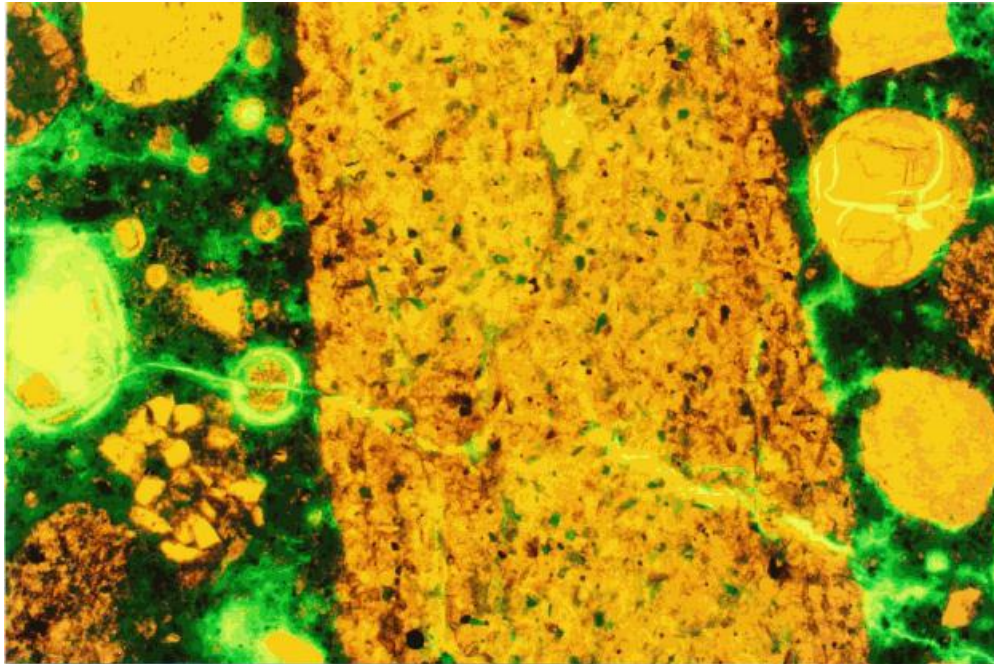
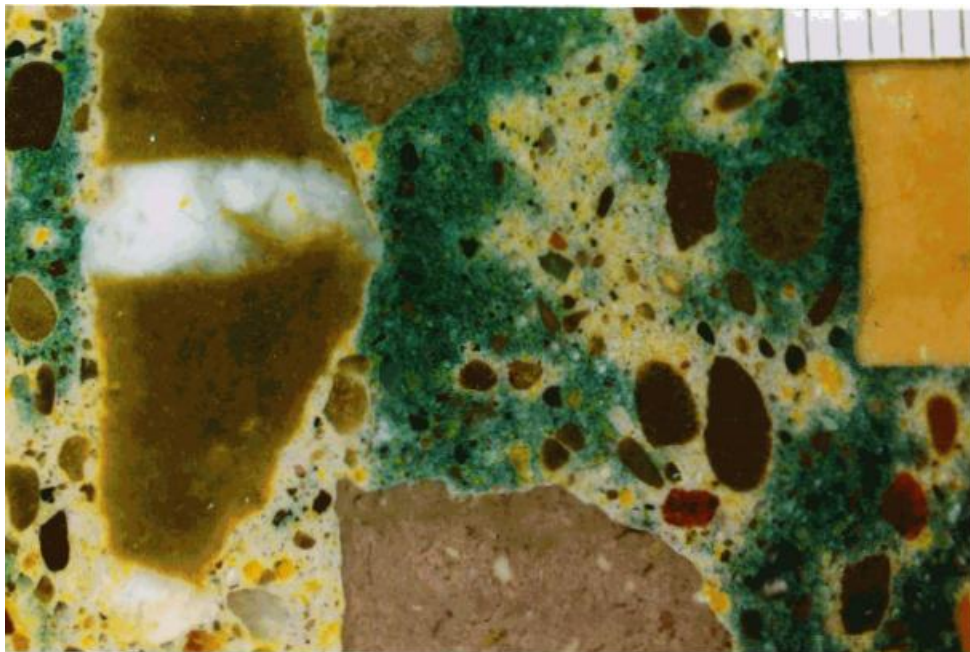
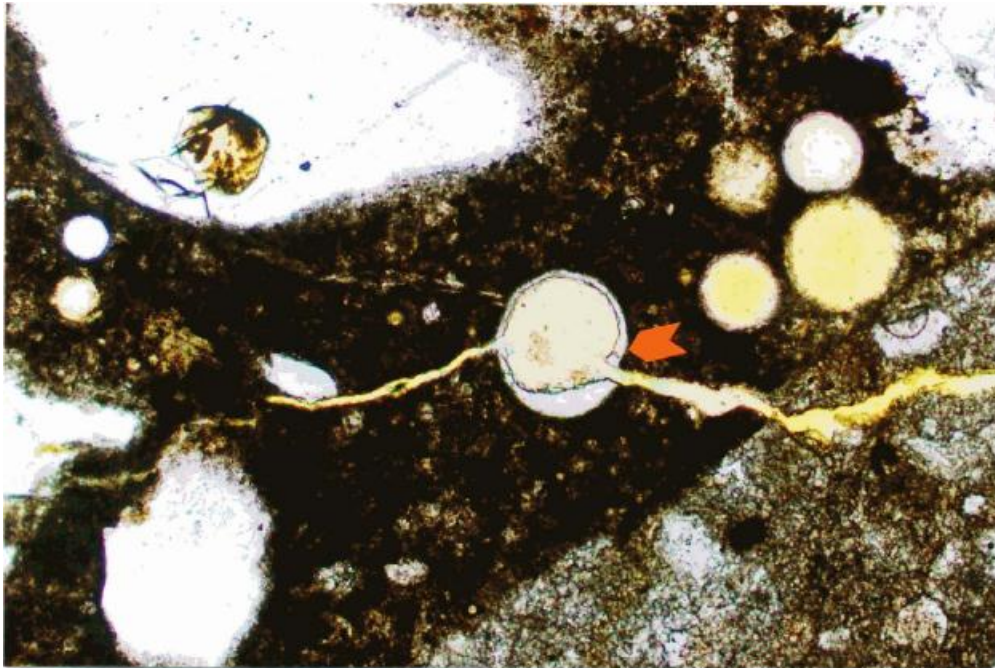


Figure 8: (Upper) Relatively thick thin section of Echo – 6 Core at 100X, showing microcrack passing out of a limestone and offsetting ASR gel (arrow) in a partially filled void, indicating the gel deposit is older than the crack. LP = 1.0 mm. (Lower) Lapped section of Victor – 2 Core at a depth of 90mm below the core top under the stereomicroscope, showing typical, irregular, green coloration of the paste, indicating use of glassy blast-furnace slag (confirmed in thin section). Millimeter scale divisions.



Airport II

Identification and Dimensions:

- Core #1: Length = 455mm; Diameter = 117mm; Intact.
Core #5: Length = 460mm; Diameter = 117mm; Intact.
Core #7: Length = 455mm; Diameter = 117mm; Intact.

Core or Fragment Surfaces:

- Core #1: Deep traction-grooved top surface with numerous fine aggregates and a few coarse aggregates exposed. Side of core is smoothly drilled. Base of core is a saw-cut surface.
- Core #5: Deep traction-grooved top surface with numerous fine aggregates and a few coarse aggregates exposed. Side of core is smoothly drilled. Base of core is a saw-cut surface.
- Core #7: Relatively shallow traction-grooves on the top surface with numerous fine and coarse aggregates exposed, as well as a mark of the original top. Side of core is smoothly drilled. Base of core is a saw-cut surface.

Large Voids, Joints, and Macrocracks (easily seen with unaided eye):

- Core #1: A few relatively large, irregularly shaped entrapped air voids occur throughout the core. A vertical macrocrack, passing through aggregates, is visible on the top surface and extends approximately 2/3rds the core diameter; depth of crack is 45 mm, terminating in entrapped air void with a diameter of 9 - 10 mm. No joints.
- Core #5: Entrapped air voids as described above. A vertical macrocrack is visible on the top surface and extends across the core diameter, passing beside a red granite coarse-aggregate particle, initialed DC on the core side, and through several aggregate particles, terminating at a depth of approximately 105 mm. No joints.
- Core #7: Entrapped air voids as described above. A narrow vertical crack is visible on the top surface and extends across approximately the core diameter; depth is approximately 83 mm, with an offset at 60 mm. No joints.

Reinforcement and Corrosion

- Core #1: None Observed.
Core #5: None Observed.
Core #7: None Observed.

Aggregates

Coarse (C):

- Core #1: Crushed gray and red granite with various crystal sizes and variations in mineralogy, plus basalt and gabbro, also of various crystal sizes.
- Core #5: As described above.

Core #7: As described above.

Fine (F):

Core #1: Sand, containing ordinary quartz & feldspar, limestone, dolostone, chert, granite, gabbro, gneiss, a wide variety of other igneous, metamorphic, and sedimentary rocks.

Core #5: As described above.

Core #7: As described above.

Gradation and Top Size:

Core #1: Evenly graded to a top size of approximately 33 mm (1 - 29 inches).

Core #5: As described above.

Core #7: As described above.

Shape and Distribution:

Core #1: Angular, equidimensional to slightly elongated CA, uniformly distributed. FA is well rounded to angular, equidimensional to slightly elongated, uniformly distributed.

Core #5: As described above.

Core #7: As described above.

Paste-Aggregate Bond:

Evaluated according to number of cross-fractured hard aggregates.

Core #1: Tight, indicated by numerous cross-fractured quartz grains.

Core #5: As described above.

Core #7: As described above.

Paste

Air Content:

Estimated on finely lapped saw-cut section and in thin section.

Core #1: 4 to 6%, air entrained.

Core #5: As described above.

Core #7: As described above.

Depth of Carbonation:**

Detected with use of variable pH indicator spray and in thin section.

Core #1: Less than 1.0mm.

Core #5: 1.0 to 2.0mm.

Core #7: 1.0 to 2.0mm, variable.

Color:

Observed on fresh fracture surface under the stereomicroscope with intense light.

Core #1: Light tan.

Core #5: Light tan.

Core #7: Light tan.

Hardness:

Resistance to scratching with a curved, sharpened, steel dental pick under the stereomicroscope.

Core #1: Hard.

Core #5: Hard.

Core #7: Hard.

Luster:

Reflectivity of fresh fracture surface under the stereomicroscope with intense light.

Core #1: Vitreous.

Core #5: Vitreous.

Core #7: Vitreous.

Calcium Hydroxide (CH):

Observed in thin section.

Core #1: 1 to 2%, occurring as small crystals within the body of the paste and, to a minor extent, as relatively coarse crystals on aggregate surfaces.

Core #5: As described above.

Core #7: As described above, except very few accumulations on aggregate surfaces.

Unhydrated Portland Cement Clinker Particles (UPCs)*:

Observed in thin section.

Core #1: 4 to 7%, the particles being comprised of impure C_3S (alite), C_2S (belite), and a matrix of mostly calcium alumina-ferrite, individual phases in particles or combined, well scattered in the paste.

Core #5: As described above.

Core #7: As described above.

Fly Ash (fa)*:

Observed in thin section.

Core #1: 15 to 20%, Class C (on the basis of carbon scarcity).

Core #5: As described above.

Core #7: As described above.

Secondary Deposits:

Observed in stereomicroscope and thin section.

Core #1: White, hardened ASR gel observed in voids located at depths of 30, 90, and 330 mm. Hardened clear gel deposits in voids also observed elsewhere in the core, but total volume of gel occurrence is very low. In thin section ASR gel observed adjacent to a coarse-aggregate microgranite gneiss particle, with microcracks in the latter leading to the gel pocket and beyond. A very soft mushy light-blue deposit (immature ASR gel?) fills a 5-mm-diameter void at a depth of 48 mm; drying a sample of this deposit resulted in a hard, clear, microcrystalline substance, having indices of refraction = 1.54, and within 20 mm of a relatively large void (8 mm) with a lining of clear hardened ASR gel.

ACR is suggested by intensely carbonated paste surrounding several dolostone particles in the fine aggregate; air voids in the zone of carbonation contain secondary

crystals of calcite, locally apparently closing the void. No associated microcracking was detected in these particles. Thin layers of ettringite occur in most voids throughout the core.

Core #5: ASR gel observed in a small void at a depth of 85 mm; and adjacent to a red granite at 295 mm; snow-white microcrystalline gel next to pink granite at 260 mm. Two adjacent void-filling deposits of microcrystalline ASR gel, with $n = 1.48$, were observed 25 mm from the saw-cut base of the core; crystal sizes approximately 2.0 microns; one filling is now white, the other is light tan. A very soft mushy light-blue deposit (immature ASR gel?) as previously described in Core #1 fills a 5-mm diameter void at a depth of 390 mm. Ettringite linings occur in virtually all air voids; crystal sizes approximately 4 to 6 microns in microcrystalline mosaics to dendritic crystals up to 30 microns long; partially isotropic; indices of refraction less than 1.548. Evidence for ACR (carbonated paste around dolostone particles) occurs around almost all the dolostone particles in the thin section.

Core #7: Exposed along the vertical macrocrack mentioned above in "Large Voids, Joints, and Macrocracks" is a very soft mushy light-blue to gray deposit (immature ASR gel?), filling a 15-mm diameter void at a depth of 60 mm; associated with ASR gel, the latter as a clear lining on the void surface. Three irregular voids at the 70-90 mm level on this same macrocrack surface are partially filled with a white microcrystalline powder interior to clear, hardened, ASR gel lining the voids. Voids containing white crystallized ASR gel are relatively common throughout the entire length of the core (as received). Evidence for ACR (carbonated paste around dolostone particles) occurs around almost all the dolostone particles in the thin section. Ettringite occurs on the surfaces of almost all voids as 20 to 30 micron-thick coatings throughout the core.

Microcracking:

Observed in fluorescent-epoxy impregnated thin section and finely lapped specimen.

Core #1: A count of 47 coarse aggregates in a lapped fluorescent-epoxy impregnated section revealed only 2 particles from within which microcracks progressed into the adjacent paste; virtually no similar microcracking was observed in particles of the fine aggregate. Abutting aggregate-to-aggregate microcracks (typical of ordinary shrinkage) are conspicuously scarce. Study of the thin section reveals a microgranite gneiss with microcracks and associated ASR gel (see under "Secondary Deposits").

Core #5: Examination of 54 coarse aggregate in a vertically oriented section (as above) reveal no aggregates with microcracks extending outward from within the particle into the adjacent paste. Abutting aggregate-to-aggregate microcracks (typical of ordinary shrinkage) are scarce.

Core #7: After examination and counting 55 coarse aggregates exposed on a lapped vertical section (as above), no microcracks extending outward from within the particle into the adjacent paste could be found. The only particles showing these types of cracks

are coarse grains of the fine aggregate. Aggregate-to-aggregate microcracks are scarce.

Estimated Water-to-(Cement + Fly Ash) Ratio:

Victor – 2: 0.40 to 0.45.

Tango – 3: As above.

Tango – 6: As above.

Echo – 2: As above.

Echo – 6: As above.

Miscellaneous:

Core #1: Lapped section extends from the top surface to a depth of 150 mm; thin section from 85 to 105 mm in a vertical plane.

Core #5: Lapped section extends from the top surface to a depth of 150 mm; thin section is transversely oriented at a depth of 150 mm,

Core #7: Lapped section extends from the top surface to a depth of 150 mm; thin section is transversely oriented at a depth of 305 mm.

Figure 1: (Upper) Thin section of Core #1 at 100X, showing ASR gel in void connected to “microgranite” coarse aggregate (right). Gel in the interior of the void is light tan and finely microcrystalline, but in the void lining it is clear and amorphous. Dark bubbles in epoxy. Depth in core is 100 mm. LP = 10 mm. (Lower) ACR carbonation of paste adjacent to reacting dolostone (left). Some of the resulting calcite occurs as void fillings (arrows). Partially cross-polarized light. 200X. LP = 0.5 mm.

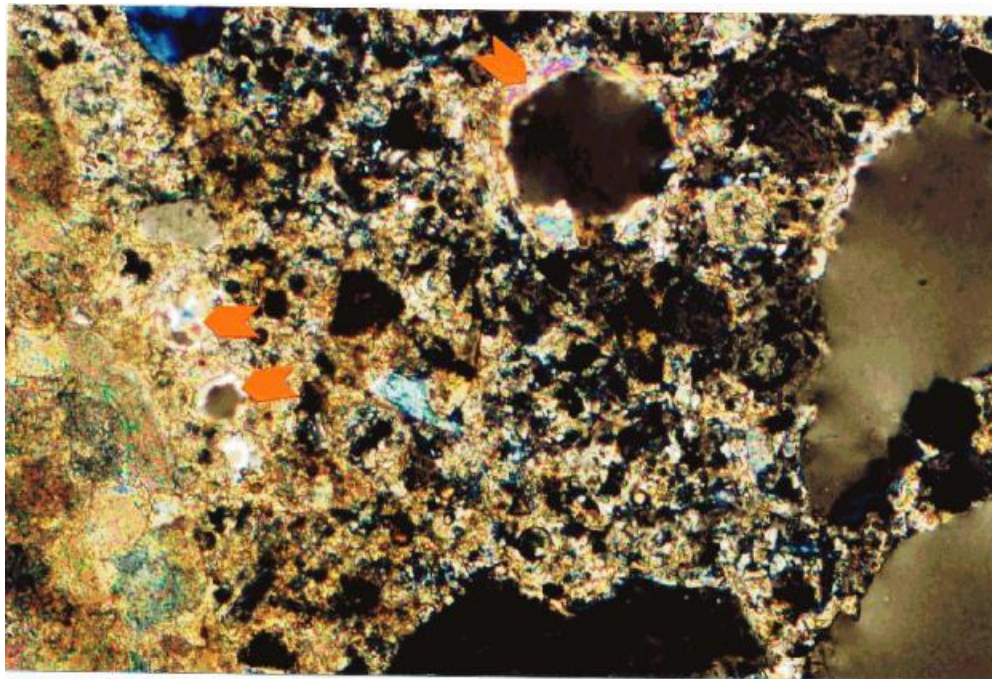
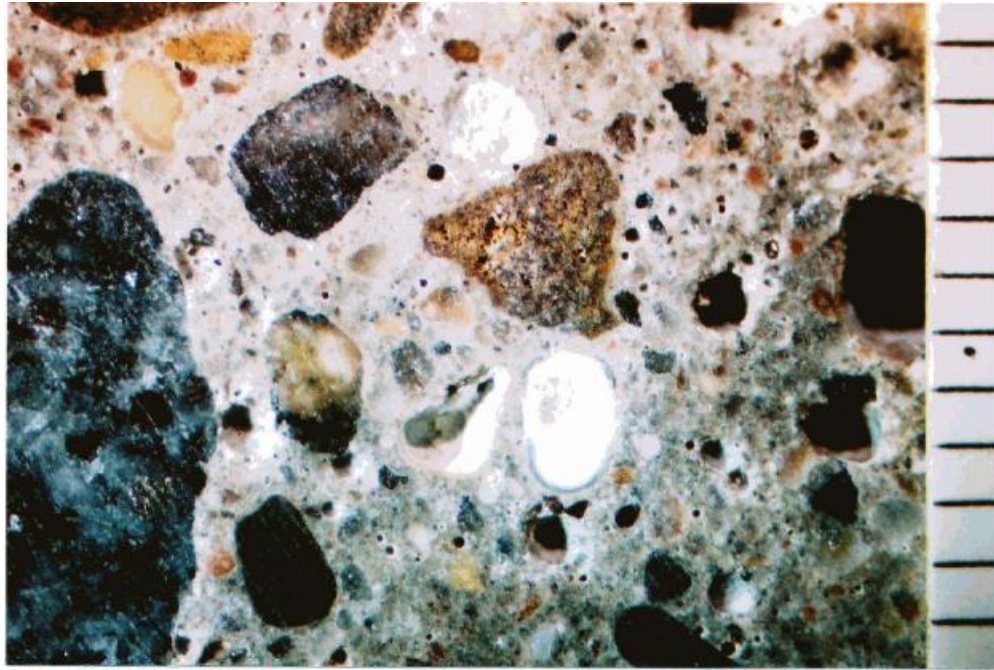


Figure 2: Lapped surface of Core # 1 under the stereomicroscope, showing three voids containing ASR gel around a microcracked fine-aggregate particle of brown siltstone. Millimeter scale divisions.



Airport III

Identification and Dimensions:

- Core 100: Length = 420mm; Diameter = 98mm; In two segments, separated at the 220mm level along a fresh fracture surface presumably produced during shipment.
- Core 106: Length = 425mm; Diameter = 98mm; In two segments, separated at the 240mm level along a fresh fracture surface presumably produced during shipment.
- Core 110: Length = 430mm; Diameter = 98mm; In two segments, separated at the 240mm level along a fresh fracture surface presumably produced during shipment.
- Core 114: Length = 428mm; Diameter = 98mm; In two segments, separated at the 240mm level along a fresh fracture surface presumably produced during shipment.

Core or Fragment Surfaces:

- Core 100: Top surface is roughened from exposed fine aggregate; faint remnants of a coarsely broomed finish. Side of core is smoothly drilled. Base of core retains 10 millimeters of an asphaltic subbase.
- Core 106: Top surface has saw-cut traction grooves approximately 2 to 3 mm deep and roughened from exposed fine aggregate; faint remnants of a coarsely broomed finish. Side of core is smoothly drilled. Base of core has up to 66 millimeters of an asphaltic subbase.
- Core 110: Top surface has saw-cut traction grooves as described above. No remains of broomed surface (if previously present). Top also exhibits a polygonal pattern of macrocracks. Side of core is smoothly drilled. Lower end of core has 30 mm of asphalt.
- Core 114: Top surface is weathered traction-grooved surface, as above, with a triple point junction from polygonal macrocracks. No remains of broomed finish, if originally present. Side is smoothly drilled. Lower end retains approximately 20 mm of asphalt.

Large Voids, Joints, and Macrocracks (easily seen with unaided eye):

- Core 100: A macrocrack, less than 0.25 mm wide partially extends over the top surface, extending downward as a microcrack at least 75 mm; macrocrack at its highest point is approximately 16 microns wide; the microcrack width near the base of the crack is roughly 1 to 2 microns.
- Core 106: Significant, large, mostly vertical, irregular elongated entrapped air voids observed at the 20, 60, 90, 130, and 160mm levels. No joints observed. A macrocrack, passing through dark coarse aggregate in the upper 20 mm of concrete, extends across part of the core top, and extends downward to the highest level of above-mentioned air

voids. Large air voids in lower half of core are generally spherical, with diameters of less than 3 mm.

Core 110: A few large, irregular, entrapped air voids are present, mainly in the upper half of the core. A void approximately 20 mm from core tap is linked to a macrocrack, the latter forming part of a polygonal system, the depth of cracking extending to approximately 50 mm. No joints observed.

Core 114: Significant, large, mostly vertical, irregular elongated entrapped air voids observed at the 60, 90, and 100mm levels; consolidation poor. No joints observed. Macrocrack seen on top surface extends to depth of approximately 50 mm, passing through aggregates and connecting to irregular large entrapped air voids.

Reinforcement and Corrosion:

Core 100: None Observed.

Core 106: None Observed.

Core 110: None Observed.

Core 114: None Observed.

Aggregates

Coarse (C):

Core 100: Partially crushed gravel, containing mainly varieties of tan sandy dolomite, cream-colored to white limestone, gray to tan sandstone (some with calcite, dolomite, and chert cements, zones of shearing, and chert grains), siltstone, minor amounts of mottled white and gray chalcedonic and microcrystalline chert, metaquartzite, dark basalt, and other rocks. Chert cements, common in the sandstones, are both microquartz and chalcedonic quartz, even in the same particle. Sandstones have wide ranges of intergranular porosity, sometimes in the same particle.

Core 106: As stated above.

Core 110: As stated above.

Core 114: As stated above.

Fine (F):

Core 100: Ordinary quartz, metaquartzite, chert, sandstone fragments as described above, and minor amounts of feldspar (mostly plagioclase), limestone, pumice, basalt, volcanic rock fragments, and others.

Core 106: As stated above.

Core 110: As stated above.

Core 114: As stated above.

Gradation and Top Size:

Core 100: Evenly graded to a top size of approximately 23mm (0.90 inch).

Core 106: As stated above.

Core 110: As stated above.

Core 114: As stated above.

Shape and Distribution:

Core 100: CA is well rounded to angular, equidimensional to slightly elongated, and uniformly distributed. FA is generally angular to subrounded, equidimensional to elongated, and uniformly distributed.

Core 106: As stated above.

Core 110: As stated above.

Core 114: As stated above.

Paste-Aggregate Bond:

Evaluated according to number of cross-fractured hard aggregates.

Core 100: Tight. Numerous quartz grains of the fine aggregate are cross-fractured.

Core 106: As stated above.

Core 110: Tight.

Core 114: Tight.

Paste**Air Content:**

Estimated on finely lapped saw-cut section and in thin section.

Core 100: 5 to 7%, air entrained; bubble clusters common.

Core 106: As stated above.

Core 110: As stated above.

Core 114: As stated above.

Depth of Carbonation:**

Detected with use of variable pH indicator spray and in thin section.

Core 100: 2 to 4mm, variable.

Core 106: 0.5mm, variable.

Core 110: 2 to 4mm, variable.

Core 114: 2 to 4mm, irregular and variable.

Color:

Observed on fresh fracture surface under the stereomicroscope with intense light.

Core 100: Medium gray.

Core 106: Medium gray.

Core 110: Medium gray.

Core 114: Light to medium gray.

Hardness:

Resistance to scratching with a curved, sharpened, steel dental pick under the stereomicroscope.

Core 100: Hard.

Core 106: Hard.

Core 110: Hard.

Core 114: Moderately hard.

Luster:

Reflectivity of fresh fracture surface under the stereomicroscope with intense light.

Core 100: Vitreous.
Core 106: Vitreous.
Core 110: Vitreous.
Core 114: Vitreous.

Calcium Hydroxide (CH):

Observed in thin section.

Core 100: 2 to 4%, occurring as irregular poikilitic crystals within the paste and, to a minor extent as relatively coarse crystals on aggregate surfaces

Core 106: As described above.

Core 110: 1 to 3%, as described above.

Core 114: 1 to 3%, as described above, but practically none as coarse crystals attached to aggregates.

Unhydrated Portland Cement Clinker Particles (UPCs)*:

Observed in thin section.

Core 100: 5 to 7%, gray Portland cement clinker. Clinker constituents are impure C₃S (alite), C₂S (belite), and a matrix of mostly calcium alumino-ferrite, individually in particles or combined, well scattered in the paste.

Core 106: As described above.

Core 110: 4 to 6%, gray Portland cement clinker as described above.

Core 114: 4 to 6%, gray Portland cement clinker as described above.

Fly Ash (fa)*:

Observed in thin section.

Core 100: Approximately 10 to 15%, Class C (on the basis of low carbon percentage).

Core 106: Estimate at 13 to 17%.

Core 110: Approximately 8 to 12%.

Core 114: Approximately 13 to 17%.

Secondary Deposits:

Core 100: Void surfaces generally free of secondary deposits, except for a few thin linings of ettringite. On the fracture surface of a chert coarse aggregate particle at a depth of approximately 90 mm from the base of the core, is a unidentified, birefringent, microcrystalline phase, with an index of refraction slightly less than 1.54, roughly equidimensional crystal sizes in the range of 2 to 4 microns; no reaction rim could be seen.

Core 106: ASR gel identified in lining of small void at depth of 70 mm (photo) and marked on fracture surface, within approximately 3 mm from a mottled gray, quartz-cemented, fine-gained sandstone. ASR gel mixed with other phases occurs in frothy voids located 40 mm from the base of the concrete.

- Core 110: Ettringite lines almost all voids from near-top surface to a depth of approximately 50 mm; at a depth of roughly 110 mm virtually none of the voids contain ettringite but it is common at a depth of approximately 310 mm. No ASR gel observed.
- Core 114: Ettringite occurs commonly in the air voids as linings. White deposits in one of the large entrapped air voids mentioned above contain (1) clear to cloudy, banded, isotropic ASR gel (2) an unidentified, birefringent, microcrystalline phase, the latter with an index of refraction slightly less than 1.54, roughly equidimensional crystal sizes in the range of 2 to 4 microns, (3) a scattering of relatively coarse irregular crystals of calcite and (4) other unidentified phases. In a second void, similar deposits were observed (minus ASR gel); with microcrystalline calcite dominating.

Microcracking:

Observed in thin section and finely lapped specimen.

- Core 100: Microcracks, apparently open, with widths on the order of 1 to 3 microns, are common in the paste throughout: the two lapped, fluorescent epoxy-impregnated, vertical sections, the latter extending to the 150mm level. Similar microcracks were observed on the transverse section. The microcracks frequently abut aggregate particle surfaces apparently perpendicularly; none were seen to originate in the body of the aggregate particle and progress into the adjacent paste. A vertical microcrack, as seen in the thin section, shows many associated subparallel microcrack (all trending in approximately the same direction); the cracks are open, approximately 4 microns wide at its terminal point and up to 80 microns wide at the upper end (some edge damage, however, was observed), passing through hard aggregates. Counting 60 coarse aggregates in the longitudinal section impregnated with fluorescent epoxy resulted in 9 observed microcracks occurring in 6 aggregate particles, the cracks passing from within the aggregate into the adjacent paste, terminating therein.
- Core 106: Counting 67 coarse aggregates exposed on a lapped fluorescent-epoxy-impregnated surface revealed nine (9) microcracks, in 6 particles, apparently originating mostly within chert-cemented sandstone (thin section for better photo) and passing into the adjacent paste; crack widths are approximately two (2) microns wide within the rock. The reaction rims, possibly combined with weathering rims, do not contain the fluorescent epoxy.
- Core 110: 53 coarse aggregates were counted, as described above, and only 5 microcracks transgressing the paste/aggregate bond line, in 4 particles, were detected; most of these were from reactions within sandstone.
- Core 114: 65 coarse aggregates were examined and counted in the fluorescent-epoxy impregnated section, resulting in 5 microcracks, in 5 particles, as described above for Core 110.

Estimated Water-to-(Cement + Fly Ash) Ratio:

Core 100: 0.37 to 0.42.

Core 106: As stated above.

Core 110: As stated above.

Core 114: As stated above.

Miscellaneous:

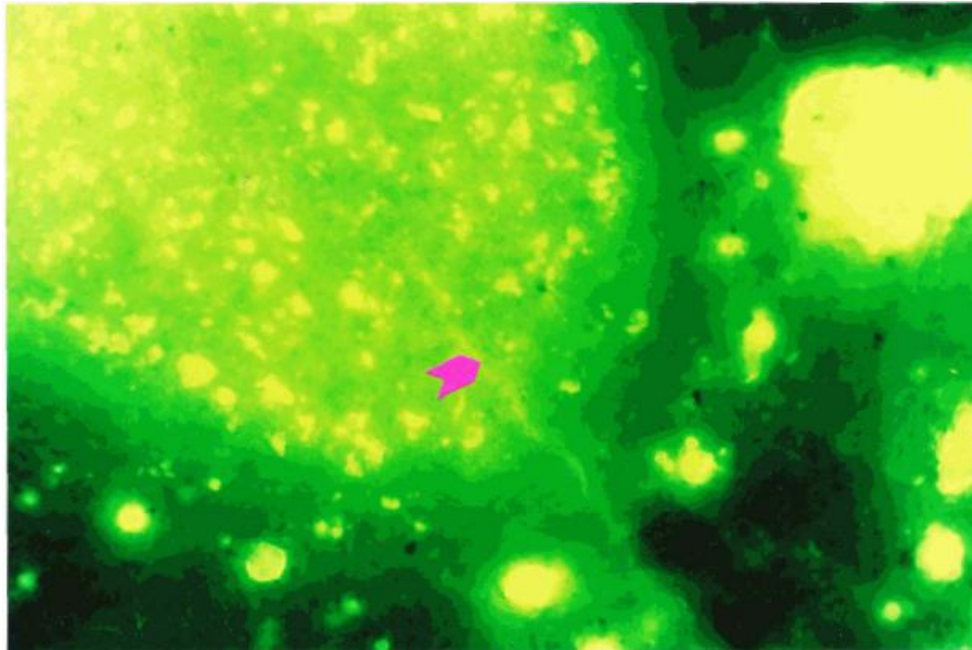
Core 100: Lapped section (longitudinal) extends from the top surface to a depth of approximately 150mm; transverse lapped section at a level of 152 mm. Thin section from the top surface to a level of approximately 45 mm.

Core 106: Lapped section (longitudinal) extends from the top surface to a depth of approximately 180mm; Thin section from the top surface to a level of approximately 45 mm.

Core 110: Lapped section (longitudinal) extends from the top surface to a depth of approximately 178mm. Thin section is horizontally oriented at a level of approximately 175mm.

Core 114: Lapped longitudinal section from top surface to a depth of 165mm. Thin section is transverse section (horizontal) at a level of 165 mm.

Figure 1: Lapped section of Core 106 at 40X magnification under reflected UV light, showing an open microcrack (magenta arrow), beginning within a porous sandstone coarse aggregate, passing into the adjacent paste where the crack terminated. Crack width approximately 4 to 10 microns, depth in core is 55mm below top surface. Incipient ASR. Length of photo (LP), left to right = 2.6 mm.



Notes for Airport I – III Petrographic Reports

*Percentage by volume of paste.

**Carbonation intensity definitions: Light – [1] Scanty, pinpoint distribution in calcium silicate hydrate (CSH), calcium hydroxide (CH) abundant. [2] Pinpoint carbonation in CSH abundant, slight crystal enlargement, but less than 3 microns, CH still abundant. Medium – [3] Almost all CSH carbonated; some CH carbonated. Extensive small-scale enlargement of paste carbonate crystals in 3 to 10 micron range, minor calcite crystallization in voids. Heavy – [4] CSH totally carbonated, traces of CH remain. Major calcite crystal enlargement to 10 microns or more, extensive development; some crystallization of calcite in voids. [5] CSH totally carbonated; traces of CH, if any. Pervasive crystal enlargement, many greater than 10 microns, abundant euhedral crystals in voids, calcite spherules possible.

Introduction for Airports IV – VIII

Dr. Prasad R. Rangaraju, Ph.D., P.E. of Clemson University, Department of Civil Engineering has contracted Schmitt Technical Services, LLC (STS) to perform petrographic examinations of core samples from the airfield pavements. The cores are from one of several airfield pavements selected to be included in Innovative Pavement Research Foundation (IPRF) Project No. 01-G-002-05-7, entitled “Performance of Concrete in the Presence of Airfield Pavement Deicers and Identification of Induced Distress Mechanisms.” Petrographic examinations were performed as part of Tasks 5, 7 and 9 of the project regarding forensic investigations of cores taken from the pavements.

Examination Procedures for Airports IV – VIII

The concrete cores were examined using selected techniques and procedures outlined in ASTM C 856, “Standard Practice for Petrographic Examination of Hardened Concrete” and the Federal Highway Administration’s Publication No. FHWA-HRT-04-150, “Petrographic Methods of Examining Hardened Concrete: A Petrographic Manual.”

Each examination included sawing each core longitudinally, followed by lapping one half the core slice with successively finer lapping grits to produce a finely ground (and nearly polished) surface. The lapped surface of the core and freshly broken surfaces of concrete were examined visually (with the unaided eye) and under a stereomicroscope at magnifications of 7 to 40X.

In addition, a thin section was made from each core, as were temporary, crushed fragment (i.e., “immersion or powder”) mounts of paste and aggregate. The thin section and immersion mounts were examined under plane and cross-polarized light at magnifications of 50 to 400X using a polarizing light microscope.

Estimates of water-to-cement ratio were done using techniques outlined in FHWA-HRT-04-150 and methods developed by Dr. Donald Campbell (unpublished).

Airport IV

Core Locations

Core locations were selected by Clemson University. Specific locations and identifications based on information conveyed by you are as follows:

<u>Core No.</u>	<u>Approximate Location</u>
1	De-Ice Pad
Echo 5 – Core 4	Echo 5 Taxiway
C7C1	Charley Connector 7 Taxiway - Core 1
G1	Golf Taxiway – Core 1

The 4 cores, (Figures 1 through 4), were received at STS on November 3, 2009. Petrographic examination was requested on each of the cores to determine the cause(s) and extent of cracking,

slab movement and other observations pertinent induced distress mechanisms occurring in the cores.

Results

Subject to the qualifications in the attached Appendix, results of the petrographic examinations are as follows:

1. Wearing surface of the four (4) cores has fine surface pitting of the cement paste extending to a depth of 1 to 2 mm (Figures 5 and 18). Cement paste adjacent to the pits appears amorphous, devoid of calcium hydroxide and recently carbonated compared to unpitted areas. These observations are often associated with minor, surficial chemical attack.⁽¹⁾ Therefore, it appears that one of the compounds (i.e., chemicals, fuels, etc.), spilled or dripped onto the pavement, is causing slow chemical attack of the wearing surface.
2. Concrete represented by the four (4) cores exhibits evidence of alkali-carbonate reaction (ACR). The alkali-reactive aggregate component is the crushed, calcitic dolomite coarse aggregate. The dolomite has a fine-grained texture with a finer matrix composed of the minerals calcite and dolomite and a reddish brown clay (Figures 6 and 9 through 11). Larger rhombic shaped dolomite crystals and an occasional quartz sand grain are within the finer matrix (Figures 10 and 11). The clay occurs as fine seams or stringers and finely disseminated particle groupings. Some of the dolomite rhombs have cores containing fine argillaceous material surrounded by an outer argillaceous-free rim of dolomite that may be slowly de-dolomitizing into calcite (Figure 6, 9 and 10). The dolomites often contain reaction rims within the outer periphery of reacting particles (Figures 19, 20 and 23). Rock textures described have been reported to typify alkali-carbonate reactive rock types and textures.⁽²⁻⁵⁾
3. Further evidence of alkali-carbonate reaction is cracking and microcracking occurring within rimmed dolomite coarse aggregate particles, with cracks radiating out from the reacting particles into adjacent cement paste in all the cores except the Deicing Pad core (Figures 7, 8, 11 through 14, 19 through 21, 23 and 24). The cracks and nearby voids are lined to filled with secondary deposits known to be expansive alkali-carbonate reaction products (Figures 7, 8, 11 through 16 and 19 through 26).⁽²⁻⁵⁾ These secondary deposits include brucite ($Mg(OH)_2$), (tentatively) various magnesium carbonate hydrate minerals, calcium acetate, calcium carbonate and an amorphous, desiccated, alkali gel (Figures 25 and 26). The white, calcium acetate (although not expansive), is characterized by turning into a flammable gel when sprayed with isopropanol. Optical properties indicate what appear to be trace amounts of magnesite ($MgCO_3$), hydromagnesite ($MgCO_3 \cdot Mg(OH)_2 \cdot 3H_2O$), lansfordite ($MgCO_3 \cdot 5H_2O$) and nesquehonite ($MgCO_3 \cdot 3H_2O$). These latter mineral occurrences require verification by x-ray diffraction and differential thermal analysis for definitive identification.
4. Some of the secondary minerals identified have been generally characterized as secondary products of alkali-carbonate reaction⁽⁴⁾; however, study of the thermodynamic and kinetic stability of phase changes of reaction products and subsequent volume

stability and their contribution to alkali-carbonate related expansion are not well understood^(4 and 6). That is to say, possibly all the reactions and secondary products of expansive alkali-carbonate reaction may not yet be fully identified, nor molar volume changes calculated and documented, particularly in the presence of acetate deicers. Further, characterization and investigation of secondary deposits in these cores (as recommended above) may yield information as to their contribution to expansion.

5. As indicated above, calcium acetate has been identified in cracks and voids of the three (3) cores that exhibit cracking. Calcium acetate is found in voids throughout the entire thickness of the pavement in each of the three (3) cores.
6. All of the concretes examined, except the De-Icer Pad Core, contain fly ash (Figures 11 and 17). Fly ash typically minimizes the potential for deleterious cracking by early reaction with the alkalis in cement to prevent substantial expansive reaction. However, it has been reported that some fly ashes, particularly those high in calcium, do not inhibit expansion by alkali-aggregate reaction, but rather, contribute soluble alkali sulfates that might increase alkali-aggregate reaction.⁽⁷⁻⁸⁾ Fly ash in the concrete pavements examined has not inhibited expansive alkali-carbonate reaction.
7. All of the cores contain what are interpreted to be cracks due to drying shrinkage at the wearing surface. The crack extends to various depths in the pavement slabs. These surficial drying shrinkage cracks allow easy ingress of moisture and deicer deeper into the pavement, thereby increasing surface area where alkali-carbonate reactions can take place. Sealing of drying shrinkage cracks (and maintaining a seal) may have lessened the effects of deleterious alkali-carbonate reactions.
8. The relative degree of alkali-carbonate reaction related cracking damage varies from none in the De-Icer Pad Core to 150 mm (5.9 in.) depth in Echo 5 Core 4 and Core C7C1 and 205 mm (8.0 in) depth in Core G1. This represents damage to the upper half of the entire pavement thickness. Echo 5 Core 4 appears to have the most visually outward signs of distress and Cores C7C1 and G1 show some cracking with the unaided eye. However, Cores C7C1 and G1 are quite progressed in internal cracking and microcracking due to alkali-carbonate reaction. The De-Icer Pad Core exhibits early signs of alkali-carbonate reaction, but no damage.
9. De-Icer Pad Core has an estimated air content of 6.5 to 8.0% and an air-void system that appears capable of protecting the concrete from freeze-thaw damage. Echo 5 Core 4 has an estimated air content of 0.5 to 2.0% to a depth of 50 mm (2.0 in.) and 3.5 to 6.0% deeper in the core, but the voids are frequently clustered together. The air-void content and air-void system in Echo 5 Core 4 are not considered capable of protecting the concrete against freeze-thaw damage. Core C7C1 has an estimated air content of 2.5 to 3.5%. The air-void content and air-void system in Core C7C1 are not considered capable of protecting the concrete against freeze-thaw damage. Core G1 has an estimated air content of 1.5 to 3.5%. The air-void content and air-void system in Core G1 are not considered capable of protecting the concrete against freeze-thaw damage. Thus, it would appear some of the pavement distress is due to cyclic freeze-thaw damage. Experience

has shown that bulk expansion by alkali-carbonate reaction, although usually less than alkali-silica reaction, can be of the same order in the presence of cyclic freezing and thawing, especially for marginal air-void systems.⁽⁹⁾ The mechanism being that cracks produced by alkali-carbonate reaction are exacerbated by critical saturation and subsequent freezing and thawing. Conversely, some older non-air-trained concretes, particularly in the Midwest, exhibit secondary alkali-aggregate reaction when containing aggregates that normally would not react without cracking first by freeze-thaw damage. Petrographic examination of these cores does not conclusively indicate which form of distress occurred first. However, based on the amount of cracking radiating from reactive aggregate particles it appears alkali-carbonate reaction is the more dominant mechanism of distress recently.

10. There is no evidence of alkali-silica reaction nor rock or mineral types in the aggregate that are considered potentially alkali-silica reactive.

Details of the petrographic examinations are provided in the following sections of this report.

Petrographic Examination

Core 1 – De-Ice Pad

General Description

The sample consists of a concrete core identified as “Core 1 De-Ice Pad” (Figure 1). The core is 214.0 mm (8.4 in.) long and has a diameter of 100.0 mm (3.9 in.).

The core top or wearing surface is a flat weathered surface (Figure 1a). There are remnants of fine ridges on the wearing surface, indicating a broom finish. There are also some lightly pitted areas at the wearing surface extending into the cement paste 1 to 2 mm (0.04 to 0.08 in.) depth (Figure 5). One side of the core top is worn smooth by the core drill bit wobbling before setting into the core hole (Figure 1a).

A 0.40 to 0.80 mm (0.015 to 0.030 in.) wide crack is present at the wearing surface (Figure 1a). The crack narrows to 0.40 mm (0.015 in.) immediately below the wearing surface. The crack is continuous, extending entirely through the core (Figure 1b). The crack narrows with depth to 0.25 mm (0.001 in.) width at the core bottom. The crack is filled with surface dirt and debris to a depth of 1 mm (0.04 in.). Below 1 mm (0.04 in.), the crack is lined to filled with fines from drilling. The crack trends parallel to the direction of embedded steel reinforcement. The crack passes around most aggregate particles, suggesting the crack formed early in the life of the concrete, before significant paste-to-aggregate bond developed. Cracking of these characteristics is typical of early shrinkage, likely as a result of drying.

An uncorroded, 12.7 mm (0.50 in.) diameter, deformed steel reinforcing bar is present at 101.6 mm (4.0 in.) depth in the core. A second similar reinforcing bar is adjacent to the first bar, but only extends 12.0 mm (0.5 in.) into the side of the core. This second bar likely represents the end of an overlapping reinforcing bar.

The core bottom is the imprint of the underlying base course.

Aggregates

Aggregate particles are uniformly dispersed throughout the concrete. Maximum aggregate size is measured as 15 mm (0.625 in.). The aggregate is fairly well-graded.

Coarse aggregate is composed of crushed calcitic dolomite. The rock has a fine-grained texture with a finer matrix composed of calcite, dolomite and reddish brown clay. Larger rhombic shaped dolomite crystals and an occasional quartz sand grain are within the finer matrix. Some of the clay occurs as fine seams or stringers. Some of the dolomite rhombs have cores containing fine argillaceous material surrounded by an outer argillaceous-free rim of dolomite that may be slowly de-dolomitizing into calcite (Figure 6).

Coarse aggregate particles are reddish pink to gray. Coarse aggregate is moderately hard; dense; angular-to-subangular; equant to slightly elongated, fossiliferous and rough textured. Many of the coarse aggregate particles contain darkened rims along their outer periphery.

Fine aggregate is natural sand containing a variety of rock and mineral types including, quartz, various types of feldspars, meta-quartzite, granite, chert, mica, dolomite fines and other rock and mineral types. The fine aggregate is predominantly composed of quartz, feldspar and meta-quartzite. Fine aggregate particles are variously colored from white to red to translucent; hard, dense, sub-rounded to well-rounded, generally spherical and having a smooth outer surface texture.

No cracking of aggregate particles is observed.

Cement Paste

The cement paste is light gray, exhibits a vitreous luster, micro-granular texture, and hackly fracture. The paste is hard, dense and tightly bonded to aggregate particles. Cement paste is carbonated to a depth of 1-to-2 mm below the wearing surface.

Residual and relict cement particles are present in a moderately abundant amount. Residual and relict cement particle content is estimated to be 12 to 15%, by volume of paste. Calcium hydroxide, a normal hydration product, is estimated to be 12-to-15% by volume of paste, as coarsely disseminated hexagonal crystals and tablets often along the fringes of aggregate particles. Supplementary cementitious materials are not detected.

Properties of the paste previously described are evaluated to provide an estimate of the water-to-cement ratio. Based on paste properties observed, water-to-cement ratio is estimated to be 0.35-to-0.45.

There are very few random microcracks present in the paste at varying depths. The microcracks pass primarily around aggregate particles and are deemed to be due to normal, early drying shrinkage of the concrete. No deterioration of the paste is observed.

Air Voids

The concrete contains numerous air-voids, ranging from mostly very fine to occasionally coarse. The voids present are generally spherical (entrained air) with a few larger, irregularly shaped voids indicative of entrapped air. The concrete is deemed air-entrained.

The air-voids are uniformly dispersed throughout the concrete. Air content is estimated to be 6.5 to 8.0%.

Traces of white, fibrous, brucite ($Mg(OH)_2$) are observed as void linings in a small number of air voids. Brucite is a common reaction product of the alkali-carbonate reaction.

Echo 5 – Core 4 (Echo 5 Taxiway)

General Description

The sample consists of a concrete core identified as “Echo 5 Core 4” (Figure 2). The core is 352.0 mm (13.9 in.) long and has a diameter of 100.0 mm (3.9 in.).

The core top or wearing surface is flat, weathered and worn, such that fine aggregate particles are partially exposed (Figure 2a). There are no remnant indications of the type of original finish on

the wearing surface. One side of the core top is worn smooth by the core drill bit wobbling before setting into the core hole (Figure 2a).

An uncorroded, 9.5 mm (0.375 in.) diameter, deformed steel reinforcing bar is present at 203.2 mm (8.0 in.) depth in the core.

At the bottom of the concrete is an underlying bituminous impregnated fiber membrane. The membrane is moderately well-bonded to the overlying concrete.

Cracks

Multiple cracks occur at the wearing surface (Figure 2a). The cracks are at oblique angles to the direction of the reinforcing steel. A portion of the wearing surface to a depth of 38 mm (1.5 in.) has spalled from the core along one side. Cracks at the wearing surface are filled and lined with calcium carbonate and brucite. The cracks pass through many coarse aggregate particles, suggesting crack formation after the development of significant paste-to-aggregate bond. Surface cracks extend to a depth of 45 to 58 mm (1.8 to 2.3 in.) where the vertical cracks intersect and truncate at a horizontal crack. The horizontal crack extends entirely through the core effectively separating the top segment from the rest of the core. The horizontal crack is lined with calcium carbonate and brucite. The horizontal crack also passes through many coarse aggregate particles suggesting crack formation after the development of significant paste-to-aggregate bond.

A second horizontal crack occurs at 100 to 150 mm (3.9 to 5.9 in.) depth. The crack extends entirely through the core effectively separating the top segment from the rest of the core. The horizontal crack is partially with calcium carbonate and brucite. The crack also passes through many coarse aggregate particles, suggesting crack formation after the development of significant paste-to-aggregate bond.

Several random cracks and microcracks occur within the top 150 mm (5.9 in.) of the core. The cracks radiate outward from dolomite coarse aggregate particles into the adjacent cementitious material paste (Figures 7, 8 and 11 through 16). The cracks are lined with a variety of white secondary deposits including brucite ($\text{Mg}(\text{OH})_2$), (tentatively) various magnesium carbonate hydrate minerals, calcium acetate, calcium carbonate and an amorphous, desiccated, alkali gel. The white, calcium acetate is characterized by turning into a flammable gel when sprayed with isopropanol. Optical properties indicate what appear to be trace amounts of magnesite (MgCO_3), hydromagnesite ($\text{MgCO}_3 \cdot \text{Mg}(\text{OH})_2 \cdot 3\text{H}_2\text{O}$), lansfordite ($\text{MgCO}_3 \cdot 5\text{H}_2\text{O}$) and nesquehonite ($\text{MgCO}_3 \cdot 3\text{H}_2\text{O}$). These latter mineral occurrences require verification by x-ray diffraction and differential thermal analysis for definitive identification.

Aggregates

Aggregates are similar to those described for Core 1. Aggregate particles are uniformly dispersed throughout the concrete. Maximum aggregate size is measured 15 mm (0.625 in.). The aggregate is fairly well-graded.

Coarse aggregate is composed of crushed calcitic dolomite. The rock has a fine-grained texture with a finer matrix composed of calcite, dolomite and reddish brown clay (Figure 9). Larger rhombic shaped dolomite crystals and an occasional quartz sand grain are within the finer matrix.

Some of the clay occurs as fine seams or stringers. Some of the dolomite rhombs have cores containing fine argillaceous material surrounded by an outer argillaceous-free rim of dolomite that is slowly de-dolomitizing into calcite (Figures 9 and 10). Conversion of dolomite to calcite is also evident adjacent to cracks that radiate out of coarse aggregate particles (Figure 12).

Coarse aggregate particles are reddish pink to gray. Coarse aggregate is moderately hard; dense; angular-to-subangular; equant to slightly elongated, fossiliferous and rough textured. Many of the coarse aggregate particles contain darkened rims along their outer periphery throughout the full depth of the core.

Fine aggregate is natural sand containing a variety of rock and mineral types including, quartz, various types of feldspars, meta-quartzite, granite, chert, mica, dolomite fines and other rock and mineral types. The fine aggregate is predominantly composed of quartz, feldspar and meta-quartzite. Fine aggregate particles are variously colored from white to red to translucent; hard, dense, sub-rounded to well-rounded, generally spherical and having a smooth outer surface texture.

Many of the dolomitic coarse aggregate particles are cracked in the upper 150 mm (5.9 in.) of the core (Figures 7 and 8).

Cement Paste

Cement paste is similar to that described for Core 1. The cement paste is brownish gray, exhibits a vitreous luster, micro-granular texture, and hackly fracture. The paste is hard, dense and tightly bonded to aggregate particles. Cement paste is carbonated to a depth of 1-to-2 mm below the wearing surface

Residual cement particles are present in a moderate amount, somewhat coarse and mostly ferrite and belite phases. Residual cement content is estimated to be 10 to 13%, by volume of paste. Calcium hydroxide, a normal hydration product, is estimated to be 5-to-8% by volume of paste, as very fine hexagonal crystals and tablets.

Residual fly ash is present, representing the use of supplementary cementitious materials in the mix (Figures 11 and 17). Residual fly ash is estimated to be 12-to-17%, by volume of paste.

Properties of the paste previously described are evaluated to provide an estimate of the water-to-cementitious materials ratio. Based on paste properties observed, water-to-cementitious materials ratio is estimated to be 0.35-to-0.45.

There is very little microcracking of the paste below 150 mm (5.9 in.) depth.

Air Voids

The concrete contains numerous air-voids, ranging from mostly very fine to occasionally coarse. The voids present are generally spherical (entrained air) with a few larger, irregularly shaped voids indicative of entrapped air. The concrete is deemed air-entrained.

However, the air-voids are not uniformly dispersed throughout the concrete. Air content is low in the top 50 mm (2.0 in.) of the pavement. Air content in the top portion of the core is estimated to be 0.5 to 2.0%. Below 50 mm (2.0 in.), the air content is estimated to be 3.5 to 6.0%, but the voids are frequently clustered together.

White secondary deposits including brucite ($\text{Mg}(\text{OH})_2$), various magnesium carbonate hydrate minerals, calcium acetate, calcium carbonate and magnesium carbonate line many voids adjacent to dolomitic coarse aggregate particles throughout the entire thickness of the pavement core. These latter mineral occurrences require verification by x-ray diffraction and differential thermal analysis for definitive identification.

C7C1 (Charley Connector 7 Taxiway - Core 1)

General Description

The sample consists of a concrete core identified as “C7C1” (Figure 3). The core is 357 mm (14.1 in.) long and has a diameter of 100 mm (3.9 in.).

The core top or wearing surface is a flat weathered surface (Figure 3a). There are remnants of fine ridges on the wearing surface, indicating a broom finish. There are also some lightly pitted areas at the wearing surface extending into the cement paste 1 to 2 mm depth (Figure 18). One side of the core top is worn smooth by the core drill bit wobbling before setting into the core hole (Figure 3a).

At the bottom of the concrete is an underlying bituminous impregnated fiber membrane. The membrane is moderately well-bonded to the overlying concrete.

No reinforcing steel or remnants thereof are present in the core.

Cracks

A 0.10 to 0.25 mm wide crack is present at the wearing surface (Figure 3a). The crack is continuous and extends to a depth of approximately 150 to 175 mm (6.0 to 7.0 in.), where it dissipates. Microcracks branch off the vertical crack at several oblique angles. The crack and microcracks most commonly pass through extensively microcracked dolomite coarse aggregate particles (Figures 19 through 21). There are also several random microcracks in the top 150 mm of the pavement. The cracks are lined with a variety of white secondary deposits including brucite ($\text{Mg}(\text{OH})_2$), (tentatively) various magnesium carbonate hydrate minerals, calcium acetate, calcium carbonate and an amorphous, desiccated, alkali gel (Figure 22). The white, calcium acetate is characterized by turning into a flammable gel when sprayed with isopropanol. Optical properties indicate what appear to be trace amounts of magnesite (MgCO_3), hydromagnesite ($\text{MgCO}_3 \cdot \text{Mg}(\text{OH})_2 \cdot 3\text{H}_2\text{O}$), lansfordite ($\text{MgCO}_3 \cdot 5\text{H}_2\text{O}$) and nesquehonite ($\text{MgCO}_3 \cdot 3\text{H}_2\text{O}$). These latter mineral occurrences require verification by x-ray diffraction and differential thermal analysis for definitive identification.

Aggregates

Aggregates are similar to those described for Core 1. Aggregate particles are uniformly dispersed throughout the concrete. Maximum aggregate size is measured 15 mm (0.625 in.). The aggregate is fairly well-graded.

Most of the coarse aggregate particles contain darkened rims along their outer periphery throughout the full depth of the core. Many of the dolomitic coarse aggregate particles are cracked in the upper 150 mm (5.9 in.) of the core (Figures 19 and 20), although random microcracking of rimmed coarse aggregate particles occurs less frequently throughout the core.

Cement Paste

Cement paste is similar to that described for Core 1. The cement paste is dark brownish gray, exhibits a vitreous luster, micro-granular texture, and hackly fracture. The paste is hard, dense and tightly bonded to aggregate particles. Cement paste is minimally carbonated to a depth of 1 mm below the wearing surface.

Residual cement particles are present in a moderate amount, somewhat coarse, with alite, ferrite and belite phases all present. Residual cement content is estimated to be 12 to 15%, by volume of paste. Calcium hydroxide, a normal hydration product, is estimated to be 6-to-10% by volume of paste, as very fine hexagonal crystals and tablets.

Residual fly ash is present, representing the use of supplementary cementitious materials in the mix. Residual fly ash is estimated to be 15-to-20%, by volume of paste.

Properties of the paste previously described are evaluated to provide an estimate of the water-to-cementitious materials ratio. Based on paste properties observed, water-to-cementitious materials ratio is estimated to be 0.35-to-0.45.

There is little microcracking of the paste below 150 mm (5.9 in.) depth.

Air Voids

The concrete contains somewhat numerous air-voids, ranging from mostly very fine to occasionally coarse. The voids present are generally spherical (entrained air) with a few larger, irregularly shaped voids indicative of entrapped air. The concrete is deemed air-entrained.

Air-voids are non-uniformly dispersed throughout the concrete, with some areas nearly of void clusters and other areas practically void free. Air content is estimated to be 2.5 to 3.5%.

White secondary deposits including brucite ($Mg(OH)_2$), various magnesium carbonate hydrate minerals, calcium acetate, calcium carbonate and magnesium carbonate line many voids adjacent to dolomitic coarse aggregate particles throughout the entire thickness of the pavement core. These latter mineral occurrences require verification by x-ray diffraction and differential thermal analysis for definitive identification.

G1 (Golf Taxiway – Core 1)

General Description

The sample consists of a concrete core identified as “G1” (Figure 4). The core is 388 mm (15.3 in.) long and has a diameter of 100 mm (3.9 in.).

The core top or wearing surface is a flat weathered surface (Figure 4a). There are remnants of fine ridges on the wearing surface, indicating a broom finish. There are also some lightly pitted areas at the wearing surface extending into the cement paste 1 to 2 mm depth. One side of the core top is worn smooth by the core drill bit wobbling before setting into the core hole (Figure 4a).

At the bottom of the concrete has the imprint of an underlying bituminous impregnated fiber membrane.

An uncorroded, 9.5 mm (0.375 in.) diameter, deformed steel reinforcing bar is partially embedded in the side of the core at 203.2 mm (8.0 in.) depth.

Cracks

Two less than 0.08 mm wide cracks occur at the wearing surface. The cracks are fine, but continuous to a depth of approximately 10 to 25 mm (0.4 to 1.0 in.) respectively, where they dissipate. The surface cracks pass primarily around aggregate particles, suggesting formation early in the life of the concrete, as by minor (due to narrow width) drying shrinkage.

Some horizontal trending and random, fine cracks and microcracks occur in the upper 150 to 205 mm (5.9 to 8.0 in.) of the core. The cracks and microcracks most commonly pass through extensively microcracked dolomite coarse aggregate particles (Figure 24). The cracks are lined with a variety of white secondary deposits including brucite ($\text{Mg}(\text{OH})_2$), (tentatively) various magnesium carbonate hydrate minerals, calcium acetate, calcium carbonate and an amorphous, desiccated, alkali gel (Figures 25 and 26). The white, calcium acetate is characterized by turning into a flammable gel when sprayed with isopropanol. Optical properties indicate what appear to be trace amounts of magnesite (MgCO_3), hydromagnesite ($\text{MgCO}_3 \cdot \text{Mg}(\text{OH})_2 \cdot 3\text{H}_2\text{O}$), lansfordite ($\text{MgCO}_3 \cdot 5\text{H}_2\text{O}$) and nesquehonite ($\text{MgCO}_3 \cdot 3\text{H}_2\text{O}$). These latter mineral occurrences require verification by x-ray diffraction and differential thermal analysis for definitive identification.

Very little cracking or microcracking is observed below 205 mm depth in the core.

Aggregates

Aggregates are similar to those described for Core 1. Aggregate particles are uniformly dispersed throughout the concrete. Maximum aggregate size is measured 15 mm (0.625 in.). The aggregate is fairly well-graded.

Most of the coarse aggregate particles contain darkened rims along their outer periphery throughout the full depth of the core. Some of the dolomitic coarse aggregate particles are cracked in the upper 150 mm to 205 mm (5.9 to 8.0 in.) of the core (Figures 23 and 24), although

random microcracking of rimmed coarse aggregate particles occur infrequently below these depths.

Cement Paste

Cement paste is similar to that described for Core 1. The cement paste is dark brownish gray, exhibits a vitreous luster, micro-granular texture, and hackly fracture. The paste is hard, dense and tightly bonded to aggregate particles. Cement paste is minimally carbonated to a depth of 1 to 3 mm below the wearing surface.

Residual cement particles are present in a moderate amount, somewhat coarse, with ferrite and belite phases most common. Residual cement content is estimated to be 12 to 15%, by volume of paste. Calcium hydroxide, a normal hydration product, is estimated to be 6-to-8% by volume of paste, as very fine hexagonal crystals and tablets.

Residual fly ash is present, representing the use of supplementary cementitious materials in the mix. Residual fly ash is estimated to be 15-to-20%, by volume of paste.

Properties of the paste previously described are evaluated to provide an estimate of the water-to-cementitious materials ratio. Based on paste properties observed, water-to-cementitious materials ratio is estimated to be 0.35-to-0.45.

There is little microcracking of the paste below 150 to 205 mm (5.9 to 8.0 in.) depth.

Air Voids

The concrete contains somewhat numerous air-voids, ranging from mostly very fine to occasionally coarse. The voids present are generally spherical (entrained air) with a few larger, irregularly shaped voids indicative of entrapped air. The concrete is deemed air-entrained.

Air-voids are non-uniformly dispersed throughout the concrete, with some areas nearly of void clusters and other areas practically void free. Air content is estimated to be 1.5 to 3.5%.

White secondary deposits including brucite ($Mg(OH)_2$), various magnesium carbonate hydrate minerals, calcium acetate, calcium carbonate and magnesium carbonate line many voids adjacent to dolomitic coarse aggregate particles throughout the entire thickness of the pavement core (Figure 25). These latter mineral occurrences require verification by x-ray diffraction and differential thermal analysis for definitive identification.

Conclusions

Petrographic examination was performed on four (4) concrete cores drilled from pavement slabs at the Colorado Springs Municipal Airport, Colorado Springs, CO. Alkali-carbonate reaction was observed in all of the cores and damage by alkali-carbonate reaction in three (3) of the four (4) cores. Evidence of significant intrusion of calcium acetate (either as a deicer or reaction product of dissolution of potassium acetate deicer, if used) was observed. Fly ash is present in the cracked concrete and appears to have been ineffective at mitigating the deleterious effects of alkali-carbonate reaction. The cracked concretes also appear to contain non-frost resistant air contents and air-void systems, such that, some of the cracking is likely due to damage by freezing and thawing while critically saturated.

Recommendations were made regarding additional characterization tests of reaction products and study of the thermodynamic and kinetic stability of phase changes of reaction products and subsequent volume stability and their contribution to alkali-carbonate related expansion.

References

- (1) Lea, F. M., *The Chemistry of Cement and Concrete*, Chemical Publishing Company, New York, NY, (1971).
- (2) Hadley, D. W., “Alkali Reactivity of Carbonate Rocks-Expansion and Dedolomitization,” Highway Research Board Proceedings, Washington, D. C., Vol. 40., pp.462-474, (1961), reprinted as Research Department Bulletin 139, Portland Cement Association, Skokie, IL.
- (3) Hadley, D. W., “Alkali Reactivity of Dolomite Carbonate Rocks,” Highway Research Record No. 45, Washington, D. C., pp.1-19, (1964), reprinted as Research Department Bulletin 176, Portland Cement Association, Skokie, IL.
- (4) Ozol, M. A., “Alkali-Carbonate Rock Reaction,” Significance of Tests and Properties of Concrete and Concrete-Making Materials, ASTM STP-169C, ASTM, Philadelphia, PA, pp. 372-387, (1994).
- (5) “Report on Alkali-Aggregate Reactivity (ACI 221.1R-98),” ACI Manual of Concrete Practice, Part 1, ACI Committee 221, American Concrete Institute, Detroit, MI, (1998).
- (6) Walker, H. N., Lane, D. S. and Stutzman, P. E., “Petrographic Methods of Examining Hardened Concrete: A Petrographic Manual.” FHWA Publication No. FHWA-HRT-04-150, Chapter 10, Federal Highway Administration, McLean, VA, (2004).
- (7) Swenson, E. G. and Gillott, J. E., “Characteristics of Kingston Carbonate Rock Reaction,” Highway Research Board Bulletin, Washington, D. C., No. 275, pp.18-31, (1960), reprinted as National Research Council of Canada, Division of Building Research, Research Paper No. 130, Ottawa, Canada.
- (8) Mehta, P. K., “Pozzolanic and Cementitious Byproducts as Mineral Admixtures for Concrete – A Critical Review,” in ACI SP 79-1, *Fly Ash, Silica Fume, Slag & Other Mineral By-Products in Concrete – Volume I*, American Concrete Institute, Detroit, MI, pp. 1-46, (1983).
- (9) Ozol, M. A. and Newlon, H. H., Jr., “Bridge Deck Deterioration Promoted by Alkali-Carbonate Reaction: A Documented Example,” Transportation Research Record No. 525, National Research Council, Washington, D. C., pp. 55-63, (1974).

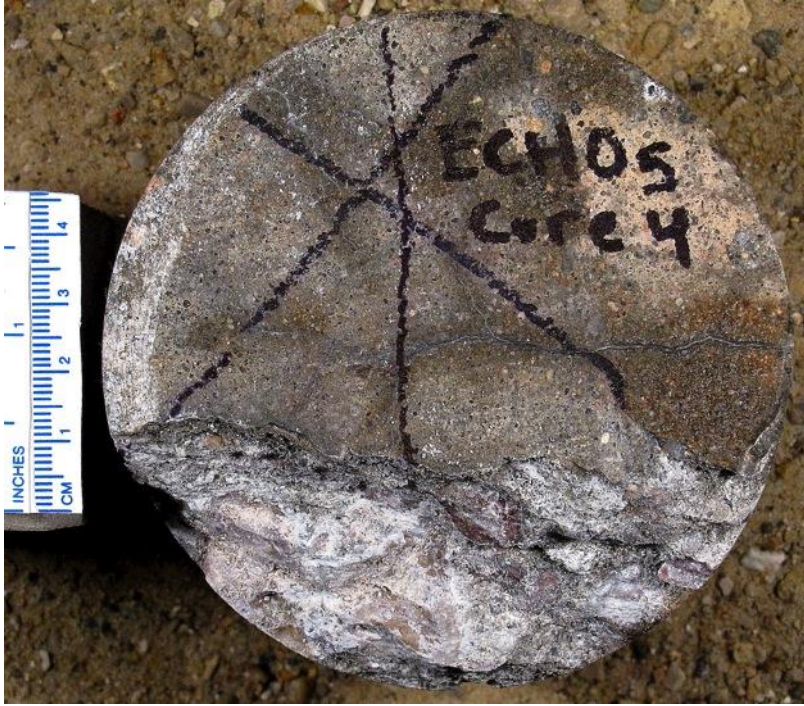


(a) Core top/wearing surface. Scale is in centimeters.



(b) Core side, top is to left. Scale is in inches.

Figure 1. Core 1 – De-Ice Pad as received for petrographic examination.



(a) Core top/wearing surface. Scale is in centimeters.



(b) Core side, top is to right. Scale is in inches.

Figure 2. Echo 5 – Core 4 (Echo 5 Taxiway) as received for petrographic examination.



(a) Core top/wearing surface. Scale is in centimeters.



(b) Core side, top is to the right. Scale is in inches.

Figure 3. Core C7C1 (Charley Connector 7 Taxiway - Core 1) as received for petrographic examination.



(a) Core top/wearing surface. Scale is in centimeters.



(b) Core side, top is to left. Scale is in inches.

Figure 4. Core G1 (Golf Taxiway – Core 1) as received for petrographic examination.



Figure 5. Close-up of the wearing surface in Core 1 (De-Ice Pad). Within the red dashed circle is an area of minor surface pitting.



Figure 6. Thin section photomicrograph of Core 1 illustrating dolomite rhomb with an argillaceous inner core and non-argillaceous outer rim and ragged upper crystal face (red arrow). 120X magnification. Vertical field of view is 0.7 mm. Plane-polarized light.

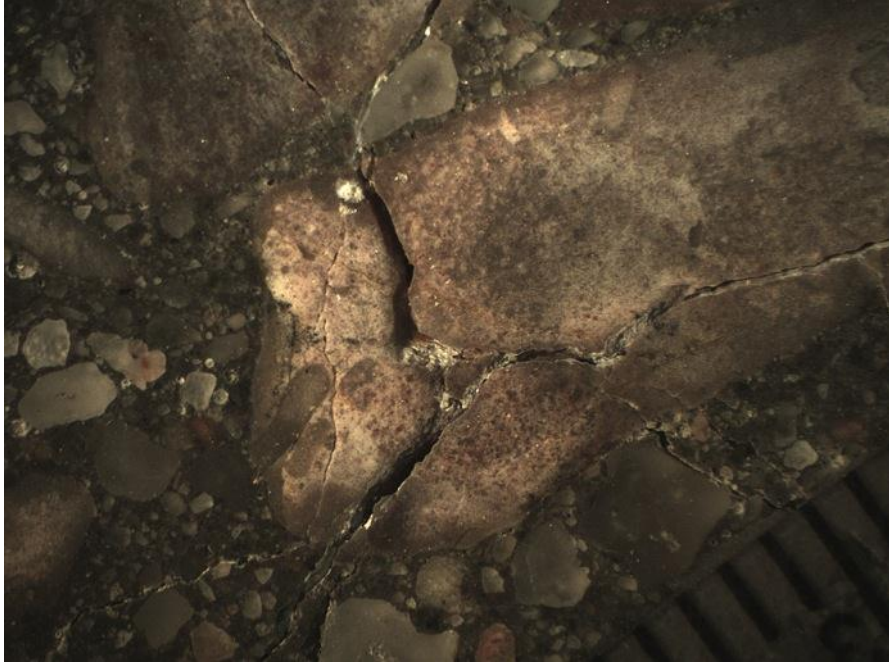


Figure 7. Magnified lapped slice of Echo 5 – Core 4 showing cracks radiating out from a rimmed, dolomite coarse aggregate particle. White, brucite (and other related) deposits line the cracks. This is typical of damage due to alkali-carbonate reaction. Scale is in millimeters.

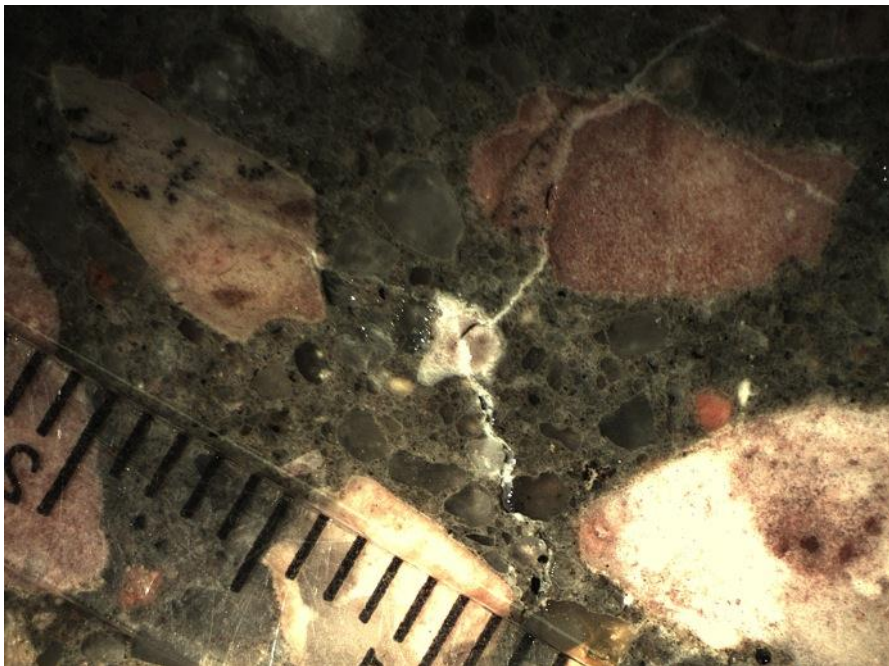


Figure 8. Photomicrograph of the magnified lapped slice of Echo 5 – Core 4 showing cracks radiating out from a small, dolomite coarse aggregate particle. White, brucite (and other related) deposits line the cracks. This is typical of damage due to alkali-carbonate reaction. Scale is in millimeters.

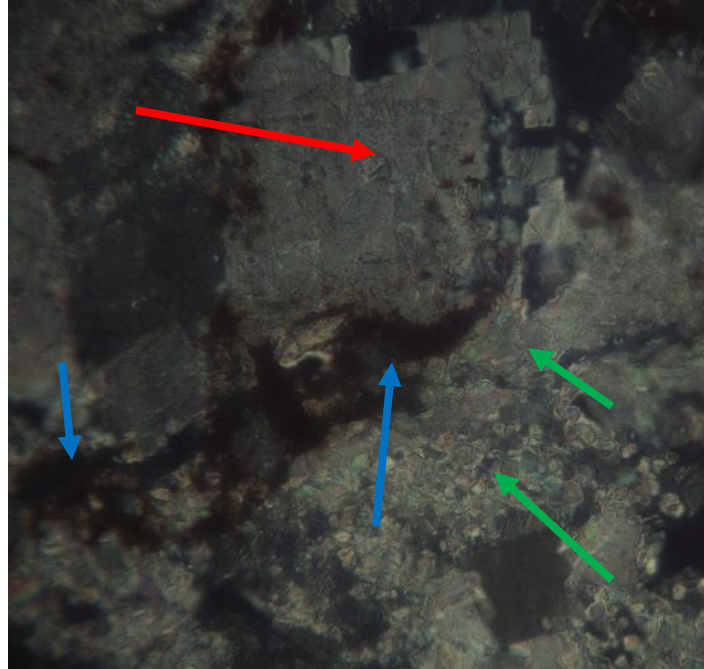


Figure 9. Thin section photomicrograph of Echo 5 – Core 4 illustrating microstructure of a dolomite coarse aggregate particle. Red arrow points to a dolomite rhomb in the process of de-dolomitization. Green arrows point to calcite converted from dolomite. Blue arrows point to brown, argillaceous material (clay) within the dolomite. Crossed-polarized light. Vertical field of view is 0.25 mm.

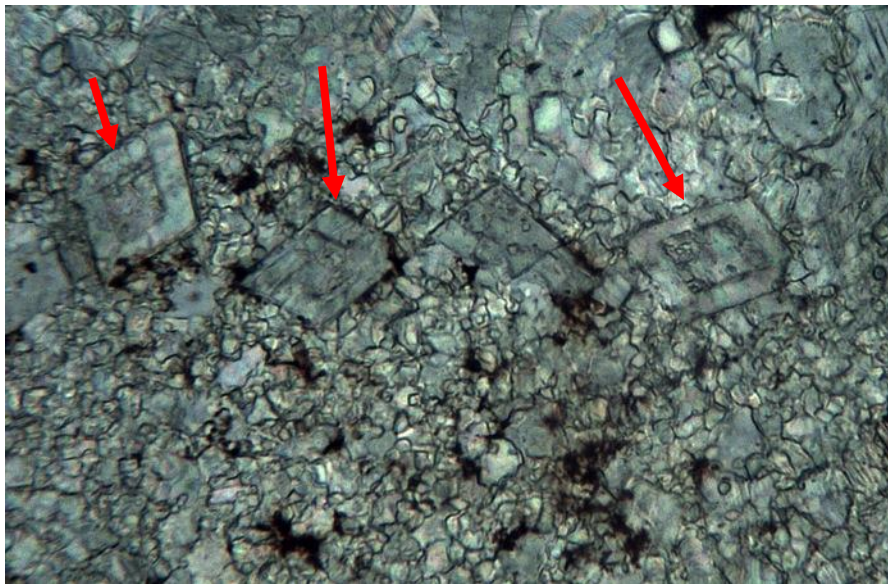


Figure 10. Thin section photomicrograph of Echo 5 – Core 4 illustrating dolomite rhombs with inner dolomitic cores and outer rims transitioning to calcite (red arrows) in a coarse aggregate particle. Brown clay is dispersed within the matrix. Vertical field of view is 0.6 mm. Plane-polarized light.

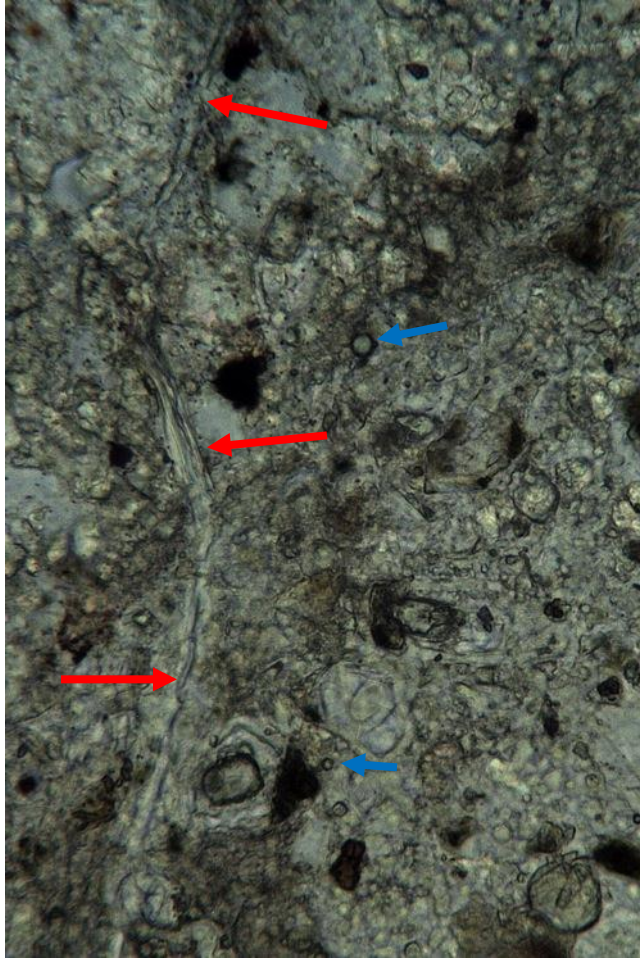


Figure 11. Thin section photomicrograph of Echo 5 – Core 4 illustrating a crack radiating out from a dolomite coarse aggregate particle (at top left) into the cementitious materials paste (red arrows). The crack is lined with brucite. Note the presence of residual fly ash particles (blue arrows). Vertical field of view is 0.25 mm. Plane-polarized light.



Figure 12. Thin section photomicrograph of Echo 5 – Core 4 illustrating a crack within a dolomite coarse aggregate particle (red arrows). The crack is lined with brucite and rock adjacent to the crack has been converted to a fine-grained calcite as compared to the coarser-grained dolomite further away from the crack. Vertical field of view is 0.60 mm. Plane-polarized light.

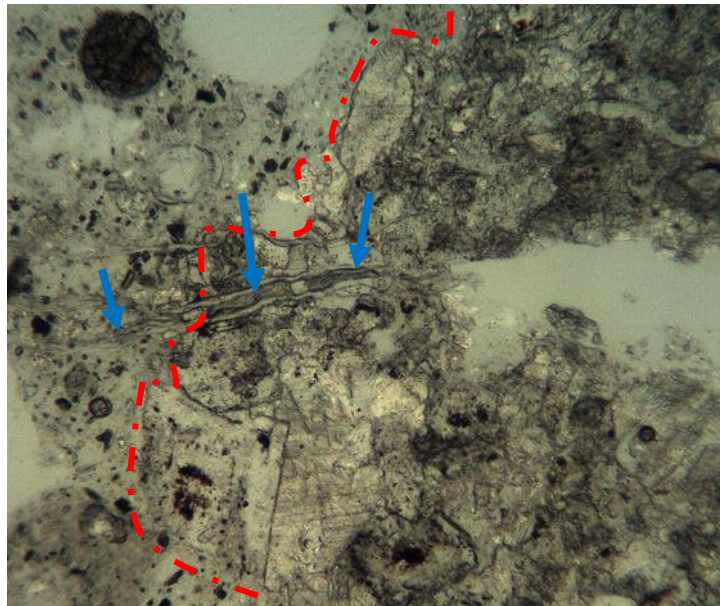


Figure 13. Thin section photomicrograph of Echo 5 – Core 4 illustrating a crack radiating out from a dolomite coarse aggregate particle (right of red dashed line) into the cementitious materials paste (blue arrows). The crack is lined with brucite. Vertical field of view is 0.60 mm. Plane-polarized light.

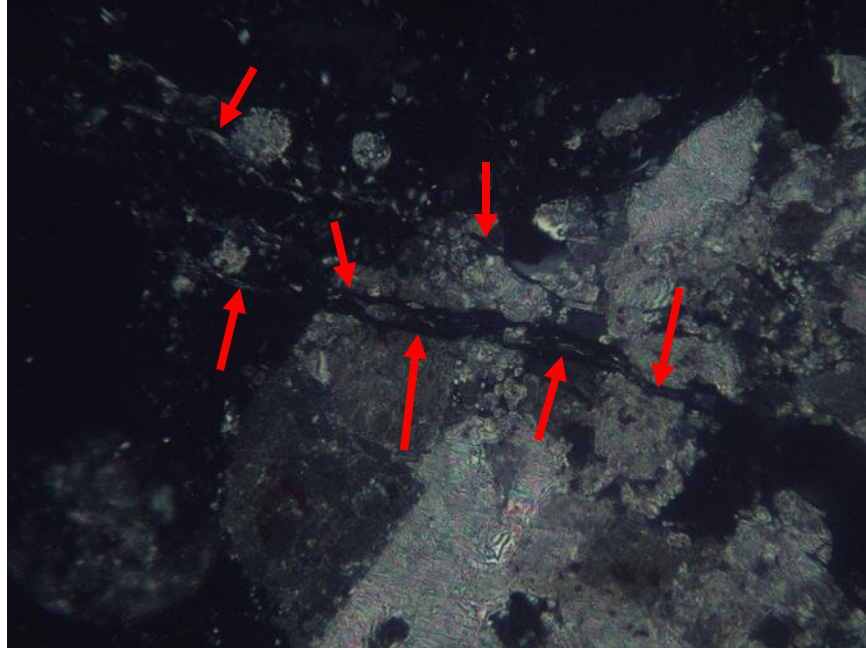


Figure 14. Thin section photomicrograph of Echo 5 – Core 4 illustrating a crack radiating out from a dolomite coarse aggregate particle (gold colored) into the cementitious materials paste (red arrows). The crack is lined with (gray appearing) brucite. Vertical field of view is 0.60 mm. Cross-polarized light.



Figure 15. Thin section photomicrograph of Echo 5 – Core 4 showing coarse, fibrous brucite (red arrow) within a dolomite coarse aggregate particle. Vertical field of view is 0.25 mm. Plane-polarized light.

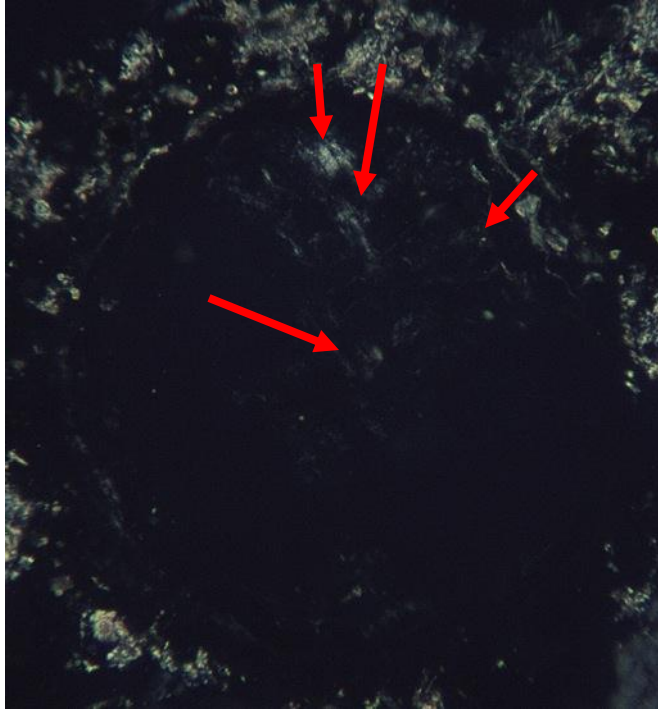


Figure 16. Thin section photomicrograph of Echo 5 – Core 4 illustrating fibrous brucite (red arrows) partially filling an air void. Vertical field of view is 0.25 mm. Crossed-polarized light.

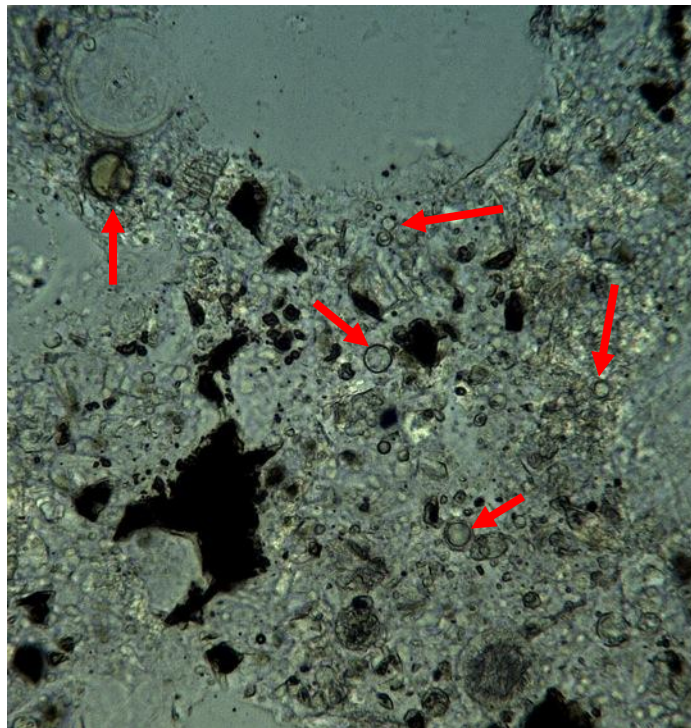


Figure 17. Thin section photomicrograph of Echo 5 – Core 4 showing the presence of residual fly ash particles (red arrows). Vertical field of view is 0.60 mm. Plane-polarized light.

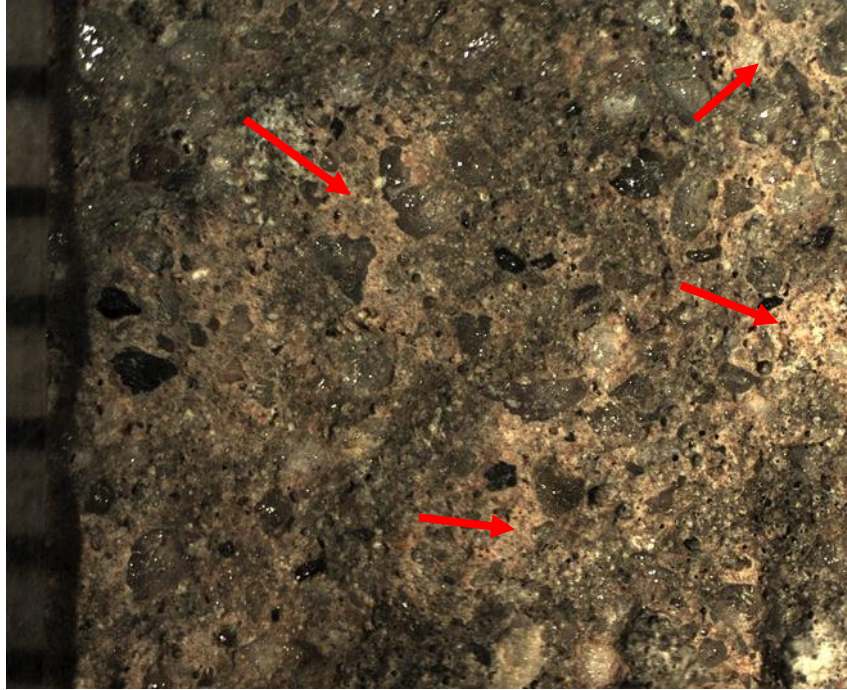


Figure 18. Close-up of the wearing surface of Core C1C7. Red arrows point to areas of minor surface pitting and fresh (pinkish) carbonation. Scale is in millimeters.

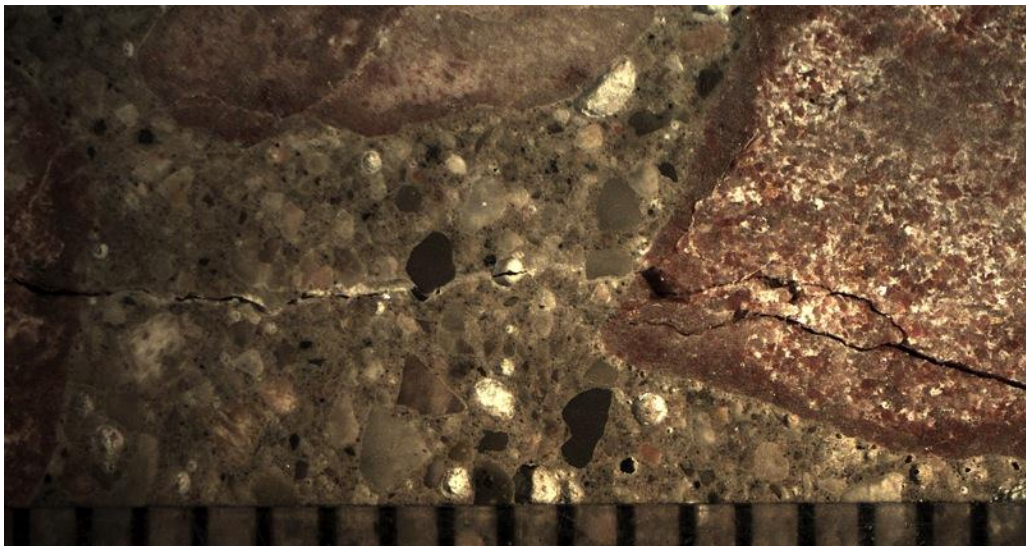


Figure 19. Magnified lapped slice of Core C1C7 showing cracks radiating out from a rimmed, dolomite coarse aggregate particle. White, brucite (and other related) deposits line the cracks and voids. This is typical of damage due to alkali-carbonate reaction. Scale is in millimeters.



Figure 20. Magnified lapped slice of Core C1C7 showing cracks radiating out from reacting dolomite coarse aggregate particles. White, brucite (and other related) deposits line the cracks and voids. This is typical of damage due to alkali-carbonate reaction. Scale is in millimeters.

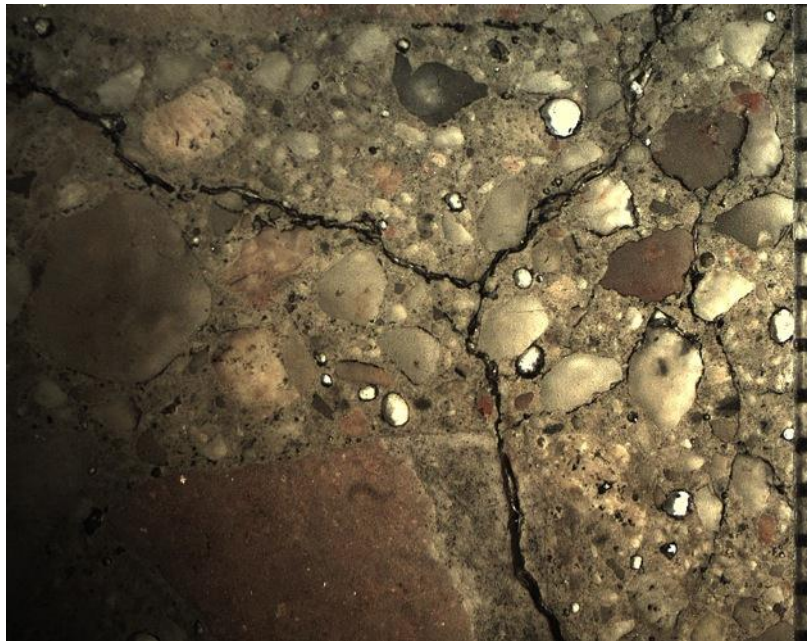


Figure 21. Magnified lapped slice of Core C1C7 showing numerous, random cracks in the cement paste. White, brucite (and other related) deposits line the cracks and voids in the field of view. This damage is due to alkali-carbonate reaction. Scale is in millimeters.



Figure 22. Crack surface in Core C1C7 lined with various, secondary deposits, including white, pearly brucite; translucent magnesite; amorphous, desiccated (and pattern cracked) alkali gel (and other related) deposits. Scale is in millimeters.



Figure 23. Magnified lapped slice of Core G1 showing cracks radiating out from a rimmed, dolomite coarse aggregate particle (red arrows). White, brucite (and other related) deposits line the cracks and voids. This is typical of damage due to alkali-carbonate reaction. Scale is in millimeters.

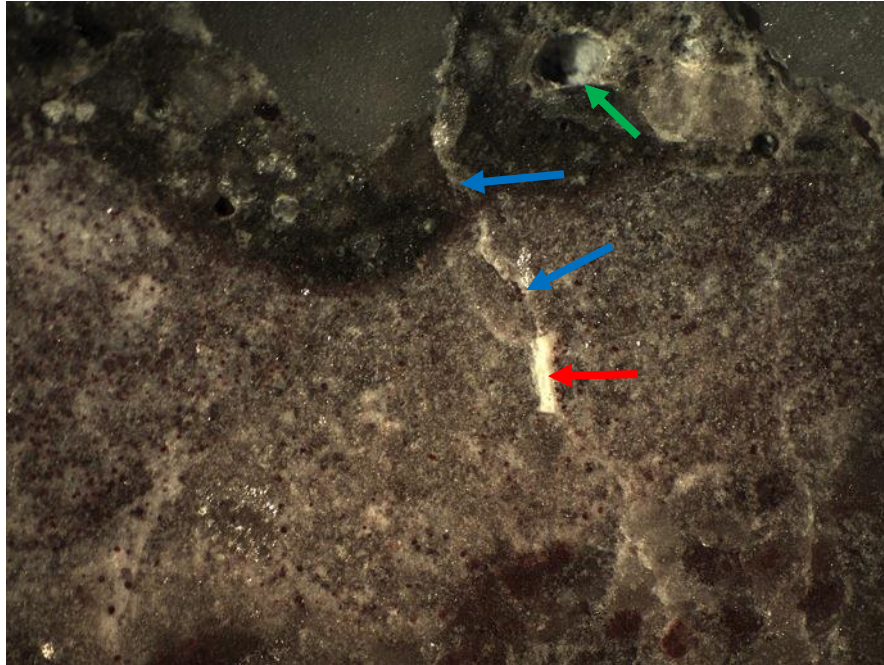


Figure 24. Magnified lapped slice of Core G1 showing a crack radiating out from a rimmed, dolomite coarse aggregate particle (blue arrows). The crack appears to originate in a coarse, fibrous, white brucite (red arrow) particle. Fine brucite lines a nearby void (green arrow).



Figure 25. Void lining in Core G1 containing various, secondary deposits, including white, pearly brucite; translucent magnesite; dull, white, botryoidal clusters of nesquehonite; amorphous, desiccated (and pattern cracked) alkali gel (and other related) deposits. Scale is in millimeters.



Figure 26. Crack surface in Core G1 lined with various, secondary deposits, including white, pearly brucite; translucent magnesite; and dull, white, botryoidal clusters of nesquehonite. Scale is in millimeters.

Airport V

Core Locations

Core locations were selected by Clemson University. Specific locations and identifications based on information conveyed by you are as follows:

<u>Core No.</u>	<u>Approximate Location</u>
4	Runway 4L22R, Lane 7, looking north
7	Runway 4L22R, Lane 5 of 6
9	Taxiway Alpha
12	Taxiway Alpha

The 4 cores, (Figures 1 through 4), were received at STS on November 18, 2009. Petrographic examination was requested on each of the cores to determine the cause(s) and extent of cracking, slab movement and other observations pertinent to induced distress mechanisms occurring in the slab.

Results

Subject to the qualifications in the attached Appendix, results of the petrographic examinations are as follows:

1. Concrete represented by the four (4) cores exhibits evidence of and damage by alkali-silica reaction (ASR). The alkali-reactive aggregate component is chert within the fine aggregate, particularly in the plus 16 mesh sieve sizes. The cherts in these concretes are beige to white to yellow and contain reactions rims along their outer periphery. The cherts are sometimes dolomitic, most are soft, porous and extensively cracked and microcracked (Figures 6 through 14).
2. Coarse aggregate is composed of blast furnace slag. The slag is vesicular, coarsely crystalline with a small amount of a very fine-grained matrix. The matrix, which is a minor constituent, is composed of glass (silica). Crystalline components are composed of the melilite, iron oxide, merwinite and pyroxene. There is no evidence of alkali-silica reaction associated with the slag coarse aggregate.
3. Evidence of deleterious alkali-silica reaction in the cores are cracking and microcracking occurring within rimmed chert aggregate particles, with cracks radiating out from the reacting particles into adjacent cement paste (Figures 5 through 14). The cracks and nearby voids are lined to filled with alkali-silica gel and innocuous secondary deposits of ettringite, calcium carbonate and calcium hydroxide.
4. The relative degree of damage by alkali-silica reaction varies from Core 4 exhibiting the most cracking, followed by Core 9 and then Cores 7 and 12 having slightly less cracking than Core 9, but still showing definitive evidence of damage.

5. Cores 4, 7 and 9 contain what are interpreted to be cracks due to drying shrinkage at the wearing surface. The cracks extend 1.5 to 2.5 in. depths in Cores 4 and 9 and 4.0 in. depth in Core 7. These drying shrinkage cracks likely allowed easy ingress of moisture and deicer deeper into the pavement, thereby increasing surface area where alkali-silica reactions can take place. Sealing of drying shrinkage cracks (and maintaining a seal) may have lessened the effects of deleterious alkali-silica reaction.
6. Residual acetate deicer has not been identified in cracks and voids of any of the cores.
7. No other forms of deterioration are detected in the concretes represented by these cores.

Details of the petrographic examinations are provided in the following sections of this report.

Petrographic Examination

Core 4

General Description

The sample consists of a concrete core identified as “Core 4 22-LR” (Figure 1). The core is 455.0 mm (17.9 in.) long and has a diameter of 96.0 mm (3.8 in.).

The core top or wearing surface is a fairly flat, weathered surface with fine aggregate particles partially exposed. The surface has been grooved (Figure 1a). Grooves are spaced 38 mm (1.5 in.) on center. Grooves are 6 mm (1/4 in.) wide and 5 mm (1/4 in.) deep.

Minor, superficially corroded, 9.0 mm (3/8 in.) diameter, deformed steel reinforcing bar is present at 143.0 mm (5.6 in.) depth. Rust stains occur as small pits along the surface of the steel reinforcement with no bar section loss apparent.

The core bottom is the imprint of a bituminous impregnated underlying base course.

Cracks

A 0.30 to 0.50 mm (0.012 to 0.020 in.) wide crack that branches off dendritically into multiple finer cracks is present at the wearing surface (Figure 1a). The cracks narrow to 0.10 mm (0.004 in.) diameter immediately below the wearing surface. The cracks extend to depths of 40-to-55 mm (1.5-to-2.2 in.) where they dissipate. This wider surface crack appears to be due to surficial drying shrinkage.

Several horizontally oriented, fine (0.15 mm or less dia.) cracks and microcracks are at 14, 47, 75 mm (0.6, 1.8 and 3.0 in.) depth and then spaced about every 10-to-20 mm apart to 200 mm (7.9 in.) depth (Figure 5).

The core was received in two pieces separated by a horizontal crack at 175-to-185 mm (6.9-to-7.3 in.) depth (Figure 1a). Cement paste is carbonated 5-to-7 mm (in.) on either side of the crack surface. The relatively deep paste carbonation suggests the crack did not form recently. The crack surface is coated with alkali-silica gel, as are voids filled with alkali-silica gel adjacent to the crack surface (Figure 6). The crack passes through several fine aggregate particles containing reaction rims along their outer periphery. Thus, it appears the crack is due to alkali-silica reaction.

Aggregates

Aggregate particles are uniformly dispersed throughout the concrete. Maximum aggregate size is measured as 19 mm (0.75 in.). The aggregate is fairly well-graded.

Coarse aggregate is composed of blast furnace slag. The slag is vesicular, coarsely crystalline with a small amount of a very fine-grained matrix. The matrix, which is a minor constituent, is composed of glass (silica). Crystalline components are composed of the melilite, iron oxide, merwinite and pyroxene. The slag aggregate does not exhibit evidence of weathering, but does yield a sulfurous odor when freshly fractured in the concrete.

Coarse aggregate particles are light to dark gray with a few particles greenish gray and tannish gray. Coarse aggregate is hard; porous due to its vesicularity but dense in its matrix; angular; equant shaped and outer surfaces of particles have a rough texture.

There is no evidence of alkali-silica reaction associated with the slag coarse aggregate.

Fine aggregate is natural sand containing a variety of rock and mineral types including, quartz, various types of feldspars, granite, chert, chalcedony, mica, dolomite and other rock and mineral types. With the exception of the chert (which will be described separately), fine aggregate particles are variously colored from white to red to translucent; hard, dense, sub-rounded to well-rounded, generally spherical and having a smooth outer surface texture.

Many of the chert particles, particularly in the plus 16 mesh sieve sizes, are beige to white to yellow and contain reaction rims along their outer periphery. The cherts are sometimes dolomitic, most are soft, porous and extensively cracked and microcracked. Cracks radiate out from chert particles often for great distances and are lined to filled with alkali-silica gel (Figure 7). This is classic evidence of damage by alkali-silica reaction. Therefore, chert in the coarser sizes of the fine aggregate is the offending reactive particle type in this concrete.

Cement Paste

The cement paste is medium greenish gray, exhibits a subvitreous luster, micro-granular texture, and hackly fracture. The paste is hard, dense and tightly bonded to aggregate particles. Cement paste is carbonated to a depth of 1-to-6 mm below the wearing surface.

Residual and relict cement particles are present in a moderate amount. Particularly abundant are residual are belite (dicalcium silicate) clusters with an abundance of interstitial calcium aluminoferrite, which is typical in older well-hydrated concretes. Residual and relict cement particle content is estimated to be 8 to 12%, by volume of paste. Calcium hydroxide, a normal hydration product, is estimated to be 7-to-10% by volume of paste, as evenly disseminated, fine hexagonal crystals. Supplementary cementitious materials are not detected; however, small particles of slag, likely fines from the coarse aggregate (and too coarse for a granulated product) are present in the paste.

Properties of the paste previously described are evaluated to provide an estimate of the water-to-cement ratio. Based on paste properties observed, water-to-cement ratio is estimated to be 0.40-to-0.45.

Cracks and microcracks are abundant throughout the paste at nearly all depths. The cracks and microcracks are lined to filled with alkali-silica gel and secondary ettringite and primarily radiate out of and pass through rimmed, chert fine aggregate particles. The cracks and microcracks are deemed to be due to expansive alkali-silica reaction.

Air Voids

The concrete contains numerous air-voids, most of which are very fine. The voids are spherical (entrained air) with some larger, irregularly shaped voids, indicative of entrapped air. The concrete is deemed air-entrained.

The air-voids are uniformly dispersed throughout the concrete. Air content is estimated to be 3.5 to 4.5%.

Etringite lines to fills many voids. Calcite lines voids in the near-surface regions of the concrete.

Core 7

General Description

The sample consists of a concrete core identified as “Core 7 4L-22R” (Figure 2). The core is 432.0 mm (17.0 in.) long and has a diameter of 100.0 mm (3.9 in.).

The core top has weathered and worn rough broom finish, such that fine aggregate particles are partially exposed (Figure 2a). There are grooves ground perpendicular to the broom finish. The grooves are spaced 38 mm (1.5 in.) apart and are 2 mm deep. Fine aggregate particles are partially exposed within the grooves, suggesting the grooves are fairly old and weathered.

A few rusted steel fragments of fine aggregate size (likely from the slag) are present at the wearing surface.

Minor surficially corroded, 9.5 mm (0.38 in.) diameter, deformed steel reinforcing bar is present at 146.0 mm (5.75 in.) depth. Some rust pitting occurs along the bar outer surface.

The imprint of a 25 mm (1 in. dia.) smooth dowel bar is along the side of the core at 247.7 mm (9.75 in.) depth. The bar itself was not submitted with the core.

Bottom of the concrete is bonded to an underlying asphaltic concrete. The asphaltic concrete is 25 mm (1 in.) thick. Bottom of the asphaltic concrete has the imprint of an underlying smooth surface, such as a geotextile. The asphaltic concrete has a 12.5 mm (0.5 in) dia. maximum sized, crushed stone as coarse aggregate and a sand as fine aggregate.

Cracks

A few very fine cracks (less than 0.08 mm. wide) occur at the wearing surface and extend vertically into the concrete to a depth of 100 mm. (4.0 in.), where the cracks dissipate. The fine cracks pass both around and through aggregate particles. These cracks may be due to drying shrinkage.

A very fine (less than 0.08 in. wide) horizontal crack occurs at 82.6 mm (3.25 in.) depth. The crack extends almost entirely through the core. The horizontal crack is partially filled with calcium carbonate and ettringite. The crack passes through and around many coarse aggregate particles, possibly suggesting crack formation after the development of some paste-to-aggregate bond, as by alkali-silica reaction.

In general, cracking due to alkali-silica reaction is relatively minor in this core.

Aggregates

Aggregates are similar to those described for Core 4. Aggregate particles are uniformly dispersed throughout the concrete. Maximum aggregate size is measured as 19 mm (0.75 in.). The aggregate is fairly well-graded.

Coarse aggregate is composed of blast furnace slag. The slag is vesicular, coarsely crystalline with a small amount of a very fine-grained matrix. The matrix, which is a minor constituent, is composed of glass (silica). Crystalline components are composed of the melilite, iron oxide, merwinite and pyroxene. The slag aggregate does not exhibit evidence of weathering, but does yield a sulfurous odor when freshly fractured in the concrete.

Coarse aggregate particles are light to dark gray with a few particles greenish gray and tannish gray. Coarse aggregate is hard; porous due to its vesicularity but dense in its matrix; angular; equant shaped and outer surfaces of particles have a rough texture.

There is no evidence of alkali-silica reaction associated with the slag coarse aggregate.

Fine aggregate is natural sand containing a variety of rock and mineral types including, quartz, various types of feldspars, granite, chert, chalcedony, mica, dolomite and other rock and mineral types. With the exception of the chert (which will be described separately), fine aggregate particles are variously colored from white to red to translucent; hard, dense, sub-rounded to well rounded, generally spherical and having a smooth outer surface texture.

Some of the coarser chert particles, particularly in the plus 16 mesh sieve sizes, are beige to white to yellow and contain brown reactions rims along their outer periphery. The chert content appears somewhat lower than in Core 4. The chert particles are sometimes dolomitic, soft, porous and microcracked. Cracks radiate out from only a few of chert particles into nearby paste (Figure 8). These few microcracks are lined with alkali-silica gel. Damage by alkali-silica reaction associated with the chert is fairly isolated in this core.

Cement Paste

Cement paste is similar to that described for Core 4. The cement paste is light-to-medium gray, exhibits a vitreous luster, micro-granular texture, and hackly fracture. The paste is hard, dense and tightly bonded to aggregate particles. Cement paste is carbonated to a depth of 5-to-10 mm below the wearing surface.

Residual cement particles are abundant and somewhat coarse, Residual cement content is estimated to be 10 to 13%, by volume of paste. Calcium hydroxide, a normal hydration product, is estimated to be 10-to-13% by volume of paste, as coarse hexagonal crystals and tablets.

Supplementary cementitious materials are not detected; however, small particles of slag, likely fines from the coarse aggregate (and too coarse for a granulated product) are present in the paste.

Properties of the paste previously described are evaluated to provide an estimate of the water-to-cement ratio. Based on paste properties observed, water-to-cement ratio is estimated to be 0.35-to-0.45.

Air Voids

The concrete contains numerous air-voids, most of which are very fine. The voids are spherical (entrained air) with some larger, irregularly shaped voids, indicative of entrapped air. The concrete is deemed air-entrained.

The air-voids are uniformly dispersed throughout the concrete. There are a few very large voids due to incomplete consolidation, but they are fairly isolated. Air content is estimated to be 3.5 to 4.5%.

Alkali-silica gel, ettringite and calcite are present as fine linings of voids. Secondary deposits do not fill any of the voids in this core, possibly suggesting a lesser amount of moisture migration than in Core 4.

Core 9

General Description

The sample consists of a concrete core identified as “Core 9 Taxiway” (Figure 3). The core is 457.0 mm (18.0 in.) long and has a diameter of 100.0 mm (3.9 in.).

The core top has weathered and worn broom finish, such that fine aggregate particles are partially exposed and polished (Figure 3a). The core bottom is a flat surface with some fine sand adherent and isolated spots of bitumen, possibly representing a bituminous impregnated underlying base course.

The core has partially penetrated an uncorroded, 9.5 mm (0.38 in.) diameter, deformed steel reinforcing bar at 254.0 mm (10.0 in.) depth.

Cracks

Two distinct fine cracks (0.08 mm. to 0.10 mm wide) occur at the wearing surface. At the wearing surface, the cracks are stained gray by secondary calcite deposits and dirt and debris. The cracks extend vertically into the concrete to a depth of 60 mm (2.4 in.), where the cracks dissipate. The fine cracks pass both around and through aggregate particles.

Horizontally oriented, fine (0.10 mm or less dia.) cracks and microcracks are concentrated at 70 to 80 mm (2.7 and 3.0 in.) depth. In addition, several random microcracks occur throughout the core. Crack surfaces are finely coated with alkali-silica gel, as are voids finely lined with alkali-silica gel. The cracks pass through and radiate from several, chert fine aggregate particles containing reaction rims along their outer periphery (Figure 9). Thus, it appears the cracks are due to alkali-silica reaction.

Aggregates

Aggregates are similar to those described for Core 4. Aggregate particles are uniformly dispersed throughout the concrete. Maximum aggregate size is as measured 19 mm (0.75 in.). The aggregate is fairly well-graded.

Coarse aggregate is composed of blast furnace slag. The slag is vesicular, coarsely crystalline with a small amount of a very fine-grained matrix. The matrix, which is a minor constituent, is composed of glass (silica). Crystalline components are composed of the melilite, iron oxide, merwinite and pyroxene. The slag aggregate does not exhibit evidence of weathering, but does yield a sulfurous odor when freshly fractured in the concrete.

Coarse aggregate particles are light to dark gray with a few particles greenish gray and tannish gray. Coarse aggregate is hard; porous due to its vesicularity but dense in its matrix; angular; equant shaped and outer surfaces of particles have a rough texture.

There is no evidence of alkali-silica reaction associated with the slag coarse aggregate.

Fine aggregate is natural sand containing a variety of rock and mineral types including, quartz, various types of feldspars, granite, chert, chalcedony, mica, dolomite and other rock and mineral types. With the exception of the chert (which will be described separately), fine aggregate particles are variously colored from white to red to translucent; hard, dense, sub-rounded to well rounded, generally spherical and having a smooth outer surface texture.

Some of the coarser chert particles, particularly in the plus 16 mesh sieve sizes, are beige to white to yellow and contain brown reactions rims along their outer periphery. The chert particles are sometimes dolomitic, soft, porous and cracked and microcracked. Cracks radiate out from chert particles into nearby paste (Figure 9). These cracks and microcracks are lined with alkali-silica gel. Therefore, damage by alkali-silica reaction associated with the chert is fairly extensive in this core and almost similar to the amount of alkali-silica related damage in Core 4.

Cement Paste

Cement paste is similar to that described for Core 4. The cement paste is medium greenish gray, exhibits a vitreous luster, micro-granular texture, and hackly fracture. The paste is hard, dense and tightly bonded to aggregate particles. Cement paste is carbonated to a depth of 1-to-3 mm below the wearing surface.

Residual cement particles are abundant and somewhat coarse, Residual cement content is estimated to be 10 to 13%, by volume of paste. Calcium hydroxide, a normal hydration product, is estimated to be 10-to-13% by volume of paste, as coarse hexagonal crystals and tablets. Supplementary cementitious materials are not detected; however, small particles of slag, likely fines from the coarse aggregate (and too coarse for a granulated product) are present in the paste.

Properties of the paste previously described are evaluated to provide an estimate of the water-to-cement ratio. Based on paste properties observed, water-to-cement ratio is estimated to be 0.35-to-0.45.

Air Voids

The concrete contains numerous air-voids, most of which are very fine. The voids are spherical (entrained air) with some larger, irregularly shaped voids, indicative of entrapped air. The concrete is deemed air-entrained.

The air-voids are uniformly dispersed throughout the concrete. Air content is estimated to be 3.0 to 4.0%.

Alkali-silica gel, ettringite and calcite are present as fine linings of voids.

Core 12

General Description

The sample consists of a concrete core half identified as “Core 12” (Figure 4). The core half is 343.0 mm (13.5 in.) long and has a core diameter of 100.0 mm (3.9 in.).

The core top has the remnants of broom finish that have been worn away by horizontal wobbling of the core bit before it set into the concrete (Figure 4a). The core bottom is an irregular broken surface within the concrete pavement. The broken surface passes both around and through aggregate particles.

Minor superficially corroded, 9.5 mm (0.38 in.) diameter, deformed steel reinforcing bar is present at 146.0 mm (5.75 in.) depth in the core. Some rust pitting occurs along the bar outer surface.

The imprint of a 12.5 mm (1/2 in. dia.) deformed reinforcing bar is at 205.0 mm (8.0 in.) depth. The bar itself was not submitted with the core. There is a small amount of corrosion product staining a crack surface adjacent to the reinforcing bar. Large voids are also present in the vicinity of the reinforcing bar, suggesting less than optimal consolidation around the reinforcing bar.

Cracks

The core was received with a horizontal crack occurring at 40.0 to 48.0 mm (1.6 to 1.9 in.) depth. The crack has effectively separated the core into two pieces (Figure 4b). Cement paste is carbonated 7.0 mm on either side of the crack surface. The relatively deep paste carbonation suggests the crack did not form recently. The crack surface is coated with drilling fines and alkali-silica gel, as are voids filled with alkali-silica gel adjacent to the crack surface. The crack passes through several fine aggregate particles containing reaction rims along their outer periphery. Thus, it appears the crack is due to alkali-silica reaction.

The core was received with a second horizontal crack occurring at 215.0 to 245.0 mm (8.5 to 9.6 in.) depth. The upper depth is at the approximate bottom of the imprint of the steel reinforcement. The crack has effectively separated the core into two pieces (Figure 4b). Cement paste along the crack surface is carbonated, but too less than 1.0 mm into the adjacent paste. The crack surface is coated with drilling fines and alkali-silica gel, as are voids filled with alkali-silica gel adjacent to the crack surface. The crack passes through several fine aggregate particles containing reaction rims along their outer periphery. This data suggests there may have been some cracking at this depth due to alkali-silica reaction, but also, this is an area of weakness to coring stresses due to the cracking but also due to poor consolidation. With the lack of carbonation, it would appear the core cracked into two pieces during coring.

Aggregates

Aggregates are similar to those described for Core 4. Aggregate particles are uniformly dispersed throughout the concrete. Maximum aggregate size is measured as 19 mm (0.75 in.). The aggregate is fairly well-graded.

Coarse aggregate is composed of blast furnace slag. The slag is vesicular, coarsely crystalline with a small amount of a very fine-grained matrix. The matrix, which is a minor constituent, is composed of glass (silica). Crystalline components are composed of the melilite, iron oxide, merwinite and pyroxene. The slag aggregate does not exhibit evidence of weathering, but does yield a sulfurous odor when freshly fractured in the concrete.

Coarse aggregate particles are light to dark gray with a few particles greenish gray and tannish gray. Coarse aggregate is hard; porous due to its vesicularity but dense in its matrix; angular; equant shaped and outer surfaces of particles have a rough texture.

There is no evidence of alkali-silica reaction associated with the slag coarse aggregate.

Fine aggregate is natural sand containing a variety of rock and mineral types including, quartz, various types of feldspars, granite, chert, chalcedony, mica, dolomite and other rock and mineral types. With the exception of the chert (which will be described separately), fine aggregate particles are variously colored from white to red to translucent; hard, dense, sub-rounded to well rounded, generally spherical and having a smooth outer surface texture.

Some of the coarser chert particles, particularly in the plus 16 mesh sieve sizes, are beige to white to yellow and contain brown reactions rims along their outer periphery. The chert particles are sometimes dolomitic, soft, porous and cracked and microcracked. Cracks and microcracks radiate out from rimmed, chert particles into nearby paste (Figures 10 through 14). These cracks microcracks are lined with alkali-silica gel (Figures 10 through 14). Therefore, damage by alkali-silica reaction is associated with the chert in this core.

Cement Paste

Cement paste is similar to that described for Core 4. The cement paste is light-to-medium gray, exhibits a vitreous luster, micro-granular texture, and hackly fracture. The paste is hard, dense and tightly bonded to aggregate particles. Cement paste is carbonated to a depth of 1-to-5 mm below the wearing surface.

Residual cement particles are abundant and somewhat coarse, Residual cement content is estimated to be 13 to 15%, by volume of paste. Calcium hydroxide, a normal hydration product, is estimated to be 10-to-13% by volume of paste, as coarse hexagonal crystals and tablets. Supplementary cementitious materials are not detected; however, small particles of slag, likely fines from the coarse aggregate (and too coarse for a granulated product) are present in the paste.

Properties of the paste previously described are evaluated to provide an estimate of the water-to-cement ratio. Based on paste properties observed, water-to-cement ratio is estimated to be 0.35-to-0.45.

Air Voids

The concrete contains numerous air-voids, most of which are very fine. The voids are spherical (entrained air) with some larger, irregularly shaped voids, indicative of entrapped air. The concrete is deemed air-entrained.

The air-voids are uniformly dispersed throughout the concrete. There are a some larger voids, particularly around the depth of the steel reinforcement that are deemed due to incomplete consolidation. Air content is estimated to be 3.5 to 4.5%.

Alkali-silica gel, ettringite and calcite are present as fine lining of voids.

Conclusions

Petrographic examination was performed on four (4) concrete cores drilled from pavement slabs at the Detroit Metropolitan Wayne County Airport, Detroit, MI. Alkali-silica reaction was observed in all of the cores as was cracking due to the reaction. The reactive aggregate is a chert in the fine aggregate, particularly plus 16 mesh sieve sizes. The coarse aggregate is a non-reactive blast furnace slag. The degree of damage varied by core location, with Core 4 from Taxiway Alpha exhibiting the highest degree of cracking, followed by Core 9 and then Cores 7 and 12 having slightly less cracking than Core 9, but still showing definitive evidence of damage.



(b) Core top/wearing surface. Scale is in centimeters.



(b) Core side, top is to right. Scale is in inches.

Figure 1. Core 4 as received for petrographic examination.



(a) Core top/wearing surface. Scale is in centimeters.



(b) Core side, top is to left. Scale is in inches.

Figure 2. Core 7 as received for petrographic examination.



(a) Core top/wearing surface. Scale is in centimeters.



(b) Core side, top is to the right. Scale is in inches.

Figure 3. Core 9 as received for petrographic examination.



(a) Core top/wearing surface. Scale is in centimeters.



(b) Core side, top is to left. Scale is in inches.

Figure 4. Core 12 as received for petrographic examination.

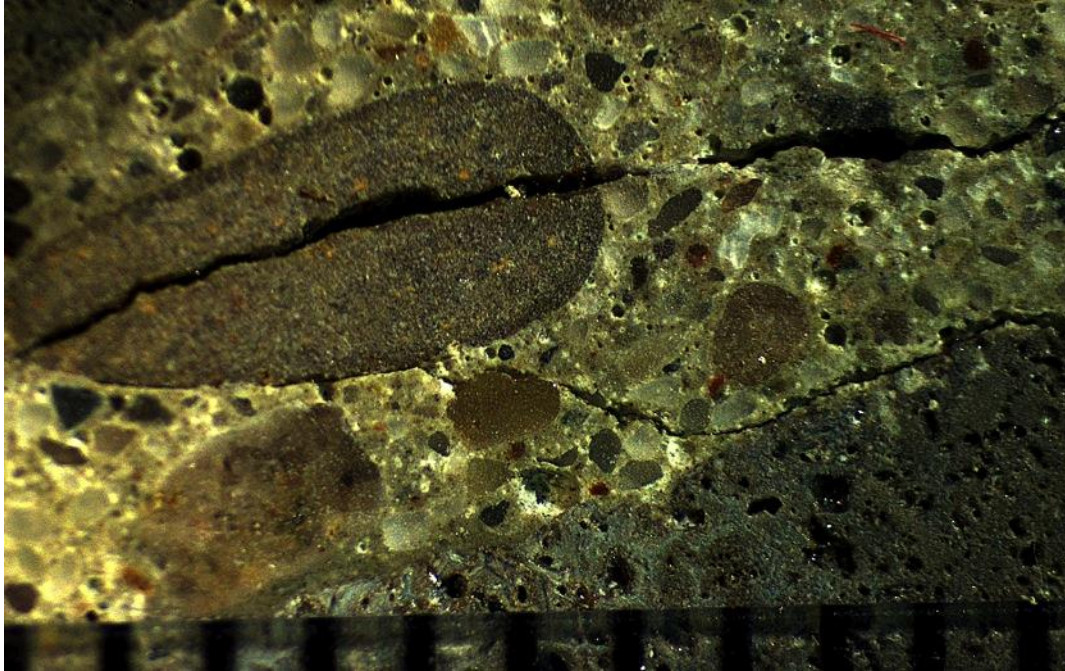


Figure 5. Lapped surface of Core 4 showing horizontal oriented cracking and microcracking. Scale is in millimeters.

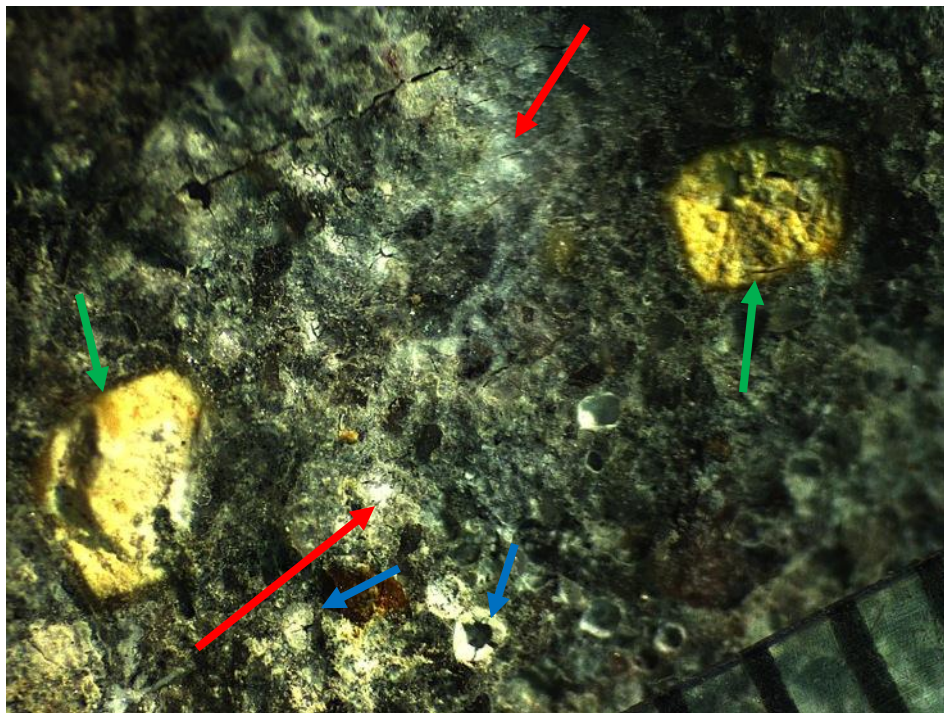


Figure 6. Magnified cracked surface in Core 4 where white alkali-silica gel lines the crack (red arrows) and voids adjacent to the crack (blue arrows). Two beige-yellow, cracked, rimmed and reacting chert particles are present along the crack (green arrows). Scale is in millimeters.



Figure 7. Lapped surface of Core 4 illustrating a crack radiating from a rimmed, beige chert particle (red arrow) into adjacent paste. The crack is filled with white alkali-silica gel (blue arrows). Scale is in millimeters.

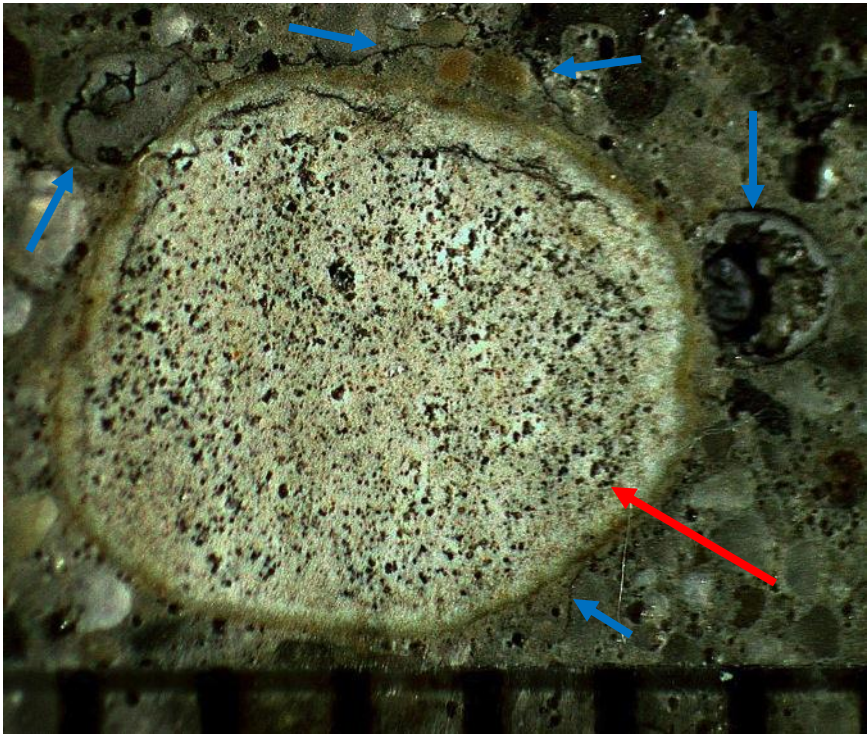


Figure 8. Photomicrograph of the magnified lapped slice of Core 7 showing cracks radiating from a rimmed, beige chert particle (red arrow) into adjacent paste. The crack and adjacent voids are filled with white alkali-silica gel (blue arrows). Scale is in millimeters.



Figure 9. Photomicrograph of Core 9 illustrating a crack radiating from a rimmed chert particle (red arrow) into adjacent paste. The crack is filled with white alkali-silica gel (blue arrows). Scale is in millimeters.

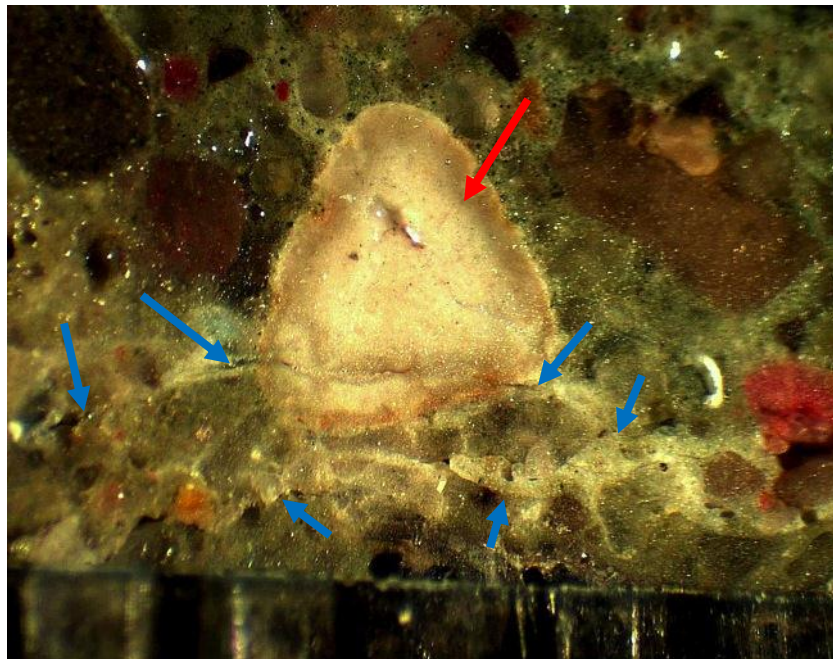


Figure 10. Photomicrograph of Core 12 showing cracks radiating from a rimmed chert particle (red arrow) into adjacent paste. The crack is filled with white alkali-silica gel (blue arrows). Scale is in millimeters.

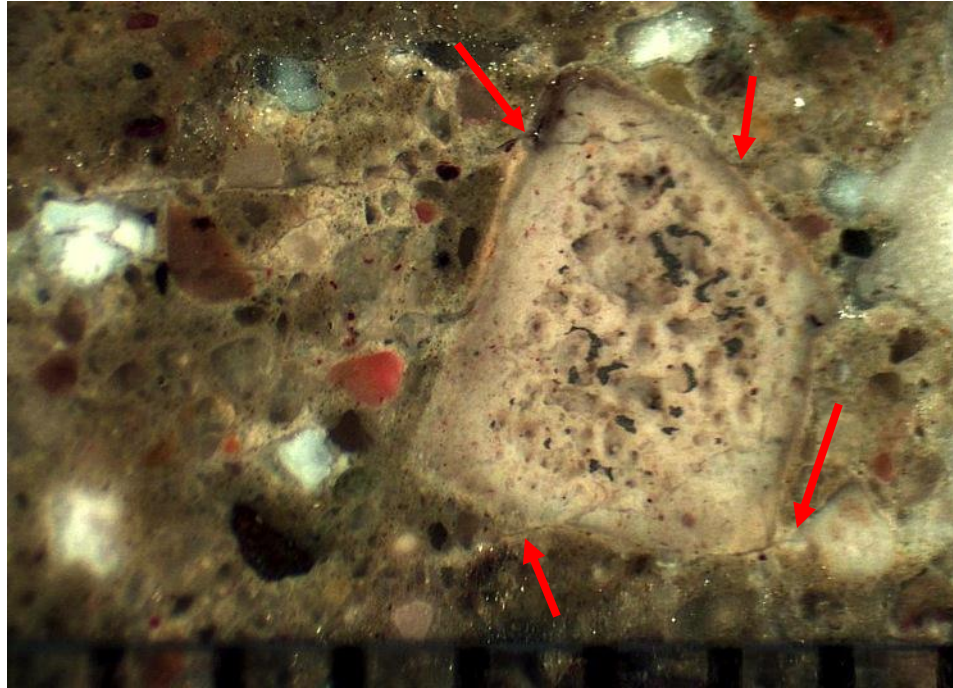


Figure 11. Photomicrograph of Core 12 illustrating cracks radiating out from a rimmed chert aggregate particle into the paste (red arrows). The cracks are lined with alkali-silica gel. Scale is in millimeters.

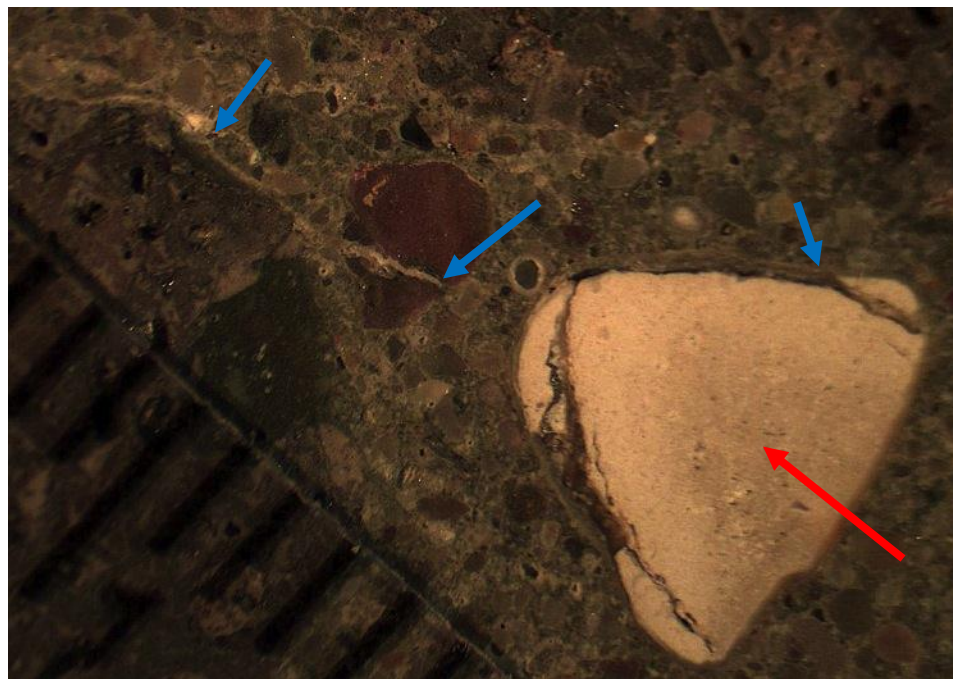


Figure 12. Photomicrograph of Core 12 showing cracks radiating from a rimmed chert particle (red arrow) into adjacent paste. The cracks are filled with white alkali-silica gel (blue arrows). Scale is in millimeters.

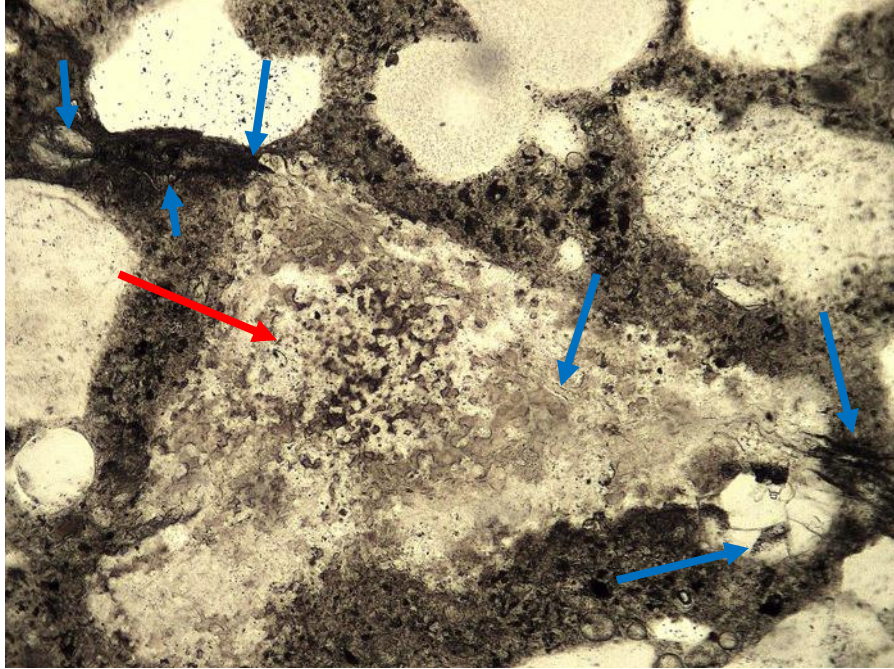


Figure 13. Thin section photomicrograph of Core 12 illustrating a crack radiating out from a chert aggregate particle (red arrow) into the cement paste. The crack and an adjacent void are lined with alkali-silica gel (blue arrows). Vertical field of view is 0.60 mm. Plane-polarized light.

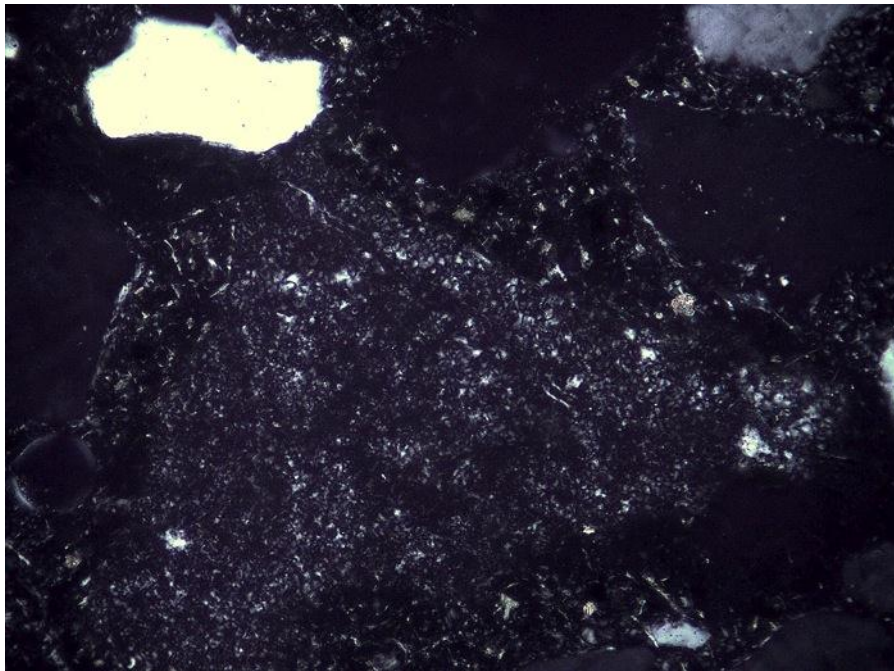


Figure 14. Thin section photomicrograph of Core 12 showing the same view as Figure 13, only in crossed polarized light. Vertical field of view is 0.60 mm.

Airport V

Core Locations

Core locations were selected by Clemson University. Cores were taken by Clemson University. The 6 cores, labeled B-1, F-2, F-3, K-1, R-5 and R-6 (Figures 1 through 6), were received at STS on February 19, 2010. Petrographic examination was requested on each of the cores to determine the cause(s) and extent of cracking, slab movement and other observations pertinent to induced distress mechanisms occurring in the slab.

Results

Subject to the qualifications in the attached Appendix, results of the petrographic examinations are as follows:

1. All six (6) cores exhibit evidence of alkali-silica reaction (ASR) and all but Core F-3 exhibit varying degrees of damage due to ASR. Core F-3 does not exhibit damage by ASR.
2. The relative degree of damage by alkali-silica reaction varies with Core R-5 exhibiting the most cracking; followed by Cores R-6 and B-1, each exhibiting similar amount of damage. Cores F-2 and K-1 exhibit slight damage.
3. The alkali-reactive aggregate components in the cores are granite gneiss comprising the coarse aggregate and chert, which is a minor component of the fine aggregate (Figures 9, 14, 15 and 21 through 24). Strain in the quartz lattice structure of the granite gneiss (due to pressure during metamorphism of the parent granite) is evidenced by undulatory extinction in quartz portions of the gneiss. Metamorphic rocks containing strained quartz are considered slowly reactive with cement alkalies.
4. Composition of the gneiss varies between cores. Cores B-1, R-5 and R-6 contain the pink feldspar mineral orthoclase, indicative of a magma melt that was higher in potassium. These three cores also exhibit the most ASR damage. Cores F-2, F-3 and K-1 lack orthoclase and have a salt and pepper (black and white) coloration. The gneiss in the latter cores contained less potassium in the magma melt. These latter cores exhibited the least to no damage by ASR. Stark and Bhatt⁽¹⁾ and Van Aardt and Visser⁽²⁾ have shown that significant amounts of alkali can be leached from alkali-bearing rocks in a calcium hydroxide (i.e., highly alkaline environment). Petrographic examination cannot discern if alkalies from the orthoclase bearing gneiss is contributing to the ASR damage in Cores B-1, R-5 and R-6.
5. Evidence of deleterious alkali-silica reaction in the cores are cracking and microcracking occurring within rimmed aggregate particles, with cracks radiating out from the reacting particles into adjacent cement paste (Figures 7, 8, 15 and 21 through 14). The cracks and nearby voids are lined to filled with alkali-silica gel and innocuous secondary deposits of

ettringite, calcium carbonate and calcium hydroxide (Figures 7, 8, 10, 19 and 21 through 23).

6. Cores B-1, K-1, R-5 and R-6 contain ground granulated blast furnace slag (GGBFS) as a supplementary cementitious material (Figures 11 and 20). Therefore, it appears the GGBFS in the quantity used has not inhibited expansive alkali-aggregate reaction.
7. Aragonite, a form of calcium carbonate, occurs along the outer fringes of coarse aggregate particles and within coarse aggregate particles at the saw-cut surfaces in Cores F-2, F-3, K-1 and less commonly in Cores R-5 and R-6. It is as if the material has exuded above the surface when moist, but now has dried and hardened (Figure 13). One possible explanation for the abundant occurrence of aragonite could be carbonation of calcium hydroxide that has been observed along aggregate particle margins in thin section of non-exposed concrete.
8. There is an abundance of ettringite lining and filling voids and cracks in all of the cores examined (Figures 7, 12, 16, 19 and 20). This may be an indication of relatively high moisture within the concrete, which is necessary for alkali-silica reaction.
9. All six (6) cores contain what are interpreted to be cracks due to drying shrinkage at the wearing surface. The cracks extend 10 mm (0.4 in.) depth in Core B-1, 45 to 70 mm (1.8 to 2.8 in.) depth in Core F-2, 15 to 20 mm (0.6 to 0.8 in.) depth in Cores F-3 and K-1, 7 to 25 mm (0.3 to 1.0 in.) depth in Core R-5 and 20 to 40 mm (0.8 to 1.6 in.) depth in Core R-7. These drying shrinkage cracks likely allowed easy ingress of moisture and deicer deeper into the pavement, thereby increasing surface area where alkali-silica reactions can take place. Sealing of drying shrinkage cracks (and maintaining a seal) may have lessened the effects of deleterious alkali-silica reaction.
10. Residual acetate deicer has not been identified in cracks and voids of any of the cores.
11. Air-voids are very non-uniformly dispersed throughout the concrete of Cores F-2 and F-3. Some areas contain few to no voids and in other areas that are clusters where the void content appears to be as high as 7% (Figures 16 and 17). Air content is estimated to range from 2.5 to 7.0% in both cores.
12. Air contents are estimated to be somewhat low with respect to freeze-thaw durability in Cores K-1 and R-5.
13. With the exception of light scaling on part of the wearing surface of Core R-5, no other forms of deterioration are detected in the concretes represented by these cores.

Details of the petrographic examinations are provided in the following sections of this report.

Petrographic Examination

Core B-1

General Description

The sample consists of a concrete core half identified as “B-1” (Figure 1). The core is 409.0 mm (16.1 in.) long and has a diameter of 143.0 mm (5.6 in.). The core half was received intact.

The core top or wearing surface is a fairly flat, weathered, finished surface with fine aggregate particles partially exposed. The wearing surface is dirty and cracked. The wearing surface contains random cracks. Immediately adjacent to the crack surfaces are gray calcium carbonate deposits (Figure 1a).

Steel reinforcement is not present in the core half received. The core bottom is the imprint of what appears to be an underlying asphalt treated base course.

Cracks

Cracks at the wearing surface are less than 0.08 mm (0.003 in.) wide and extend to about 10 mm (0.4 in.) depth where they dissipate. The cracks pass around aggregate particles. These surface cracks appear to be due to surficial drying shrinkage.

A relatively small number of random, fine (less 0.08 mm dia.) microcracks occur throughout the core (Figures 7 and 8). The microcracks appear to originate within granite gneiss coarse aggregate particles (Figure 9) and some of the chert fine aggregate particles and radiate out into adjacent paste for a few centimeters. The microcracks and voids intersected by the microcracks are lined with alkali-silica gel (Figure 10). Thus, the microcracks appear to be due to alkali-silica reaction.

Aggregates

Aggregate particles are uniformly dispersed throughout the concrete. Maximum aggregate size is measured as 31 mm (1-1/4 in.). The aggregate is fairly well-graded.

Coarse aggregate is composed of crushed granite gneiss. The granite has, by pressure and temperature, been deformed such that the particles exhibit a gneissic texture. That is, light and dark minerals of the rock have segregated, such that there are linear bands of light minerals and alternating linear bands of dark minerals within the rock. Quartz in the gneiss is highly strained as evidenced by undulatory extinction under cross-polarized light. The crushed particles also have what appears to be reaction rims along their outer periphery.

Coarse aggregate particle color is a mixture of pink, black and white. Coarse aggregate is hard; dense; angular; somewhat elongate to equant shaped and outer surfaces of particles have a rough texture.

Fine aggregate is natural sand containing a variety of rock and mineral types including, quartz, various types of feldspars, granite, quartzite, mica, hornblende, chert and a minor amount of other rock and mineral types. Fine aggregate particles are variously colored from white to red to

translucent; hard, dense, angular to well-rounded, generally spherical and having a smooth outer surface texture.

Cement Paste

The cement paste is beige with an occasional greenish tint. The paste exhibits a vitreous luster, micro-granular texture, and hackly fracture. The paste is hard, dense and tightly bonded to aggregate particles. Cement paste is carbonated to a depth of 1-to-2 mm below the wearing surface.

Residual and relict cement particles are present in a moderate amount, particularly evident are residual belite (dicalcium silicate) clusters with interstitial calcium aluminoferrite, which is typical in well-hydrated concretes. Residual and relict cement particle content is estimated to be 5 to 7%, by volume of paste. Calcium hydroxide, a normal hydration product, is estimated to be 6-to-8% by volume of paste, as coarse hexagonal crystals.

Ground granulated blast furnace slag is present as a supplementary cementitious material. Some of the slag has hydrated into yellowish amorphous relicts in the paste (Figure 11). Residual slag content is estimated to be 20 to 25%, by volume of paste.

Properties of the paste previously described are evaluated to provide an estimate of the water-to-cementitious materials ratio. Based on paste properties observed, water-to-cementitious materials ratio is estimated to be 0.35-to-0.40.

Air Voids

The concrete contains numerous air-voids, most of which are very fine. The voids are spherical (entrained air) with few larger, irregularly shaped voids, indicative of entrapped air. The concrete is deemed air-entrained.

The air-voids are uniformly dispersed throughout the concrete. Air content is estimated to be 4.5 to 5.5%.

Ettringite lines many of the voids (Figure 12).

Core F-2

General Description

The sample consists of a concrete core half identified as “F-2” (Figure 2). The core is 417.0 mm (16.4 in.) long and has a diameter of 143.0 mm (5.6 in.). The core half was received intact.

The core top or wearing surface is a fairly flat, weathered, finished surface with fine aggregate particles partially exposed. The wearing surface contains random, fine cracks. Immediately adjacent to the crack surfaces are gray calcium carbonate deposits (Figure 2a).

Steel reinforcement is not present in the core half received. The core bottom is the imprint of what appears to be an underlying asphalt treated base course.

Along the “as-received” saw cut surface white deposits are observed growing out of the coarse aggregate particles (Figure 13). These deposits have been optically identified as aragonite.

Cracks

Cracks at the wearing surface are 0.08 to 0.1 mm (0.003 to 0.004 in.) wide and extend 45 to 70 mm (1.8 to 2.8 in.) depth where they terminate in granite gneiss coarse aggregate particles (Figure 14). The cracks pass both around and through aggregate particles. These cracks are lined only with dirt, debris and a small amount of calcium carbonate.

A relatively small number of random and horizontal trending, fine (less 0.08 mm dia.) microcracks occur throughout the core (Figure 15). The microcracks are primarily in the top 50 mm (2.0 in.) of the concrete slab. The microcracks pass around and through granite gneiss coarse aggregate particles and fine aggregate particles. The microcracks and voids immediately adjacent to the microcracks are lined intermittently with ettringite. No alkali-silica gel is detected associated with the cracks.

Aggregates

Aggregate particles are uniformly dispersed throughout the concrete. Maximum aggregate size is measured as 31 mm (1-1/4 in.). The aggregate is fairly well-graded.

Aggregates are similar to those described for Core B-1; however, the granite gneiss is nearly white and black with virtually no pink colored feldspars. This indicates the original granite was poor in the feldspar mineral orthoclase and the magma melt was lower in potassium than the gneiss represented in Core B-1.

Along the outer fringes of coarse aggregate particles at the saw-cut surface is a white deposit that has exuded above the surface and is now dry and hardened. The deposit has been optically identified as aragonite, a form of calcium carbonate, which could be due to carbonation of calcium hydroxide observed along aggregate particle margins in thin section of non-exposed concrete.

Cement Paste

The cement paste is medium gray. The paste exhibits a subvitreous luster, micro-granular texture, and hackly fracture. The paste is hard, dense and tightly bonded to aggregate particles. Cement paste is carbonated to a depth of 1 mm below the wearing surface.

Residual and relict cement particles are present in a moderate amount, particularly evident are residual belite (dicalcium silicate) clusters with interstitial calcium aluminoferrite, which is typical in well-hydrated concretes. Residual and relict cement particle content is estimated to be 12 to 15%, by volume of paste.

Calcium hydroxide, a normal hydration product, is estimated to be 9-to-12% by volume of paste, as coarse hexagonal crystals. Calcium hydroxide is particularly abundant along the outer fringes of aggregate particles and has carbonated to calcium carbonate along the “as-received” saw cut core surface. Some ettringite is also seen along aggregate fringes. Ground granulated blast furnace slag is not present in this core half.

Properties of the paste previously described are evaluated to provide an estimate of the water-to-cement ratio. Based on paste properties observed, water-to-cement ratio is estimated to be 0.35-to-0.40.

Air Voids

The concrete contains primarily clusters of air-voids, most of which are very fine. The voids are spherical (entrained air) with few larger, irregularly shaped voids, indicative of entrapped air. The concrete is deemed air-entrained.

Some areas contain few to no voids and in other areas are clusters where the void content appears to be as high as 7% (Figures 16 and 17). The air-voids are very non-uniformly dispersed throughout the concrete. Air content is estimated to be 2.5 to 7.0%.

Ettringite lines most of the voids (Figure 17).

Core F-3

General Description

The sample consists of a concrete core half identified as “F-3” (Figure 3). The core is 408.0 mm (16.0 in.) long and has a diameter of 145.5 mm (5.7 in.). The core half was received intact.

The core top or wearing surface is a fairly flat, weathered, finished surface with fine aggregate particles partially exposed. The wearing surface contains random, fine cracks. The surface has been spray painted orange.

Steel reinforcement is not present in the core half received. The core bottom is the imprint of what appears to be an underlying asphalt treated base course.

Cracks

Cracks at the wearing surface are 0.08 mm (0.003 in.) wide and extend 15 to 20 mm (0.6 to 0.8 in.) depth where they dissipate in cement paste. The cracks pass both around and through aggregate particles. These cracks are not lined with any secondary deposits. The cracks appear to be due to drying shrinkage.

No other cracks are detected in the body of the core.

Aggregates

Aggregate particles are uniformly dispersed throughout the concrete. Maximum aggregate size is measured as 31 mm (1-1/4 in.). The aggregate is fairly well-graded.

Aggregates are very similar to those described for Core B-1; however, the granite gneiss is nearly white and black with virtually no pink colored feldspars. This indicates the original granite was poor in the feldspar mineral orthoclase and the magma melt was lower in potassium than the gneiss represented in Core B-1.

As in Core F-2, along the outer fringes of coarse aggregate particles at the saw-cut surface is a white deposit that has exuded above the surface and is now dry and hardened. The deposit has been optically identified as aragonite, a form of calcium carbonate, which could be due to carbonation of calcium hydroxide observed along aggregate particle margins in thin section of non-exposed concrete.

Alkali-silica gel soaked paste is immediately adjacent to a few of the rimmed coarse aggregate particles, but there is no damage associated with the gel.

Cement Paste

The cement paste is medium gray. The paste exhibits a subvitreous luster, micro-granular texture, and hackly fracture. The paste is hard, dense and tightly bonded to aggregate particles. Cement paste is carbonated to a depth of 1 to 3 mm below the wearing surface.

Residual and relict cement particles are present in a moderate amount, particularly evident are residual belite (dicalcium silicate) clusters with interstitial calcium aluminoferrite, which is typical in well-hydrated concretes. Residual and relict cement particle content is estimated to be 10 to 13%, by volume of paste.

Calcium hydroxide, a normal hydration product, is estimated to be 9-to-12% by volume of paste, as coarse hexagonal crystals. Calcium hydroxide is particularly abundant along the outer fringes of aggregate particles and has carbonated to calcium carbonate along the “as-received” saw cut core surface. Some ettringite is also seen along aggregate fringes.

Ground granulated blast furnace slag is not present.

Properties of the paste previously described are evaluated to provide an estimate of the water-to-cement ratio. Based on paste properties observed, water-to-cement ratio is estimated to be 0.35-to-0.40.

Air Voids

The concrete contains primarily clusters of air-voids, most of which are very fine. The voids are spherical (entrained air) with few larger, irregularly shaped voids, indicative of entrapped air. The concrete is deemed air-entrained.

Some areas contain few to no voids and in clusters void content appears to be as high as 7%. The air-voids are very non-uniformly dispersed throughout the concrete. Air content is estimated to be 2.5 to 7.0%.

Ettringite lines most of the voids.

Core K-1

General Description

The sample consists of a concrete core half identified as “K-1” (Figure 4). The core is 56.0 mm (2.2 in.) long and has a diameter of 145.5 mm (5.7 in.). The core half was received intact.

The core top or wearing surface is a fairly flat, weathered, finished surface with fine aggregate particles partially exposed. The wearing surface contains random cracks (Figure 4a). Immediately adjacent to crack surfaces are gray calcium carbonate deposits (Figure 4a).

Steel reinforcement is not present in the core half received. The core bottom is a smooth sawn surface.

Cracks

Cracks at the wearing surface are 0.1 to 0.25 mm (0.004 to 0.01 in.) wide and extend 15 to 20 mm (0.6 to 0.8 in.) depth where they dissipate in cement paste. The cracks pass both around and through aggregate particles. These cracks are lined only with dirt, debris and a small amount of calcium carbonate (Figure 18). No alkali-silica gel is detected associated with the cracks. Paste adjacent to the cracks is carbonated, possibly suggesting the cracks did not form recently.

The concrete contains numerous random microcracks in the body of the core (Figure 18). The microcracks appear to originate within granite gneiss coarse aggregate particles and some of the chert fine aggregate particles and radiate out into adjacent paste for a few centimeters. Thus, the microcracks appear to be due to alkali-silica reaction.

Aggregates

Aggregate particles are uniformly dispersed throughout the concrete. Maximum aggregate size is measured as 31 mm (1-1/4 in.). The aggregate is fairly well-graded.

Aggregates are very similar to those described for Core B-1; however, the granite gneiss is nearly white and black with virtually no pink colored feldspars. This indicates the original granite was poor in the feldspar mineral orthoclase and the magma melt was lower in potassium than the gneiss represented in Core B-1.

As in Cores F-2 and F-3, along the outer fringes of coarse aggregate particles at the saw-cut surface is a white deposit that has exuded above the surface and is now dry and hardened. The deposit has been optically identified as aragonite, a form of calcium carbonate, which could be due to carbonation of calcium hydroxide observed along aggregate particle margins in a thin section of non-exposed concrete.

Alkali-silica gel soaked paste is immediately adjacent to a few of the rimmed coarse aggregate particles, a few chert fine aggregate particles and lining some voids, but there is no damage associated with the gel.

Cement Paste

The cement paste is light to medium gray. The paste exhibits a subvitreous luster, micro-granular texture, and hackly fracture. The paste is hard, dense and tightly bonded to aggregate particles. Cement paste is carbonated to a depth of 1 to 2 mm below the wearing surface.

Residual and relict cement particles are present in a moderate amount, particularly evident are residual belite (dicalcium silicate) clusters with interstitial calcium aluminoferrite, which is typical in well-hydrated concretes. Residual and relict cement particle content is estimated to be 8 to 12%, by volume of paste.

Calcium hydroxide, a normal hydration product, is estimated to be 10-to-15% by volume of paste, as coarse hexagonal crystals. Calcium hydroxide is particularly abundant along the outer fringes of aggregate particles and has carbonated to calcium carbonate along the “as-received” saw cut core surface. Some ettringite is also seen along aggregate fringes.

Ground granulated blast furnace slag is present as a supplementary cementitious material. Some of the slag has hydrated into yellowish amorphous relicts in the paste (Figure 19). Residual slag content is estimated to be 5 to 10%, by volume of paste.

Properties of the paste previously described are evaluated to provide an estimate of the water-to-cementitious materials ratio. Based on paste properties observed, water-to-cementitious materials ratio is estimated to be 0.35-to-0.40.

Air Voids

The concrete contains voids that are spherical (entrained air) with few larger, irregularly shaped voids, indicative of entrapped air. The concrete is deemed air-entrained.

Some areas contain few to no voids, but in general, the air content is low. Thus, air-voids are very non-uniformly dispersed throughout the concrete. Air content is estimated to be 0.5 to 3.0%.

Ettringite lines many of the voids (Figures 19 and 20).

Core R-5

General Description

The sample consists of a concrete core half identified as “R-5” (Figure 5). The core is 413.0 mm (16.3 in.) long and has a diameter of 143.5 mm (5.6 in.). The core half was received intact.

The core top or wearing surface is a fairly flat, weathered surface having the remnants of a broom finish with fine aggregate particles partially exposed and some very light scaling of surface mortar. The wearing surface contains map and random cracks (Figure 5a).

Steel reinforcement is not present in the core half received. The core bottom is the imprint of what appears to be an underlying asphalt treated base course.

Cracks

Cracks at the wearing surface are 0.1 to 0.25 mm (0.004 to 0.01 in.) wide and extend 7 to 25 mm (0.3 to 1.0 in.) depth where they dissipate in cement paste and occasionally into rimmed coarse aggregate particles. The cracks pass both around and through aggregate particles. These cracks are lined only with a black substance, dirt, debris and a small amount of calcium carbonate. No alkali-silica gel is detected associated with the cracks. Paste adjacent to the cracks is carbonated, possibly suggesting the cracks did not form recently.

The concrete contains numerous random and horizontal microcracks in the body of the core, many of which radiate out of rimmed coarse aggregate particles and chert fine aggregate particles into the adjacent paste for up to several inches (Figures 21 and 22). Alkali-silica gel

lines many of the microcracks. Thus, the cracking appears to be due to alkali-silica reaction, although some of the surface cracks could be due to minor surficial drying shrinkage.

Aggregates

Aggregate particles are not uniformly dispersed throughout the concrete. The top 25 mm (1 in.) of the slab is devoid of coarse aggregate, suggesting high vibration levels during consolidation. Maximum aggregate size is measured as 31 mm (1-1/4 in.). The aggregate is fairly well graded.

Aggregates are very similar to those described for Core B-1, and therefore, orthoclase (and pink color of the gneiss) is more prominent in the coarse aggregate of this core. Unlike Cores F-2 and F-3, there are only a few white, aragonite deposits along the outer fringes of coarse aggregate particles.

Alkali-silica gel lined voids are immediately adjacent to a few of the rimmed coarse aggregate particles.

Cement Paste

The cement paste is light to medium gray. The paste exhibits a subvitreous luster, micro-granular texture, and hackly fracture. The paste is hard, dense and tightly bonded to aggregate particles. Cement paste is carbonated to a depth of 1 to 2 mm below the wearing surface.

Residual and relict cement particles are present in a moderate amount, particularly evident are residual belite (dicalcium silicate) clusters with interstitial calcium aluminoferrite, which is typical in well-hydrated concretes. Residual and relict cement particle content is estimated to be 10 to 12%, by volume of paste.

Calcium hydroxide, a normal hydration product, is estimated to be 8-to-10% by volume of paste, as coarse hexagonal crystals. Calcium hydroxide is particularly abundant along the outer fringes of aggregate particles and has carbonated to calcium carbonate along the “as-received” saw cut core surface. Some ettringite is also seen along aggregate fringes.

Ground granulated blast furnace slag is present as a supplementary cementitious material. Some of the slag has hydrated into yellowish amorphous relicts in the paste. Residual slag content is estimated to be 8 to 12%, by volume of paste.

Properties of the paste previously described are evaluated to provide an estimate of the water-to-cementitious materials ratio. Based on paste properties observed, water-to-cementitious materials ratio is estimated to be 0.35-to-0.40.

Air Voids

The concrete contains voids that are spherical (entrained air) with few larger, irregularly shaped voids, indicative of entrapped air. The concrete is deemed air-entrained.

Some areas contain few voids, but in general, the air content is marginally low. Thus, air-voids are very non-uniformly dispersed throughout the concrete. Air content is estimated to be 2.0 to 4.5%.

Ettringite lines many of the voids.

Core R-6

General Description

The sample consists of a concrete core half identified as “R-6” (Figure 6). The core is 406.5 mm (16.0 in.) long and has a diameter of 143.5 mm (5.6 in.). The core half was received intact.

The core top or wearing surface is a fairly flat, weathered surface having the remnants of a deep broom finish with fine aggregate particles partially exposed. The wearing surface contains random cracks (Figure 6a). The core bottom is a flat sawn surface.

Steel reinforcement is present in the core half received. A 12.7 mm (1/2 in.) diameter, smooth surfaces reinforcing bar extends nearly vertically through the core (Figure 6c). The vertical bar is intersected by two 9.5 mm (3/8 in.) diameter, smooth surfaced reinforcing bars oriented horizontally in the core at 230 mm (9 in.) depth. None of the reinforcement is corroded.

Cracks

Cracks at the wearing surface are 0.3 to 0.4 mm (0.01 to 0.02 in.) wide and extend 20 to 40 mm (0.8 to 1.6 in.) depth where they primarily terminate in rimmed coarse aggregate particles, although a few dissipate in cement paste. The cracks pass both around and through aggregate particles. These cracks are lined only with a black substance, dirt, debris and a small amount of calcium carbonate. Alkali-silica gel is present in the deeper reaches of these cracks.

The concrete contains numerous random and horizontal microcracks in the body of the core, many of which radiate out of rimmed coarse aggregate particles and chert fine aggregate particles into the adjacent paste for up to several inches (Figures 23 and 24). Alkali-silica gel lines many of the microcracks and voids adjacent to microcracks and rimmed coarse aggregate particles and chert fine aggregate particles. Thus, the cracking appears to be due to alkali-silica reaction, although some of the surface cracks could be due to minor surficial drying shrinkage.

Aggregates

Aggregate particles are uniformly dispersed throughout the concrete. Maximum aggregate size is measured as 31 mm (1-1/4 in.). The aggregate is fairly well-graded.

Aggregates are very similar to those described for Core B-1, and therefore, orthoclase (and pink color of the gneiss) is more prominent in the coarse aggregate of this core. Unlike Cores F-2 and F-3, there are only a few white, aragonite deposits along the outer fringes of coarse aggregate particles.

Alkali-silica gel lined voids are immediately adjacent to a many of the rimmed coarse aggregate particles and chert fine aggregate particles.

Cement Paste

The cement paste is light gray. The paste exhibits a subvitreous luster, micro-granular texture, and hackly fracture. The paste is hard, dense and tightly bonded to aggregate particles. Cement paste is carbonated to a depth of 1 to 2 mm below the wearing surface.

Residual and relict cement particles are present in a moderate amount, particularly evident are residual belite (dicalcium silicate) clusters with interstitial calcium aluminoferrite, which is typical in well-hydrated concretes. Residual and relict cement particle content is estimated to be 8 to 10%, by volume of paste.

Calcium hydroxide, a normal hydration product, is estimated to be 10-to-12% by volume of paste, as coarse hexagonal crystals. Calcium hydroxide is particularly abundant along the outer fringes of aggregate particles and has carbonated to calcium carbonate along the “as-received” saw cut core surface. Some ettringite is also seen along aggregate fringes.

Ground granulated blast furnace slag is present as a supplementary cementitious material. Some of the slag has hydrated into yellowish amorphous relicts in the paste. Residual slag content is estimated to be 20 to 25%, by volume of paste.

Properties of the paste previously described are evaluated to provide an estimate of the water-to-cementitious materials ratio. Based on paste properties observed, water-to-cementitious materials ratio is estimated to be 0.35-to-0.40.

Air Voids

The concrete contains voids that are spherical (entrained air) with few larger, irregularly shaped voids, indicative of entrapped air. The concrete is deemed air-entrained.

Air-voids are uniformly dispersed throughout the concrete. Air content is estimated to be 4.5 to 6.0%.

Alkali-silica gel and ettringite line many of the voids.

Conclusions

Petrographic examination was performed on six (6) concrete cores drilled from pavement slabs at the Raleigh Durham International Airport, Morrisville, NC. Evidence of alkali-silica reaction was observed in all six (6) cores examined. Cracking damage and indications of expansion due to the reaction were detected in all cores except Core B-1. The reactive aggregate is granite gneiss comprising the coarse aggregate and chert, which is a minor component of the fine aggregate. The degree of damage varied by core location, with Core R-5 exhibiting the most cracking; followed by Cores R-6 and B-1, each exhibiting similar amount of damage and Cores F-2 and K-1 exhibit only slight damage.

References

- (1) Stark, D. and Bhatta, M. S. Y., "Alkali-Silica Reactivity: Effect of Alkali in Aggregate on Expansion," Alkalies in Concrete, ASTM STP-930, ASTM, Philadelphia, PA, pp. 16-30, (1986).
- (2) Van Aardt, J. H. P. and Visser, S., "Calcium Hydroxide Attack on Feldspars and Clays: Possible Relevance to Cement-Aggregate Reactions," Cement and Concrete Research, Vol. I, No. 6, pp. 643-648, (1977).



(c) Core top/wearing surface. Scale is in inches and centimeters.



(d) Core outside, top is to left. Scale is in inches.



(e) Core inside, top is to left. Scale is in inches.

Figure 1. Core B-1 as received for petrographic examination.



(a) Core top/wearing surface. Scale is in inches and centimeters.



(b) Core outside, top is to left. Scale is in inches.



(c) Core inside, top is to left. Scale is in inches.

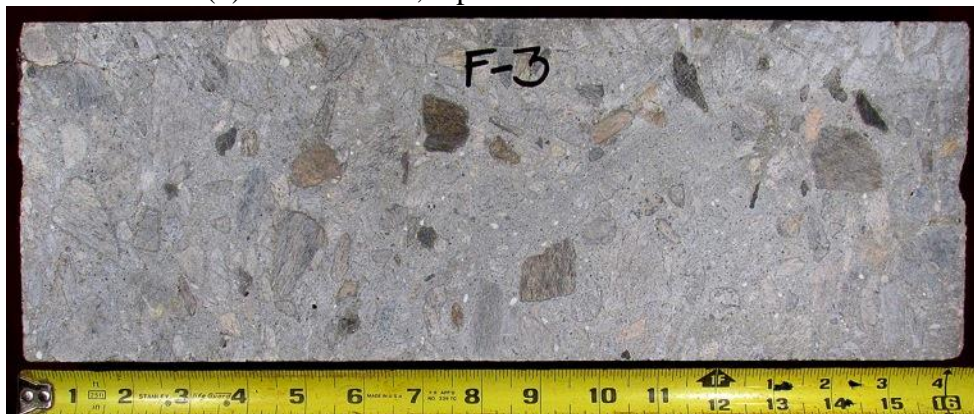
Figure 2. Core F-2 as received for petrographic examination.



(a) Core top/wearing surface. Scale is in centimeters.



(b) Core outside, top is to left. Scale is in inches.



(c) Core inside, top is to the left. Scale is in inches.

Figure 3. Core F-3 as received for petrographic examination.



(b) Core top/wearing surface. Scale is in centimeters.



(c) Core side, core top is toward the top of the photograph. Scale is in inches.

Figure 4. Core K-1 received for petrographic examination.



(a) Core top/wearing surface. Scale is in centimeters.



(b) Core outside, top is to left. Scale is in inches.



(c) Core inside, top is to the right. Scale is in inches.

Figure 5. Core R-5 as received for petrographic examination.



(a) Core top/wearing surface. Scale is in centimeters.



(b) Core outside, top is to left. Scale is in inches.



(c) Core inside, top is to the right. Scale is in inches.

Figure 6. Core R-6 as received for petrographic examination.

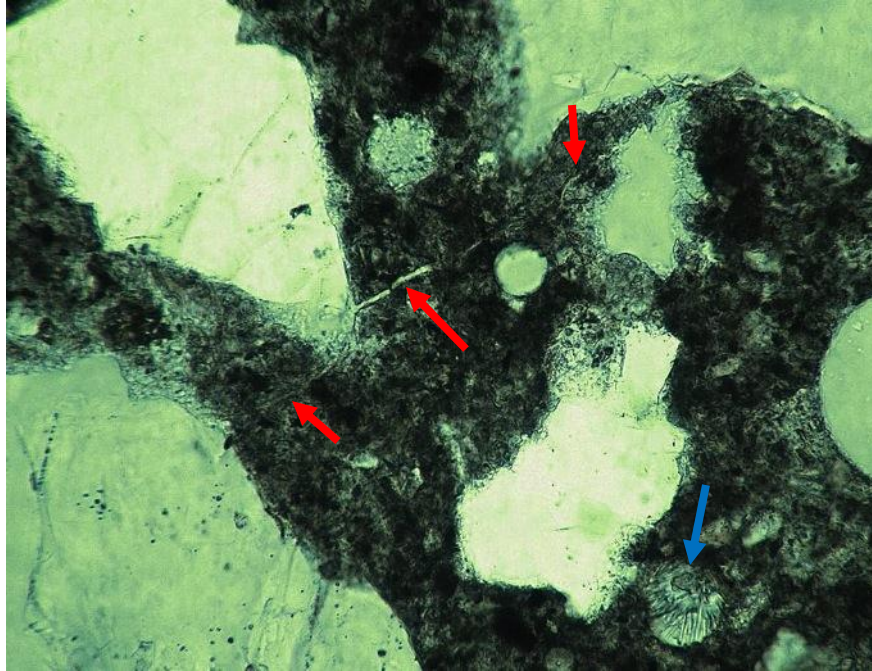


Figure 7. Thin section photomicrograph of a portion Core B-1 where alkali-silica gel lines a crack (red arrows) and a void is filled with ettringite (blue arrows). Vertical field of view is 0.60 mm. Plane-polarized light.

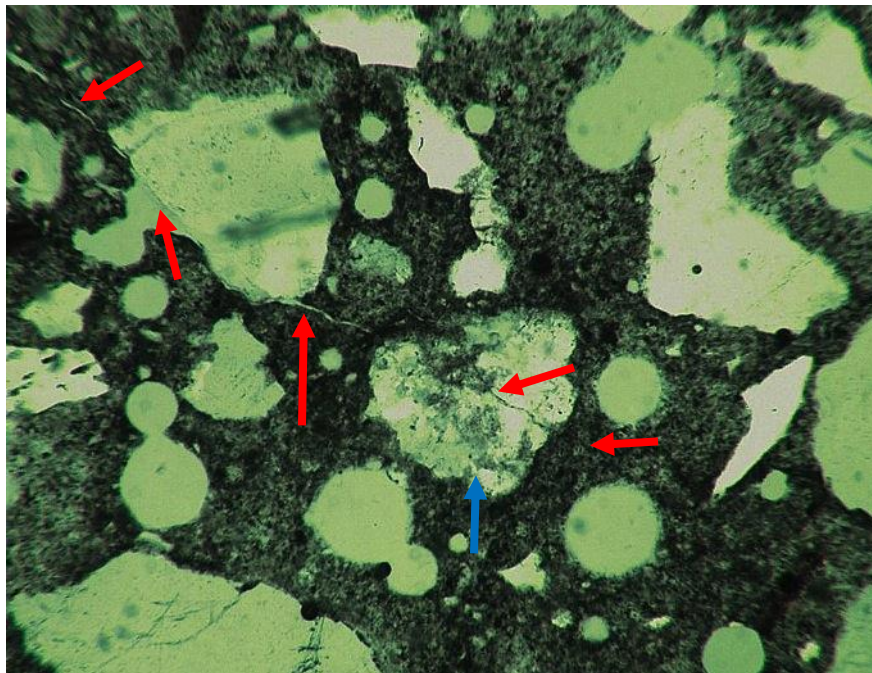


Figure 8. Thin section photomicrograph of a portion Core B-1 where alkali-silica gel lines a crack (red arrows) and the crack radiates out from a reacting particle (blue arrow). Vertical field of view is 1.1 mm. Plane-polarized light.



Figure 9. Photomicrograph of Core B-1 illustrating a rimmed gneiss particle (red arrow). Scale is in millimeters.

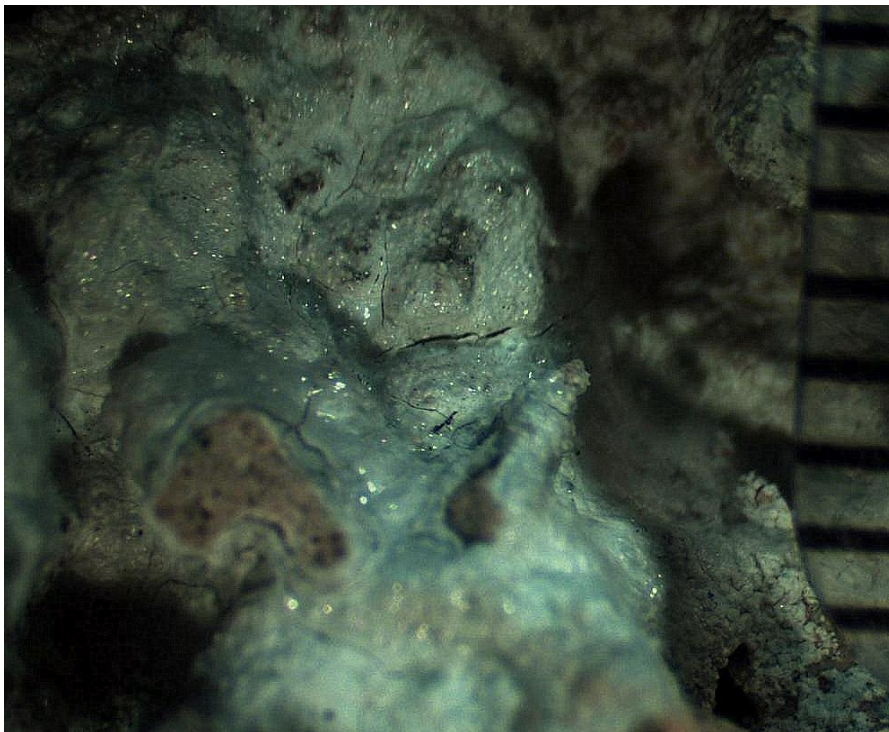


Figure 10. Alkali-silica gel lining an entrapped air void of Core B-1. Scale is in millimeters.

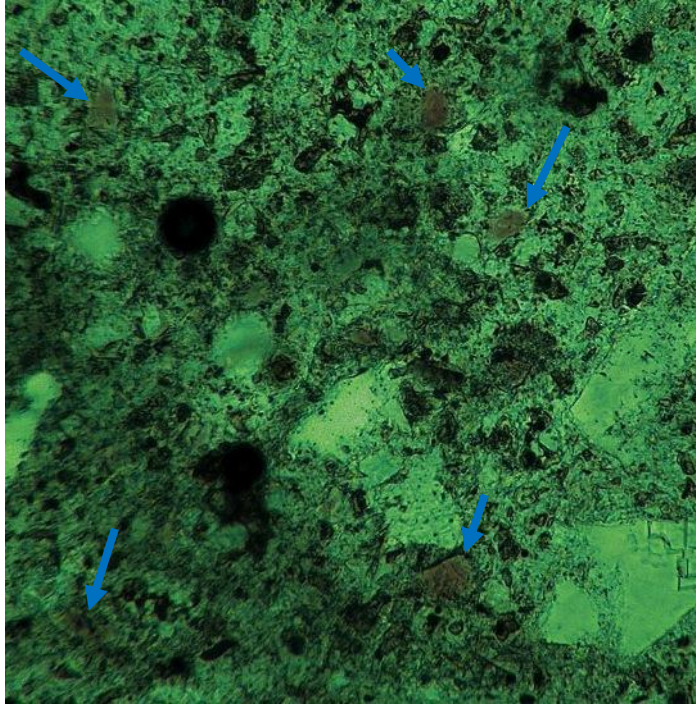


Figure 11. Thin section photomicrograph of a portion Core B-1 illustrating brown slag relicts (blue arrows). Vertical field of view is 0.60 mm. Plane-polarized light.

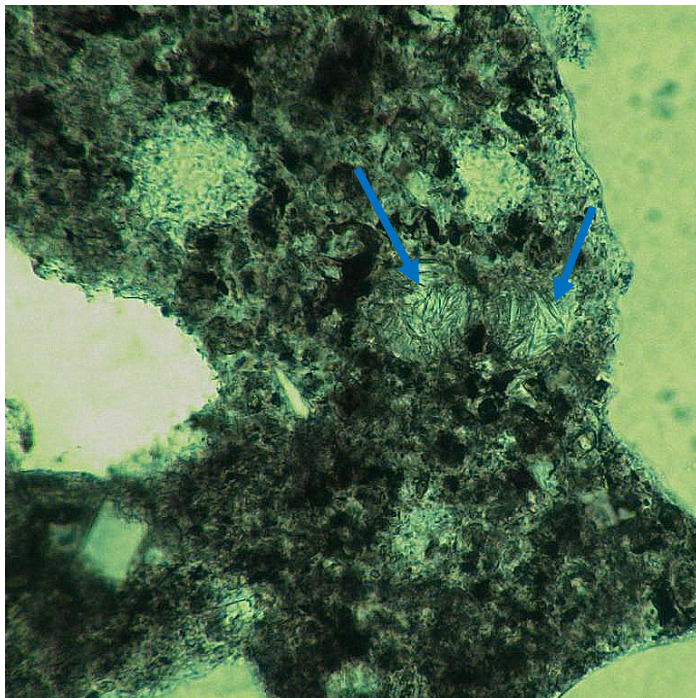


Figure 12. Thin section photomicrograph of a portion Core B-1 showing voids filled with ettringite (blue arrows). Vertical field of view is 0.60 mm. Plane-polarized light.

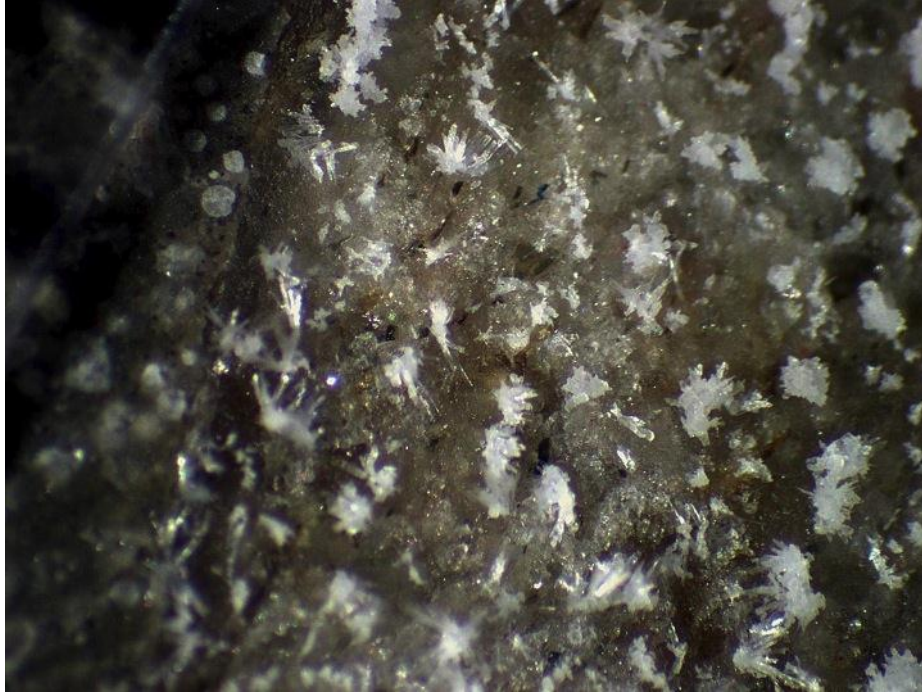


Figure 13. Photomicrograph of Core F-2 illustrating aragonite crystals growing out of a granite gneiss particle along a sawn surface. Scale is in millimeters.

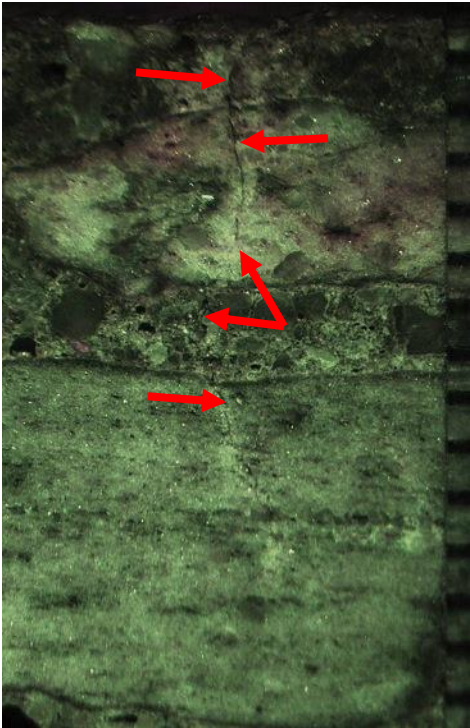


Figure 14. Photomicrograph of Core F-2 illustrating a surface crack extending through two rimmed gneiss particles (red arrows). Scale is in millimeters.

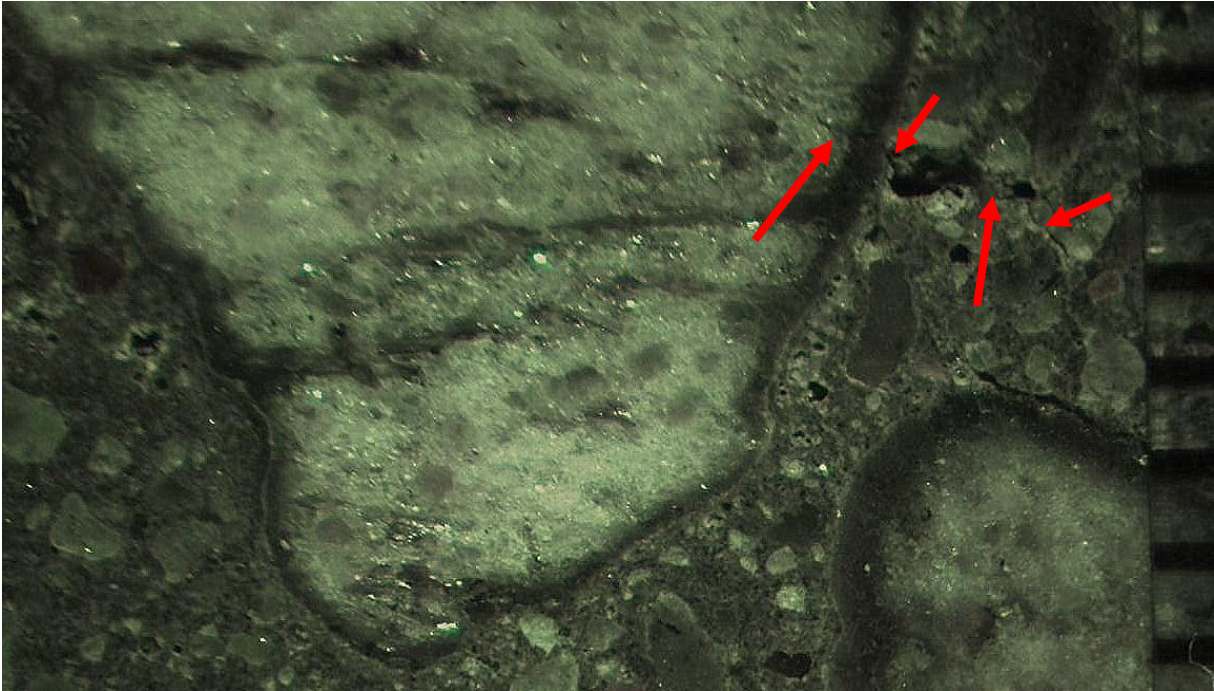


Figure 15. Photomicrograph of Core F-2 showing a cracked and rimmed gneiss particle with the crack radiating into adjacent paste (red arrows). Scale is in millimeters.



Figure 16. Photomicrograph of Core F-2 illustrating air-void clusters (within red circles) and ettringite filled voids (red arrows). Scale is in millimeters.

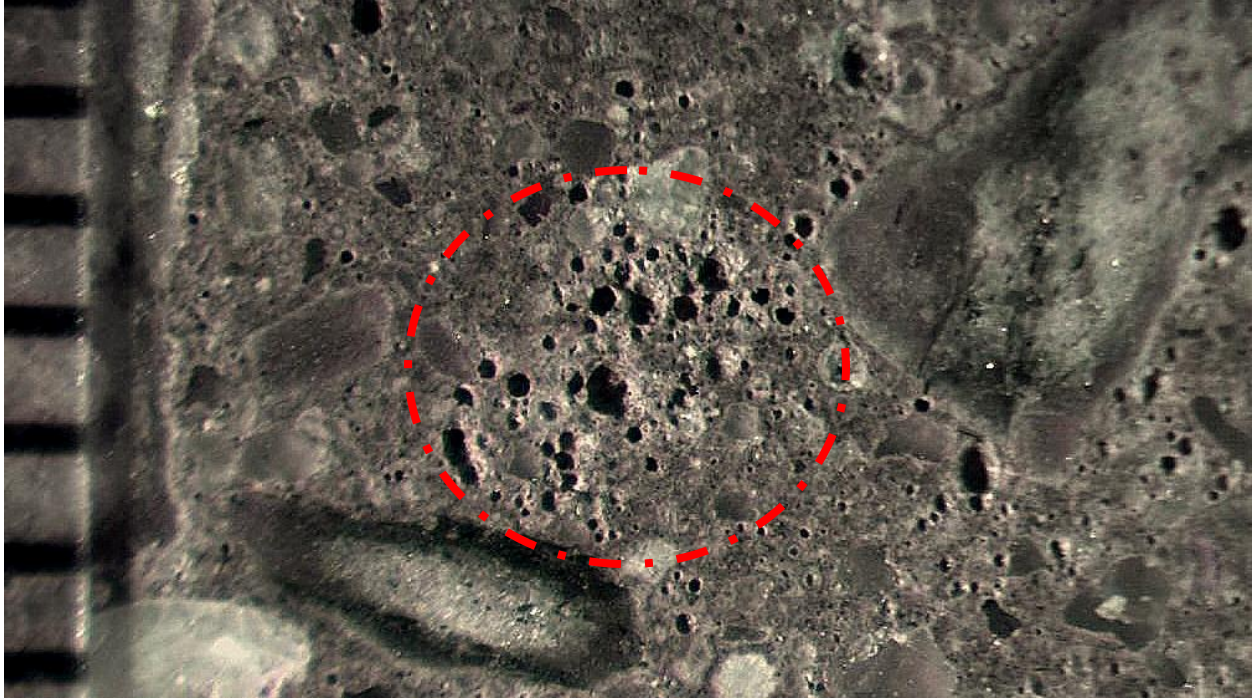


Figure 17. Photomicrograph of Core F-2 illustrating air-void clusters (within red dashed circle). Scale is in millimeters.

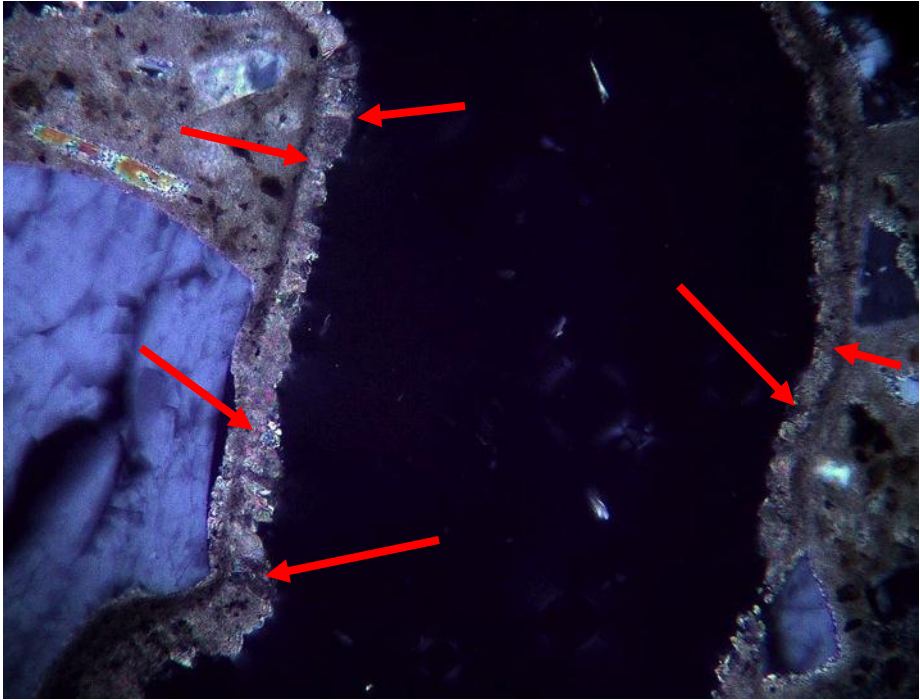


Figure 18. Thin section photomicrograph of Core K-1 along a crack extending down from the pavement wearing surface. The crack is lined with calcite (red arrows). Vertical field of view is 0.60 mm. Cross-polarized light.

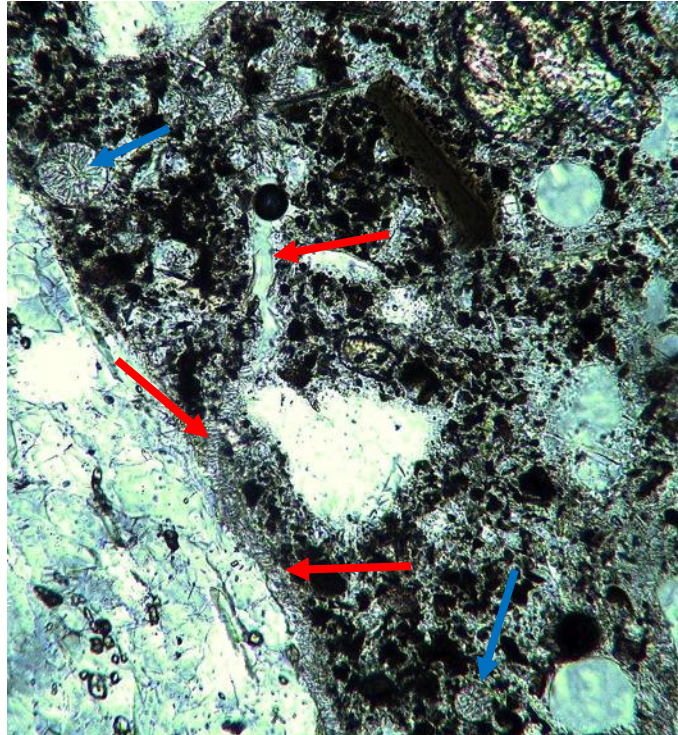


Figure 19. Thin section photomicrograph of Core K-1 showing a microcrack (red arrows) and voids lined to filled with ettringite (blue arrows). Vertical field of view is 0.60 mm. Plane-polarized light.

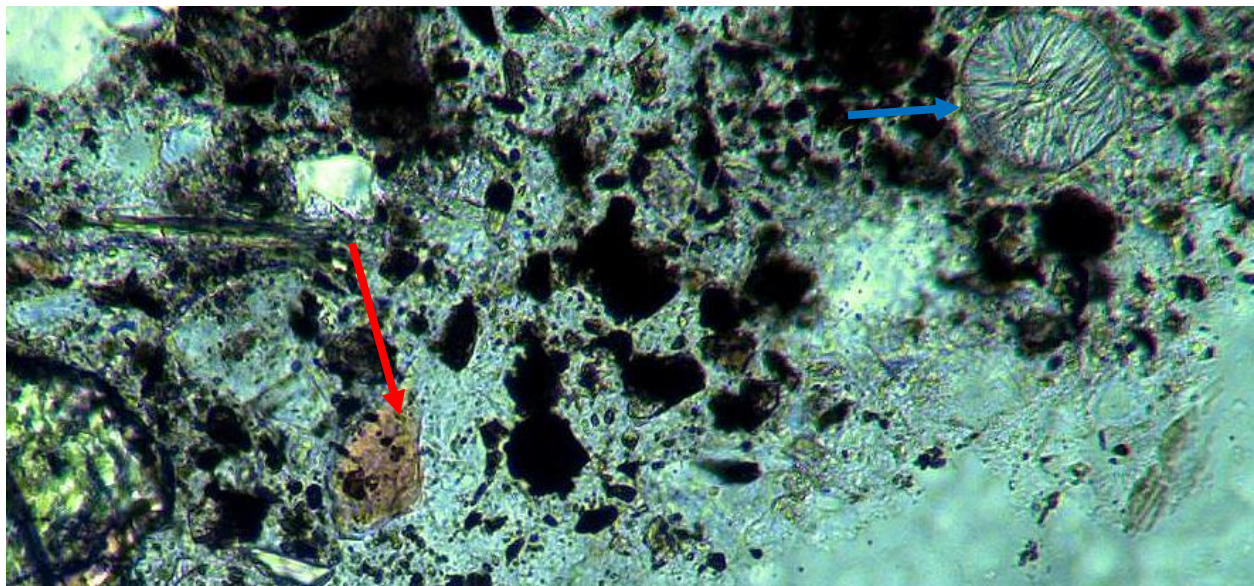


Figure 20. Thin section photomicrograph of Core K-1 illustrating a slag relict (red arrow) and a void filled with ettringite (blue arrow). Vertical field of view is 0.60 mm. Plane-polarized light.

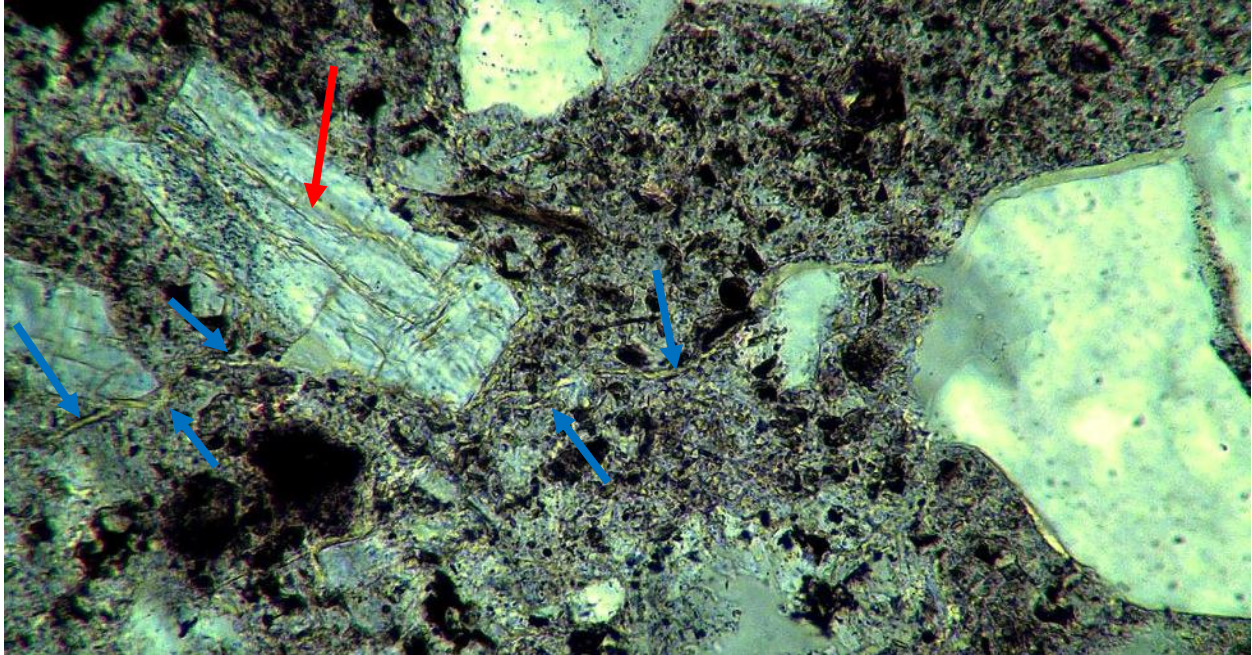


Figure 21. Thin section photomicrograph of Core R-5 illustrating a cracked and reacting aggregate particle (red arrow) with crack radiating out into adjacent paste and filled alkali-silica gel (blue arrows). Vertical field of view is 0.60 mm. Plane-polarized light.

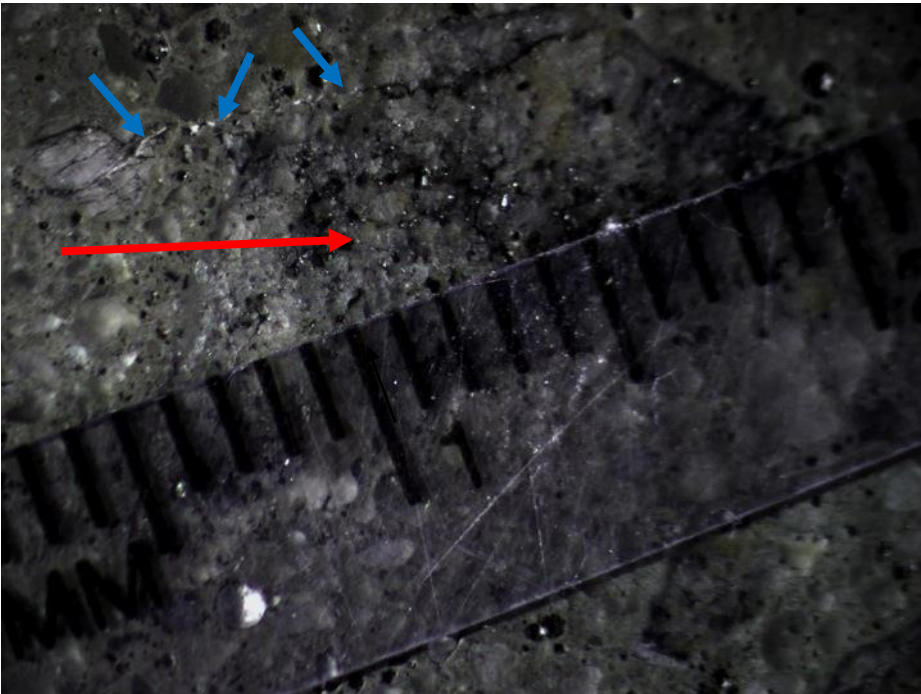


Figure 22. Photomicrograph of Core R-5 showing a cracked and rimmed gneiss particle (red arrow) with an alkali-silica gel filled crack radiating into adjacent paste (blue arrows). Scale is in millimeters.



Figure 23. Photomicrograph of alkali-silica gel lining a crack in Core R-6. The reacting gneiss particles are delineated by red arrows. Scale is in millimeters.

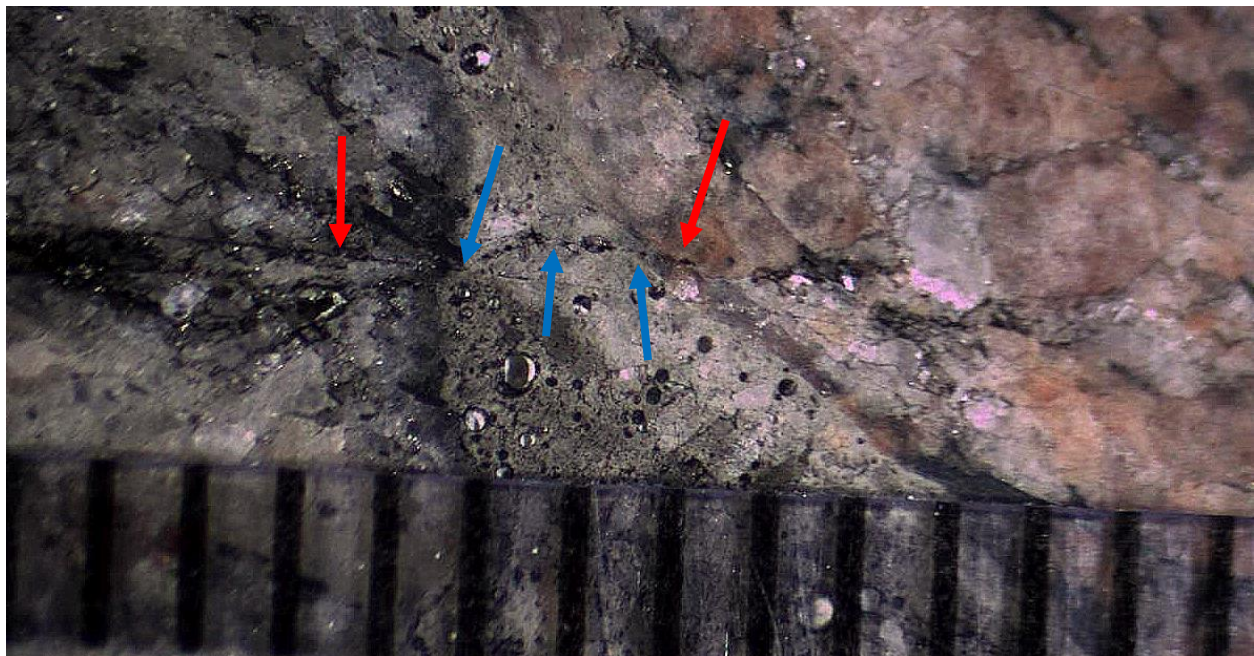


Figure 24. Photomicrograph of Core R-6 showing cracked and rimmed gneiss particles (red arrows) with an alkali-silica gel filled crack radiating from both particles (blue arrows). Scale is in millimeters.

Airport VII

Core Locations

Core locations were selected by Clemson University. Specific locations and identifications based on information conveyed by you are as follows:

<u>Core No.</u>	<u>Approximate Location</u>
A3	Hanger Area Slabs, NE of Taxiway B, between Taxiways D and E
D8	Terminal Area Slabs, NE of Taxiway B and south of Taxiway F

The 2 cores, (Figures 1 and 2), were received at STS on May 5, 2011. Petrographic examination was requested on each of the cores to determine the cause(s) and extent of cracking, slab movement and other observations pertinent to induced distress mechanisms occurring in the slab.

Results

Subject to the qualifications in the attached Appendix, results of the petrographic examinations are as follows:

1. Coarse aggregate in both cores (A3 and D8) is composed of crushed limestone. Portions of some limestone particles are cherty. There is minor evidence of alkali-silica reaction associated with chert in a few of the coarse aggregate. This minor evidence includes alkali-silica gel in voids adjacent to the chert, but no cracking damage associated with the particles or in paste around the gel (Figure 3). The limestone is not dolomitic; and therefore, not of a variety susceptible to alkali-carbonate reaction.
2. Both cores contain fine cracks (0.008 in. or less wide) at the pavement-wearing surface that extend an inch or two into the concrete and dissipate. The cracks go through some aggregate particles, but pass around most aggregate particles, suggesting early formation, such as a result of drying shrinkage. The surface cracks in Core A3 have autogenously healed with calcium carbonate, perhaps with some iron impurities giving the carbonate deposits a slight red to yellow tinge.
3. The top 2-to-3 inches of Core A3 has been poorly consolidated and contains numerous large voids (honeycomb) that are up to ¼ in. wide (Figure 4). Most of these voids are lined with calcium carbonate, ettringite and alkali-silica gel (Figure 5). The carbonate is readily dissolved by drops of dilute hydrochloric acid.
4. Entrained air content in the near-surface honeycomb areas is lower than in the body of the concrete (Figures 6 and 7), possibly suggesting the concrete in the honeycombed area was a later load of concrete that experienced premature (i.e., false or flash) set which did not have enough agitation for air void development.

5. The fine aggregate in both cores is natural sand containing discrete chert particles among other lithologies. Again, there is minor evidence of alkali-silica reaction associated with chert in the fine aggregate, in the form of alkali-silica gel in voids adjacent to a few of the chert particles (Figure 8), but no cracking damage associated with the fine aggregate particles or in paste around the gel in either core.
6. There are some horizontal trending, but somewhat discontinuous microcracks occurring at depths of 3 to 7 inches in both cores, although slightly more abundant in Core D8. The microcracks may be associated with alkali-silica reaction, but are more typical of early stages of freeze-thaw damage or other forms of damage not readily identifiable in the cores examined.
7. Both concretes contain fly ash as a supplementary cementitious material (Figure 9), estimated to be in the 10-to-15% range (by volume of paste). The fly ash also likely inhibited concrete represented by these cores from participating in extensive deleterious alkali-silica reaction. Other damaged or highly cracked areas may not contain fly ash and this should be investigated further.
8. Water-to-cementitious materials ratio is estimated to be low to moderately low, in the 0.35-to-0.40 range.
9. Paste is only minimally carbonated (less than 1 mm. deep), suggesting the concrete was well cured.

Details of the petrographic examinations are provided in the following sections of this report.

Petrographic Examination

Core A3

General Description

The sample consists of a concrete core identified as “Core A3” (Figure 1). The core is 375.0 mm (14.7 in.) long and has a diameter of 102.0 mm (4.0 in.).

The core top or wearing surface is a fairly flat, weathered (finished) surface with many fine aggregate particles partially exposed.

The top 2-to-3 inches of the pavement has been poorly consolidated and contains numerous large voids (honeycomb) that are up to ¼ in. wide (Figure 4). Most of these voids are lined with calcium carbonate, ettringite and alkali-silica gel (Figure 5). Entrained air content in the near-surface honeycomb areas is lower than in the body of the concrete (Figures 6 and 7), possibly suggesting the concrete in the honeycombed area was a later load of concrete that experienced premature (i.e., false or flash) set.

Steel reinforcement is not present in the core. Nor is there any evidence of damage due to corrosion of steel reinforcement in this core.

The core bottom is the imprint of what appears to be a white, lime-treated underlying base course.

Cracks

Fine cracks (0.008 in. or less wide) at the pavement-wearing surface extend an inch or two into the concrete and dissipate. The cracks go through some aggregate particles, but pass around most aggregate particles, suggesting early formation, such as a result of drying shrinkage. The surface of the cracks have autogenously healed with calcium carbonate, perhaps with some iron impurities giving the carbonate deposits a slight red to yellow tinge.

There are some horizontal trending, but somewhat discontinuous microcracks occurring at depths of 3 to 7 inches. The microcracks may be associated with alkali-silica reaction, but are more typical of early stages of freeze-thaw damage or other forms of damage.

Aggregates

Aggregate particles are uniformly dispersed throughout the concrete. Maximum aggregate size is measured as 19 mm (0.75 in.). The aggregate is fairly well graded.

Coarse aggregate is composed of crushed limestone. The limestone is more often sparitic (coarse grained) to infrequently micritic (fine grained). The limestone contains numerous fossils and is sometimes cherty. There is minor evidence of alkali-silica reaction associated with chert in a few of the coarse aggregate particles, in the form of alkali-silica gel in voids adjacent to the chert, but no cracking damage associated with the particle or in paste around the gel. The limestone is not dolomitic; and therefore, not of a variety susceptible to alkali-carbonate reaction.

Coarse aggregate particles are beige to light to dark gray. Coarse aggregate is hard; somewhat dense; angular; equant shaped and outer surfaces of particles have a rough texture.

Fine aggregate is natural sand containing a variety of rock and mineral types including, quartz, various types of feldspars, metaquartzite, meta-argillite, chert, limestone fines and other rock and mineral types. Fine aggregate particles are variously colored from brown to translucent; hard, dense, sub-rounded to well rounded, generally spherical and having a smooth outer surface texture.

Some of the chert and meta-argillite particles contain reaction rims along their outer periphery. As in the coarse aggregate, there is minor evidence of alkali-silica reaction associated with chert and meta-argillite in a few of the fine aggregate particles. Minor evidence includes alkali-silica gel in voids adjacent to the chert (Figure 8) and meta-argillite, but no cracking damage associated with the particle or in paste around the gel.

Cement Paste

The cement paste is dark brownish gray, exhibits a vitreous luster, micro-granular texture, and hackly fracture. The paste is hard, dense and tightly bonded to aggregate particles. Cement paste is carbonated to a depth of 1-to-2 mm below the wearing surface.

Residual cement particles are present in a moderate amount. Residual cement particle content is estimated to be 10-to-12%, by volume of paste. Calcium hydroxide, a normal hydration product, is estimated to be 10-to-12% by volume of paste, as evenly disseminated, fine hexagonal crystals.

The concrete contains fly ash as a supplementary cementitious material, estimated to be in the 10-to-15% range (by volume of paste). The fly ash also likely inhibited concrete represented by these cores from participating in deleterious alkali-silica reaction.

Properties of the paste previously described are evaluated to provide an estimate of the water-to-cementitious materials ratio. Based on paste properties observed, water-to-cementitious materials ratio is estimated to be 0.35-to-0.40.

Air Voids

The concrete contains numerous air-voids, many below 2-to-3 inches, which are very fine. The voids are spherical (entrained air) with some larger, irregularly shaped voids, indicative of entrapped air, particularly in the top 2-to-3 inches of the core. The concrete is deemed air-entrained.

Air content is estimated to be 2.5-to-4.5% in the top 2-to-3 inches of the core and 4.5-to-6.0% at greater depths in the core. Ettringite lines to fills many voids. Calcite lines voids in the near-surface regions of the concrete, as does innocuous alkali-silica gel.

Core D8

General Description

The sample consists of a concrete core identified as “Core D8” (Figure 2). The core is 362.0 mm (14.3 in.) long and has a diameter of 102.0 mm (4.0 in.).

The core top or wearing surface is a fairly flat, weathered (finished) surface with many fine aggregate particles partially exposed.

Steel reinforcement is not present in the core. Nor is there any evidence of damage due to corrosion of steel reinforcement in this core.

The core bottom is an irregular broken surface, passing primarily through aggregate particles. A few deposits of alkali-silica gel fill voids adjacent to chert aggregate particles, but there is no damage observed associated with the gel deposits.

Cracks

Fine cracks (0.008 in. or less wide) at the pavement-wearing surface extend an inch or two into the concrete and dissipate. The cracks go through some aggregate particles, but pass around most aggregate particles, suggesting early formation, such as a result of drying shrinkage.

There are some horizontal trending, but somewhat discontinuous microcracks occurring at depths of 3-to-7 inches. The microcracks are more common in this core than in Core A3. Some of the microcracks extend out from chert particles into adjacent paste and are filled with alkali-silica gel. Other microcracks do not extend out from chert particles and may be associated with alkali-silica reaction, but are more typical of early stages of freeze-thaw damage or other forms of damage.

Aggregates

Aggregates are similar to those described for Core A3. Aggregate particles are uniformly dispersed throughout the concrete. Maximum aggregate size is measured as 19 mm (0.75 in.). The aggregate is fairly well-graded.

As in Core A3, there is minor evidence of alkali-silica reaction associated with chert in a few of the coarse aggregate particles and a few chert and meta-argillite fine aggregate particles. Minor evidence includes alkali-silica gel in voids adjacent to the reacting particles (Figure 4), but no cracking damage associated with the particle or in paste around the gel.

Cement Paste

Cement paste is similar to that described for Core A3. The cement paste is brownish gray, exhibits a vitreous luster, micro-granular texture, and hackly fracture. The paste is hard, dense and tightly bonded to aggregate particles. Cement paste is carbonated to a depth of less than 1mm below the wearing surface.

Residual cement particles are present in a moderate amount. Residual cement particle content is estimated to be 10-to-12%, by volume of paste. Calcium hydroxide, a normal hydration product, is estimated to be 10-to-12% by volume of paste, as evenly disseminated, fine hexagonal crystals.

The concrete contains fly ash as a supplementary cementitious material (Figure 9), estimated to be 10-to-15% range (by volume of paste). The fly ash also likely inhibited concrete represented by these cores from participating in deleterious alkali-silica reaction.

Properties of the paste previously described are evaluated to provide an estimate of the water-to-cementitious materials ratio. Based on paste properties observed, water-to-cementitious materials ratio is estimated to be 0.35-to-0.40.

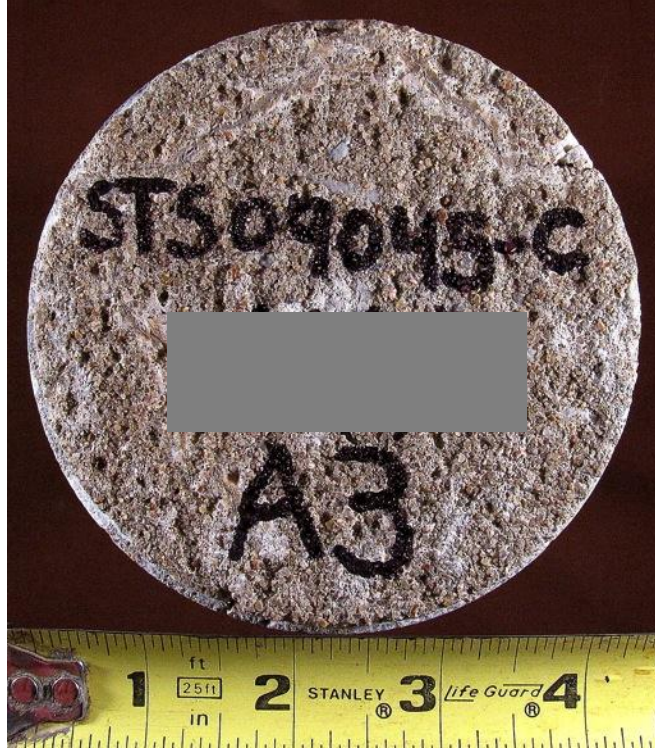
Air Voids

The concrete contains numerous air-voids, most of which are very fine. The voids are spherical (entrained air) with some larger, irregularly shaped voids, indicative of entrapped air. The concrete is deemed air-entrained.

The air-voids are uniformly dispersed throughout the concrete. Air content is estimated to be 6.0-to-7.5%. Most of the voids are clean, but a few are partially lined with calcium carbonate.

Conclusions

Petrographic examination was performed on two (2) concrete cores drilled from pavement slabs at Airport VII. Minor evidence of alkali-silica reaction was observed associated with chert in the coarse aggregate and chert and meta-argillite in the fine aggregate. The reaction is manifested as alkali-silica gel in voids associated with some of the reaction particles, but no definitive damage is observed in Core A3 as a result of the reaction. This is likely due to the presence of fly ash as a supplementary cementitious material. The fly ash also likely inhibited major deleterious alkali-silica reaction. There is minor microcracking due to alkali silica reaction in Core D8. Concrete quality in the two cores is judged to be very good.



(a) Core top/wearing surface. Scale is in inches.



(b) Core side, top is to right. Scale is in inches.

Figure 1. Core A3 as received for petrographic examination.



(a) Core top/wearing surface. Scale is in inches.



(b) Core side, top is to left. Scale is in inches.

Figure 2. Core D8 as received for petrographic examination.



Figure 3. Photomicrograph along a freshly fractured surface of Core D8. Red arrow points to a reacting chert coarse aggregate particle with an alkali-silica gel filled void (green arrow) adjacent to the reacting particle. Scale is in millimeters.

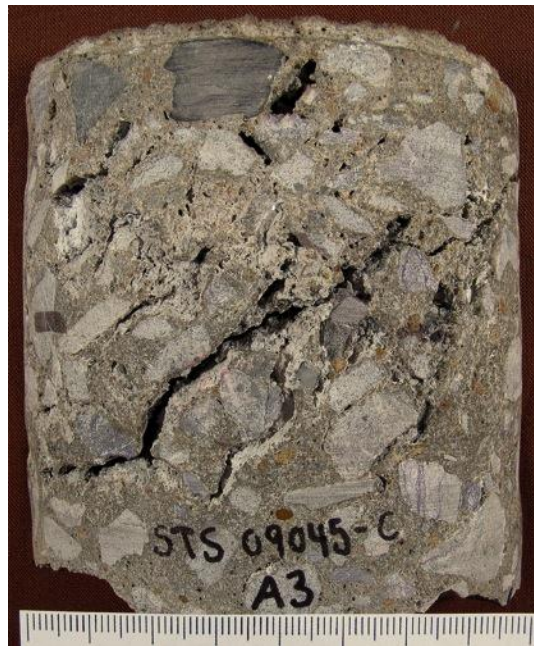


Figure 4. Honeycomb or poor consolidation in the upper 2-to-3 inches of Core A3. Scale is in millimeters.

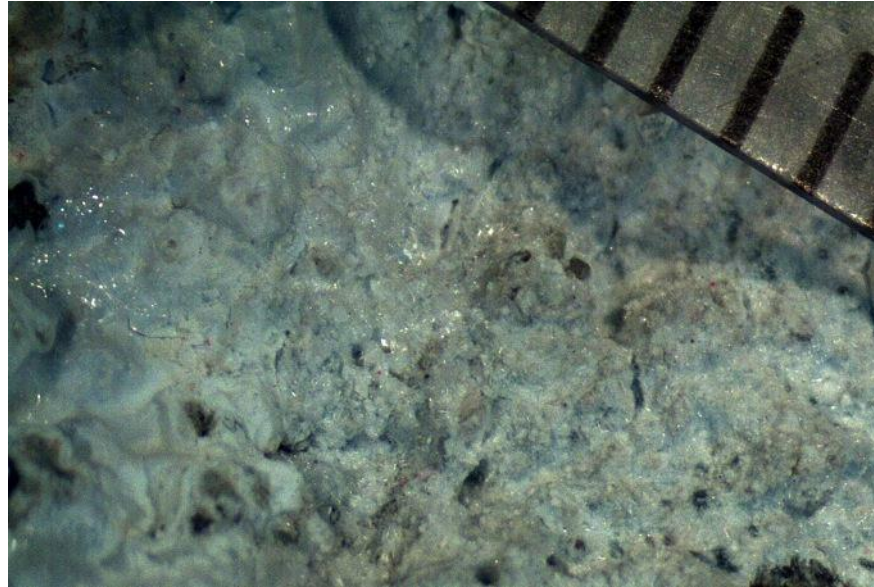


Figure 5. Photomicrograph along a large, poorly consolidated void (honeycomb) in Core A3. The void is lined with calcium carbonate, ettringite and wet appearing alkali-silica gel. Scale is in millimeters.

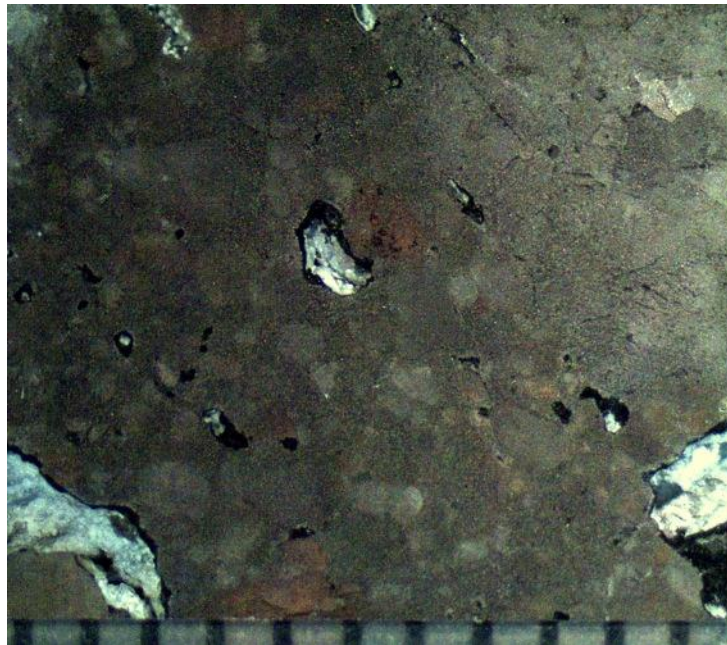


Figure 6. Photomicrograph along the lapped surface within the upper area of poor consolidation in Core A3. Air content is low, estimated to be 2.5-to-4.5% in the top 2-to-3 inches. Scale is in millimeters.

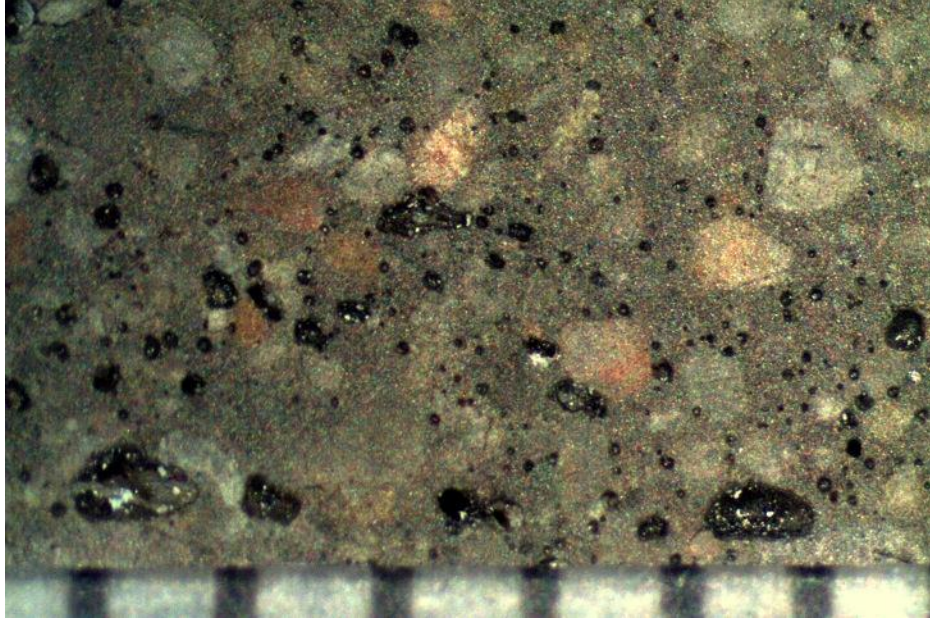


Figure 7. Photomicrograph along the lapped surface in the bottom half of Core A3. Air content is estimated to be 4.5-to-6.0% in this view. Scale is in millimeters.

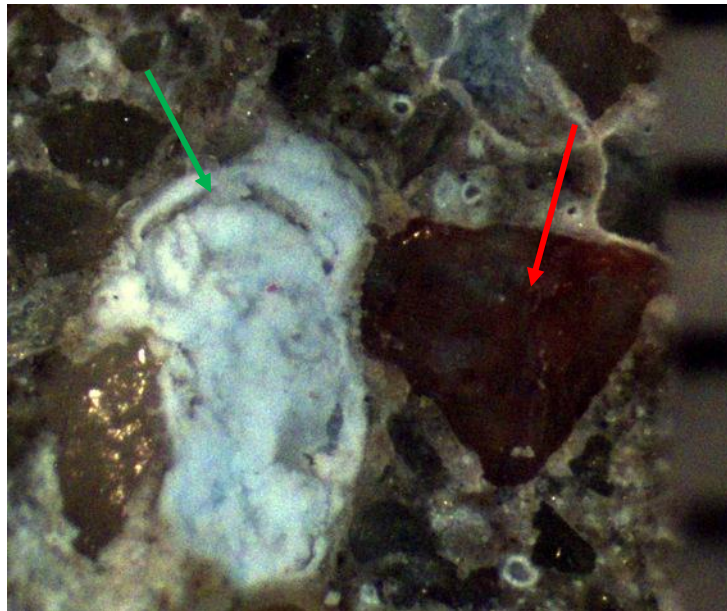


Figure 8. Photomicrograph along a freshly fractured surface of Core A3. Red arrow points to a reacting chert fine aggregate particle with an alkali-silica gel filled void (green arrow) adjacent to the reacting particle. Scale is in millimeters.

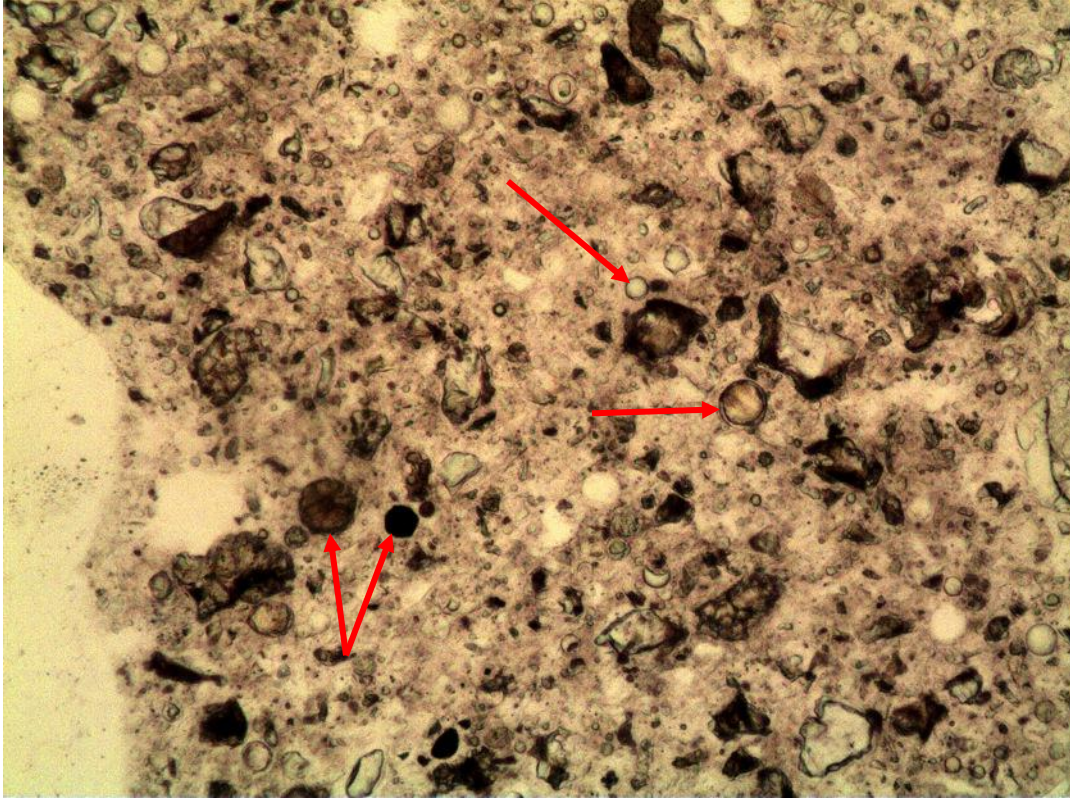


Figure 9. Thin section photomicrograph of Core D8. Red arrow points to fly ash particles that are present as supplementary cementitious materials in both cores. Plane polarized light. Vertical field of view is 0.6 mm.

Airport VIII

Core Locations

Core locations were selected by Clemson University. Specific locations and identifications based on information conveyed by you are as follows:

<u>Core No.</u>	<u>Approximate Location</u>
C1	R/W 1R North End
C7	Gate A-26

The 2 cores, (Figures 1 and 2), were received at STS on July 21, 2011. Petrographic examination was requested on each of the cores to determine the cause(s) and extent of cracking, slab movement and other observations pertinent to induced distress mechanisms occurring in the slab.

Results

Subject to the qualifications in the attached Appendix, results of the petrographic examinations are as follows:

1. Concrete represented by the two (2) cores exhibits evidence of and damage by alkali-silica reaction (ASR). The alkali-reactive aggregate component is chert and metaquartzite within the fine aggregate, particularly in the plus 16 mesh sieve sizes. The cherts and metaquartzites in these concretes are white, brown and tan and contain reactions rims along their outer periphery (Figures 4, 6, 9 and 10). The cherts and metaquartzites are cracked and microcracked and frequently the cracks are lined with gel as is adjacent paste.
2. Coarse aggregate is composed of crushed diabase. The diabase is medium grained, dense and hard. This rock type does not contain any reactive form of silica, and hence, there is no evidence of alkali-silica reaction associated with the diabase coarse aggregate.
3. Evidence of deleterious alkali-silica reaction in the cores are cracking and microcracking occurring within rimmed chert and metaquartzite fine aggregate particles, with cracks radiating out from the reacting particles into adjacent cement paste (Figures 5 through 8). The cracks and nearby voids are lined to filled with alkali-silica gel and innocuous secondary deposits of ettringite, calcium carbonate and calcium hydroxide.
4. The relative degree of damage by alkali-silica reaction is relatively minor. That is, not easily discernible in the two cores with the naked eye, but evident by microscopic observation.
5. Core C1 contains what is interpreted to be a surface crack due to alkali-silica reaction at the wearing surface. The crack extends nearly 1 in. into the core, but also extends well into and terminates within a sound diabase coarse aggregate particle. In addition, the top 2 mm. (0.08 in.) of concrete nearest the wearing surface is an incipient popoff due to

expansion (Figure 3). This appears similar to a drying shrinkage crack, but by virtue of cracking within a hard coarse aggregate particle, the origin must be due to a stress greater than concrete drying shrinkage.

6. Residual acetate deicer has not been identified in cracks and voids of any of the cores.
7. No other forms of deterioration are detected in the concretes represented by these cores.

Details of the petrographic examinations are provided in the following sections of this report.

Petrographic Examination

Core C1

General Description

The sample consists of a concrete core identified as “Core C1” (Figure 1). The core is 366.0 mm (14.4 in.) long and has a diameter of 93.0 mm (3.7 in.).

The core top or wearing surface is a fairly flat, weathered (finished) surface with many fine aggregate particles partially exposed.

Steel reinforcement is not present in the core. Nor is there any evidence of damage due to corrosion of steel reinforcement in this core.

The core bottom is the imprint of an underlying base course.

Cracks

A 0.15 mm. (0.006 in.) wide crack occurs at the wearing surface. The crack extends nearly 1 in. into the core, but also extends well into and terminates within a sound diabase coarse aggregate particle. In addition, the top 2 mm. (0.08 in.) of concrete nearest the wearing surface is an incipient popoff due to expansion (Figure 3).

A few microcracks at the wearing surface are less than 0.08 mm (0.003 in.) wide or less and extend 15 to 20 mm (0.6 to 0.8 in.) depth where they dissipate in cement paste. The cracks pass both around and through aggregate particles. These cracks are not lined with any secondary deposits. The cracks appear to be due to drying shrinkage.

A relatively small number of random, fine (less 0.08 mm dia.) microcracks occur throughout the core. The microcracks appear to originate within chert and metaquartzite fine aggregate particles (Figure 4 and 5) and radiate out into adjacent paste for a few centimeters. The microcracks and voids intersected by the microcracks are lined with alkali-silica gel (Figure 5 and 6). Thus, the microcracks appear to be due to alkali-silica reaction.

Aggregates

Aggregate particles are uniformly dispersed throughout the concrete. Maximum aggregate size is measured as 32 mm. (1.25 in.). The aggregate is fairly well graded.

Coarse aggregate is composed of crushed diabase. The diabase is medium grained, black with white speckles, hard, dense, angular; equant to flat and elongated in shape and outer surfaces of particles have a rough texture.

There is no evidence of alkali-silica reaction associated with the coarse aggregate.

Fine aggregate is natural sand containing a variety of rock and mineral types including, quartz, various types of feldspars, granite, chert, chalcedony, mica, metaquartzite and other rock and mineral types. With the exception of the chert and metaquartzite (which will be described separately), fine aggregate particles are variously colored from white to red to translucent; hard, dense, sub-rounded to well rounded, generally spherical and having a smooth outer surface texture.

The cherts and metaquartzites are white, brown and tan and contain reaction rims along their outer periphery (Figures 4 through 6). The cherts and metaquartzites, particularly in the plus 8 mesh sieve sizes, are cracked and microcracked and frequently the cracks are lined with gel, as is adjacent paste. Cracks radiate out from reacting particles into adjacent paste and are lined to filled with alkali-silica gel. This is classic evidence of damage by alkali-silica reaction. Therefore, chert and metaquartzite in the coarser sizes of the fine aggregate is the offending reactive particle type in this concrete.

Cement Paste

The cement paste is grayish brown, exhibits a vitreous luster, micro-granular texture, and hackly fracture. The paste is hard, dense and tightly bonded to aggregate particles. Cement paste is carbonated to a depth of 2 mm below the wearing surface.

Residual cement particles are present in a moderate low amount, but relict or ghosts of cement particles are evident indicating the paste is well hydrated. Residual and relict cement particle content is estimated to be 5-to-8%, by volume of paste. Calcium hydroxide, a normal hydration product, is estimated to be 9-to-12% by volume of paste, as evenly disseminated, generally coarse hexagonal tablets and masses. Supplementary cementitious materials are not detected.

Properties of the paste previously described are evaluated to provide an estimate of the water-to-cement ratio. Based on paste properties observed, water-to-cement ratio is estimated to be 0.35-to-0.40.

Air Voids

The concrete contains some very fine air-voids indicative of entrained air. The concrete also contains with some larger, irregularly shaped voids, indicative of entrapped air. The concrete is deemed air-entrained. However, air content in general is considered low. The air-voids are uniformly dispersed throughout the concrete. Air content is estimated to be 1.5 to 3.0%.

Alkali-silica gel, calcite and ettringite line about half the voids.

Core C7

General Description

The sample consists of a concrete core identified as “C7” (Figure 2). The core is 366.0 mm (14.4 in.) long and has a diameter of 93.0 mm (3.7 in.).

The core top or wearing surface is a fairly flat, weathered (finished) surface with many fine aggregate particles partially exposed.

Steel reinforcement is not present in the core. Nor is there any evidence of damage due to corrosion of steel reinforcement in this core.

The core bottom is the imprint of an underlying base course.

Cracks

A few very fine microcracks (less than 0.08 mm. wide) occur at the wearing surface and extend vertically into the concrete to a depth of 6-to-15 mm. (0.2-to-0.60 in.), where the cracks dissipate. The fine cracks pass primarily around aggregate particles. These cracks appear to be due to drying shrinkage.

A relatively small number of random, fine (less 0.08 mm dia.) microcracks occur throughout the core. The microcracks appear to originate within chert and metaquartzite fine aggregate particles (Figure 5) and radiate out into adjacent paste for a few centimeters. The microcracks and voids intersected by the microcracks are lined with alkali-silica gel . Thus, the microcracks appear to be due to alkali-silica reaction.

Aggregates

Aggregates are similar to those described for Core C1. Aggregate particles are uniformly dispersed throughout the concrete. Maximum aggregate size is measured as 32 mm. (1.25 in.). The aggregate is fairly well graded.

As in Core C1, there are cherts and metaquartzites containing reaction rims along their outer periphery. The cherts and metaquartzites, particularly in the plus 8 mesh sieve sizes, are cracked and microcracked and frequently the cracks are lined with gel as is adjacent paste is. Cracks radiate out from reacting particles into adjacent paste and are lined to filled with alkali-silica gel (Figure 7 through 10). This is classic evidence of damage by alkali-silica reaction. Therefore, chert and metaquartzite in the coarser sizes of the fine aggregate is the offending reactive particle type in this concrete. Evidence of deleterious alkali-silica reaction is slightly more prevalent in this core, as compared to Core C1. However, the reaction is still judged to be minor.

Cement Paste

Cement paste is similar to that described for Core C1. Cement paste is carbonated to a depth of 1 mm below the wearing surface. Supplementary cementitious materials are not detected. Based on paste properties observed, water-to-cement ratio is estimated to be 0.35-to-0.40.

Air Voids

The concrete contains numerous air-voids, most of which are very fine. The voids are spherical (entrained air) with some larger, irregularly shaped voids, indicative of entrapped air. The concrete is deemed air-entrained.

The air-voids are uniformly dispersed throughout the concrete. Air content is estimated to be 4.5 to 5.5%.

Alkali-silica gel, ettringite and calcite are present as partial fine linings of voids.

Conclusions

Petrographic examination was performed on two (2) concrete cores drilled from pavement slabs at the Washington Dulles Airport, Chantilly, VA. Alkali-silica reaction was observed in both cores as was cracking due to the reaction. The reactive aggregates are chert and metaquartzite in the fine aggregate, particularly plus 8 mesh sieve sizes. The coarse aggregate is a non-reactive crushed diabase. The degree of damage is relatively minor in both cores but slightly more prevalent in Core C7.



(a) Core top/wearing surface. Scale is in inches.

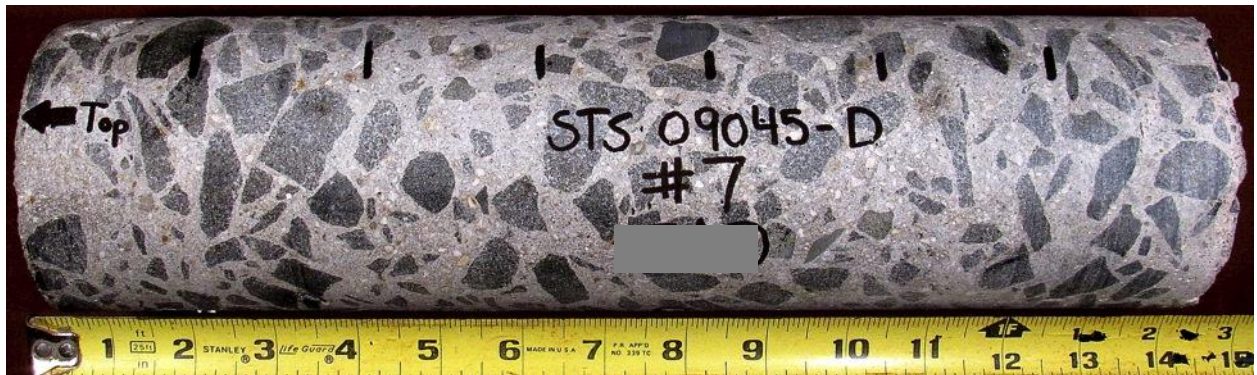


(b) Core side, top is to right. Scale is in inches.

Figure 1. Core C1 as received for petrographic examination.



(a) Core top/wearing surface. Scale is in inches.



(b) Core side, top is to left. Scale is in inches.

Figure 2. Core C7 as received for petrographic examination.

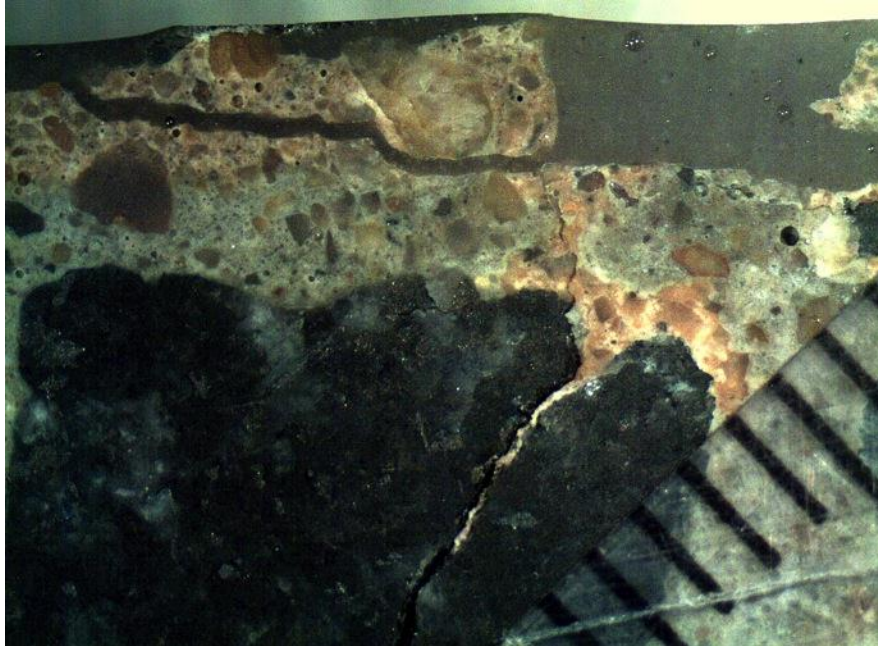


Figure 3. Photomicrograph of Core C1 showing a surface crack extending into the core well into a sound diabase coarse aggregate particle. In addition, the top 2 mm. (0.08 in.) of concrete nearest the wearing surface is an incipient popoff due to expansion. Scale is in millimeters.

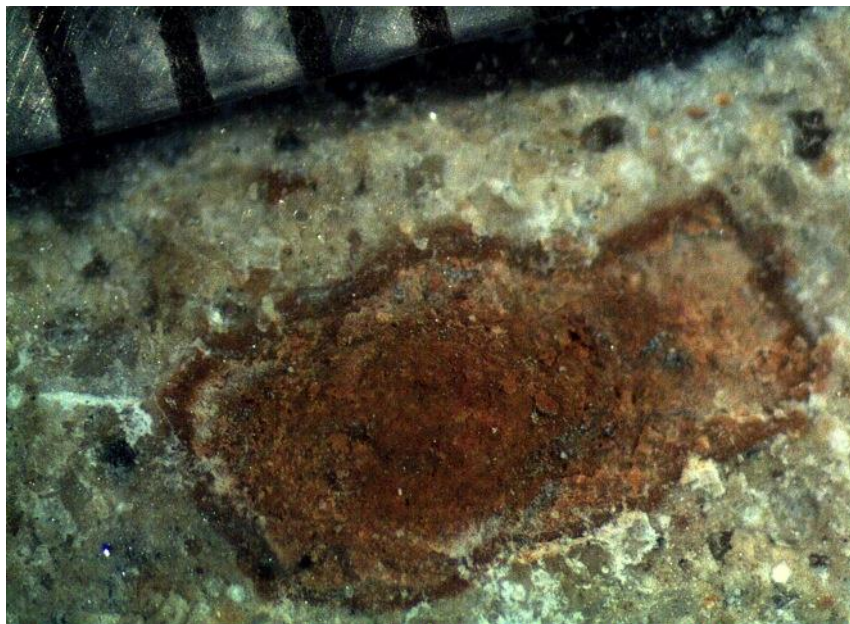


Figure 4. Photomicrograph of Core C1 illustrating a reacting chert particle. Scale is in millimeters.



Figure 5. Lapped surface of Core C1 showing horizontal oriented cracking and microcracking extending outward from a metaquartzite fine aggregate particle (red arrow). Scale is in millimeters.



Figure 6. Magnified cracked surface in Core C1 where white alkali-silica gel lines the crack and voids adjacent to the crack. Several, cracked, rimmed and reacting chert and metaquartzite particles are present along the crack (green arrows). Scale is in millimeters.

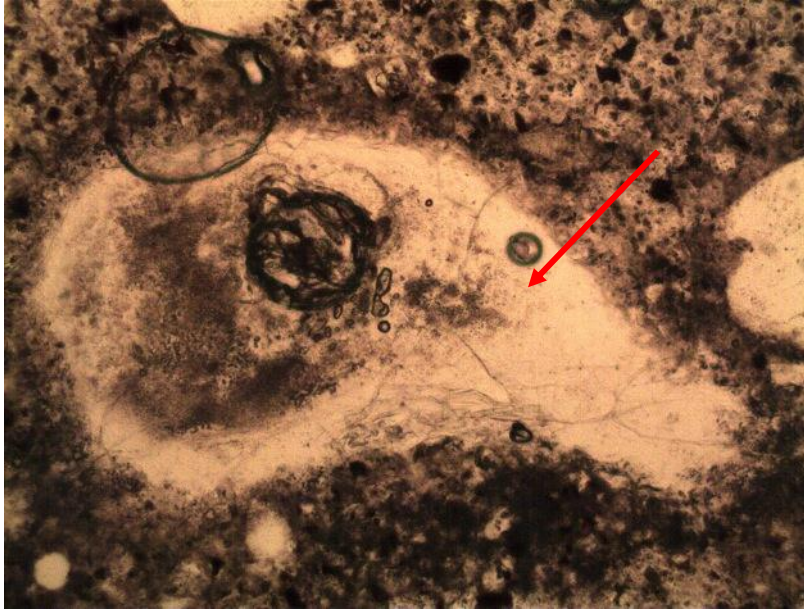


Figure 7. Thin section photomicrograph of a reacting chert particle in Core C7. Cracks radiate from a rimmed, beige chert particle (red arrow) into adjacent paste. The cracks are filled with alkali-silica gel and paste is soaked by gel. Vertical field of view is 1.1 mm. Plane polarized light.

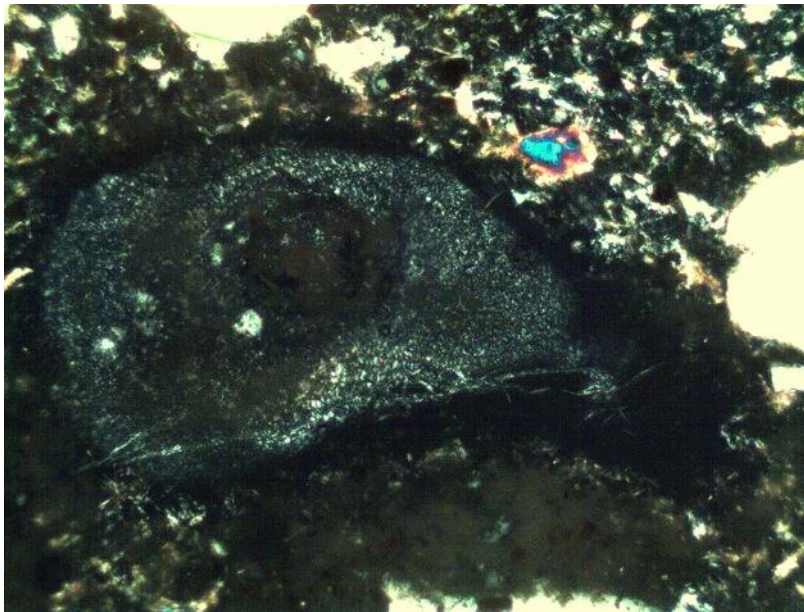


Figure 8. Thin section photomicrograph of the same reacting chert particle as in Figure 7. Gel filled cracks are slightly more apparent. Vertical field of view is 1.1 mm. Cross-polarized light.

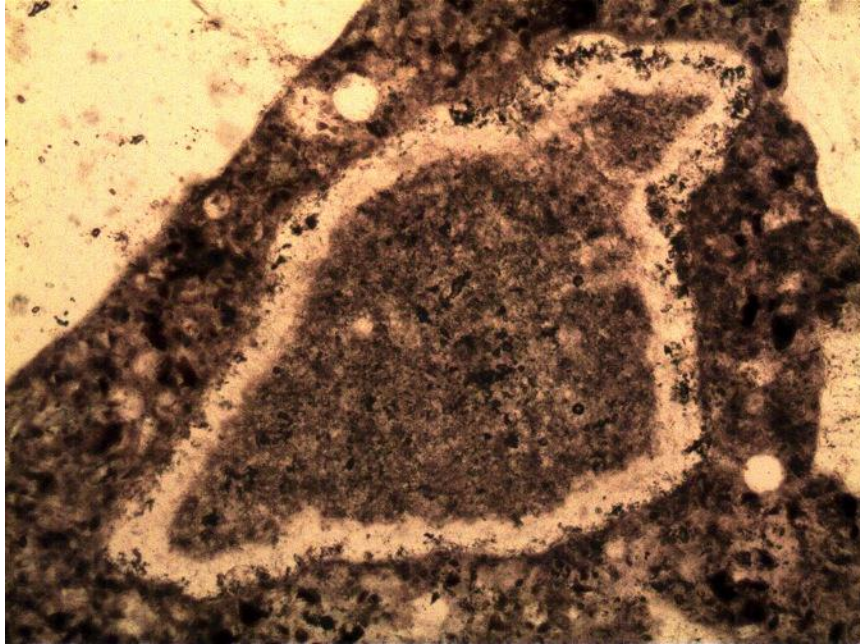


Figure 9. Thin section photomicrograph of a rimmed chert particle in Core C7. Vertical field of view is 1.1 mm. Plane polarized light.

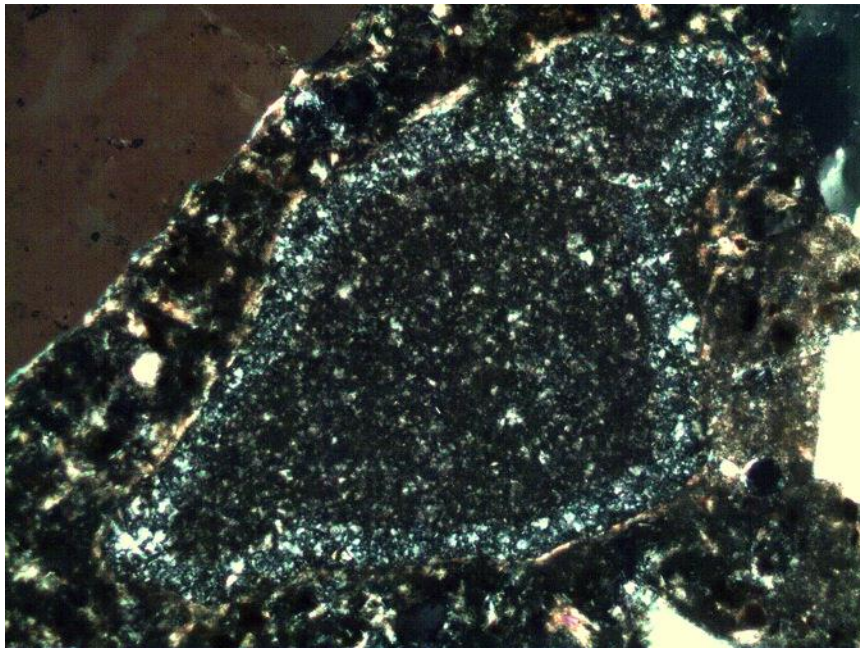


Figure 10. Thin section photomicrograph of the same rimmed chert particle as in Figure 9. Vertical field of view is 1.1 mm. Cross-polarized light.

Appendix For Airports IV – VIII

Document Qualifications

Standard of Care

This report has been prepared for the exclusive use of the Client for specification application to their project. This report is not intended for use by others. Schmitt Technical Services, LLC (STS) has provided professional services consistent with generally accepted evaluative and geologic practices. No other warranties are expressed or implied. The opinions and recommendations submitted in these reports are based on interpretation of field observations, samples taken from specific locations and/or field and/or laboratory test results.

Samples

The samples taken during the field observations depict conditions only at specific locations and times indicated in the report. Conditions at other locations may differ from conditions where sampling was conducted. The passage of time may also result in changes in conditions interpreted to exist at the locations where sampling was conducted.

Completion of Characterization of Site Conditions

The scope of services described in this report is based on a limited number of samples. The nature and variations in other locations may exist and may not become evident until repairs are performed. If variations or other latent conditions become evident, additional evaluation and testing may be warranted.

Conceptual Level of Project Scope

The field activities, testing procedures and evaluative approaches used in this study are consistent with those normally used in testing of construction materials and products. The number of samples and tests and scope of testing were done within Client's budget, but represents less data than that generally needed to evaluate the extent of less than expected performance.

Test Repair and Repair Observations and Testing

Since findings, discussion and observations are based on limited numbers of observations and tests, the Client should be particularly sensitive to the potential need for adjustment in extent of repair, repair procedures and repair materials in the field. It is in the best interest of the client to retain STS to observe and test repair materials and repairs to observe general compliance with repair design concepts, specifications and contractor/manufacturer recommendations and to assist in development of changes should field conditions differ from those anticipated before the start of repair construction.

Limitations-Repair Construction Considerations

The recommendations made in the report are not intended to dictate type of repair materials to be used, construction methods or construction sequences. Prospective contractors and material suppliers must evaluate potential repair problems on the basis of their knowledge and experience

in the local area and on the basis of similar project in other localities, taking into account their own proposed repair construction methods and procedures.

Testing Conducted by Others

When subcontracted outside field and/or laboratory services and analyses are used, STS will rely upon the data provided by the outside field service or laboratory, and will not conduct an independent evaluation of the reliability of their data.